Durham E-Theses

Magnetic anisotropy and domain structure in gadolinium

Smith, Ronald Leslie

How to cite:

Smith, Ronald Leslie (1978) *Magnetic anisotropy and domain structure in gadolinium*, Durham theses, Durham University. Available at Durham E-Theses Online: http://etheses.dur.ac.uk/8210/

Use policy

The full-text may be used and/or reproduced, and given to third parties in any format or medium, without prior permission or charge, for personal research or study, educational, or not-for-profit purposes provided that:

- a full bibliographic reference is made to the original source
- a link is made to the metadata record in Durham E-Theses
- the full-text is not changed in any way

The full-text must not be sold in any format or medium without the formal permission of the copyright holders.

Please consult the full Durham E-Theses policy for further details.

Academic Support Office, Durham University, University Office, Old Elvet, Durham DH1 3HP
e-mail: e-theses.admin@dur.ac.uk Tel: +44 0191 334 6107
http://etheses.dur.ac.uk

'MAGNETIC ANISOTROPY AND DOMAIN STRUCTURE IN GADOLINIUM'

BY

RONALD LESLIE SMITH B.Sc.

The copyright of this thesis rests with the author. No quotation from it should be published without his prior written consent and information derived from it should be acknowledged.

A thesis submitted to the University of Durham in candidature for the degree of Doctor of Philosophy.

October 1978.

Durham University SCIENCE - 7 FEB 1979 SECTION Library

TO MY FAMILY AND
ELISABETH

ABSTRACT

The magnetocrystalline anisotropy constants of high quality single crystals of gadolinium have been measured using torque magnetometry. The redetermination of the anisotropy constants was necessary due to the poor agreement between the previous measurements which had been made on uncharacterized material of varying quality. The easy direction of magnetization was determined from the anisotropy constants and it is in good agreement with the direct measurements of Corner and Tanner (1976), made on the same crystal, and the neutron diffraction results of Cable and Wollan (1968). It is suggested that the lack of agreement in the previous determinations of the constants was due to the quality of the crystals used, particularly with respect to their oxygen content. A treatment of the magnetostatic energy of nonmagnetic inclusions in gadolinium and their contribution to the total anisotropy is given which can explain the discrepancies between the results of the various previous investigations of the easy direction and anisotropy.

The magnetic domain structure of gadolinium was investigated using the Bitter wet colloid technique and a dry colloid technique suitable for low temperature work (90K to 291K). The formation of domains at the Curie temperature (291K) and also the disappearance of a clear domain structure at about 230K, below which there is an easy cone of magnetization, was observed. No magnetic domains were observed below 230K. Around 230K it was expected that there would not be a clear domain structure due to the low value of the anisotropy but the reasons for the non-appearance of domains below about 150K, where the anisotropy is large again, are not clear as Corner and Saad (1977a) have observed clear domain patterns on gadolinium at 77K.

ACKNOWLEDGEMENTS.

I would like to take this opportunity to make the following acknowledgements.

I would like to thank Professor A.W.Wolfendale for accepting me as a research student and for allowing me the use of the facilities of the Physics Department. I would also like to express my thanks to the University of Durham for the provision of a Research Studentship.

My special thanks go to Dr. W.D.Corner for his excellent supervision over the past three years. I would also like to thank Dr. B.K.Tanner for his ideas and enthusiasm.

Thanks also go to all the departmental technical and secretarial staff of the department, especially Mr. K.G.Moulson and Mr. A.E. Lanigan, the solid state group technicians, and Mr. J.Scott, the departmental glassblower. I would like to thank Mrs C.G. Rowes and Mrs J.T.McGough for typing this thesis.

Finally my thanks go to past and present members of the solid state research group, in particular Mr. I.B.MacCormack who proof read the manuscript, for help, advice and friendship.

Some of the material inChapter five has been published in,

Proc. Conf. on Rare Earths and Actinides, Durham 1977 Inst. Phys. Conf. Ser. No. 37 and J.Phys. F. 1977 7 L229.

CONTENTS. PAGE

Chapter Four Contd.

Chapter Six Contd.

Chapter Eight Contd.

CHAPTER ONE

Introduction to Magnetism

1.1 Magnetism

The phenomenon of magnetism has been the subject of experimental observation for over 3,000 years and is, perhaps, the oldest aspect of solid state physics. Yet it was not until the early part of this century that the origins of magnetism became clear with the discovery of quantum mechanics. Magnetism is probably the most common manifestation of the quantum mechanical nature of matter. It is incapable of being understood otherwise for a strictly classical system in thermal equilibrium can display no magnetic moment. The magnetic moment of a free atom has three sources:

a) The intrinsic quantum mechanical spin of an electron

b) The orbital angular momentum of an electron about the nucleus

c) The change in the orbital moment induced by an external magnetic field

It follows that for atoms with filled electron shells, giving zero total spin and orbital moment, only the third effect can induce a magnetic moment.

To quantify magnetic substances we introduce a macroscopic quantity, the magnetisation $\underline{M}$, which is defined as the magnetic moment per unit volume. The magnetic susceptibility per unit volume K is defined in S.I. units, which are used throughout this thesis, as

$$K = \frac{\underline{M}}{\underline{H}} \qquad (1.1)$$

using the Sommerfeld convention where

$$\underline{B} = \mu_0 \ (\underline{H} + \underline{M}) \qquad (1.2)$$

$$= \underline{B}_0 + \mu_0 \underline{M}$$

Durham University SCIENCE - 7 FEB 1979 SECTION Library

relates the magnetic flux density $\underline{B}$ in Webers m^{-2}(Tesla) with the magnetic field strength $\underline{H}$ in A m^{-1}. $\underline{M}$ is then measured in A m^{-1} and K is dimensionless. K is not in general a constant and its magnitude and variations with magnetic field strength and temperature can be used to distinguish types of magnetic behaviour. The constant μ_o, known as the absolute permeability of free space, relates the values of $\underline{B}$ and $\underline{H}$ when there is no medium present and has the value $4\pi \times 10^{-7}$ H m^{-1}.

Another quantity which is used to distinguish the various types of magnetism is the relative permeability μ_r.

$$\mu_r = \frac{\underline{B}}{\underline{B}_o} = 1 + \mu_o \frac{\underline{M}}{\underline{B}_o}$$

$$= 1 + K \qquad (1.3)$$

Where $\underline{B}o$ is the magnetic flux density due to a magnetic field strength $\underline{H}$ in free space.

$$\underline{B}_o = \mu_o \underline{H} \qquad (1.4)$$

Equations (1.1) to (1.4) define the basic quantities in a magnetic field. Further effects of magnetic fields acting on matter will be discussed as required in subsequent chapters.

The various types of magnetic behaviour will now be discussed.

1.2 Diamagnetism

Diamagnetism is the only form of magnetism that is exhibited by all atoms and is due to the change in orbital moment induced by an external magnetic field. K is negative and very small, of the order of 10^{-5}. The occurrence of diamagnetism is understood by considering the precession of the electron orbits about the applied magnetic field (Larmor precession). Then in accordance with Lenz's Law the direction of the magnetic moment produced is such as to oppose the magnetic field producing it. This magnetic moment, μ_{dia}, can be calculated classically (after allowing electrons to have stable orbits) or more correctly quantum mechanically, the result being the same in both cases (for details see Van Vleck 1932).

$$\underline{\mu}_{dia} = - \frac{Z e^2 \underline{B}}{4 m} \langle \rho^2 \rangle \qquad (1.5)$$

where Z is the atomic number
e is the electronic charge
m is the electronic mass
$\langle \rho^2 \rangle$ is the mean square of the perpendicular distance of the electron from the field axis through the nucleus.

The mean square distance of the electron from the nucleus is

$$\langle r^2 \rangle = \frac{3}{2} \langle \rho^2 \rangle$$

and if we have N atoms per unit volume the diamagnetic susceptibility is

$$K_{dia} = - \frac{\mu_o NZ e^2}{6m} \langle r^2 \rangle \qquad (1.6)$$

Equation (1.6) gives the basic properties of diamagnetism which can be summarised as:

a) The diamagnetic susceptibiltiy is always negative since $\langle r^2 \rangle > 0$

b) Diamagnetism is a property of all matter

c) K_{dia} is not explicitly temperature dependent

d) The amount of magnetisation is proportional to $\langle r^2 \rangle$ and small variations in K_{dia} with temperature may be interpreted as a slight dependence of $\langle r^2 \rangle$ on temperature.

To calculate theoretically the value of the diamagnetic susceptibility we need only to estimate $\langle r^2 \rangle$. For a hydrogen like atom we can use Bohr quantum theory, but in more complicated atoms the effect of other electrons must be taken into account. This can be achieved by the introduction of a screening factor σ. To give more accurate results though, it is best to construct the electron orbitals using Hartree or Hartree-Fock wave functions and hence find the mean of theelectron charge distributions. A comparison of these calculations with experimental results is given in Kubo and Nagamiya (1969). The agreement is found to be good for the rare gases and some ions.

When a material shows any other magnetic effect the contribution of diamagnetism, being extremely small, can usually be neglected.

1.3 Paramagnetism

In the case of paramagnetism there is a small positive susceptibility (approximately 10^{-3}) which is independant of the applied field strength but has a simple temperature dependance. This temperature dependance can be expressed as

$$K = \frac{C}{T} \qquad (1.7)$$

the Curie Law, or

$$K = \frac{C^1}{T-\theta_p}$$

the Curie-Weiss Law. C, C^1 are constants and θ_p is a constant known as the paramagnetic Curie temperature. The two types of behaviour are illustrated in Figure 1.1.

Paramagnetism occurs in materials where the atoms or molecules have a permanent magnetic moment and the Curie or Curie-Weiss behaviour is explained as a compensation process between the ordering effect of the applied magnetic field and the disordering effects of thermal motion.

Langevin developed the classical theory of paramagnetism by considering a perfect gas modied by the presence of a magnetic field. Here interactions between the molecular moments are neglected and, using Boltzmann statistics, he obtained an expression:

$$\frac{\langle\mu\rangle}{\mu} = \coth\alpha - \frac{1}{\alpha} \equiv L(\alpha) \qquad (1.9)$$

where $\alpha = \frac{\mu \underline{B}_o}{k T}$

$\langle\mu\rangle$ is the mean resolved moment along the field direction $\underline{B}o$

$L(\alpha)$ is known as the Langevin Function

A more rigorous treatment was developed by Brillouin where each atom or ion had an angular momentum quantum number J and an associated magnetic

moment $Jg\mu_B$, where g is the Landé splitting factor and μ_B the Bohr magneton ($\mu_B = \frac{e\hbar}{2m}$). The allowed orientations of M_J, the resolved values of J along $\underline{B}_o$, can have 2J+1 values. Applying Boltzmann statistics to calculate the population of the levels and then summing over the allowed levels we obtain (see Morrish (1965) for details)

$$\frac{\langle\mu\rangle}{\mu} = \frac{2J+1}{2J} \coth\left(\frac{2J+1}{2}\right)\alpha - \frac{1}{2J}\coth\left(\frac{\alpha}{2J}\right)$$

$$= B(\alpha) \qquad (1.10)$$

$B(\alpha)$ is the Brillouin function with $\alpha = Jg\mu_B \frac{\underline{B}_o}{kT}$

If we let the moments assume any orientations, ($J \to \infty$) as in the classical case, then

$$B(\alpha) \longrightarrow \coth\alpha - \frac{1}{\alpha} = L(\alpha)$$

For moderate fields and temperatures not too low α is small and

$$K = \frac{\underline{M}}{\underline{H}} = \frac{N\langle\mu\rangle}{\underline{H}} = \left(\frac{J+1}{3J}\right)\frac{(N J g \mu_B)^2 \underline{B}_o}{N k T, \underline{H}}$$

$$= \frac{N^2 g^2 J(J+1)\mu_B{}^2 \mu_o}{3RT} \qquad (1.11)$$

The quantity $g[J(J+1)]$ is known as the effective number of Bohr magnetons, P_{eff}, and equation (1.11) gives the Curie Law $K \propto \frac{1}{T}$. A more exact quantum mechanical derivation of equation (1.11) is also given by Morrish (1965).

The Curie-Weiss Law (equation 1.8) can be explained if it is assumed that there is an internal molecular field due to the partial orientation of the atomic moments. This gives a total effective field

$$\underline{H}_{eff} = \underline{H}_{app} + N_w \underline{M} \qquad (1.12)$$

where N_w is the Weiss molecular field constant. Now from equation (1.11)

$$\underline{M} = \frac{\underline{H}}{T} N^2 g^2 \frac{J(J+1)}{3R}\mu_B{}^2$$

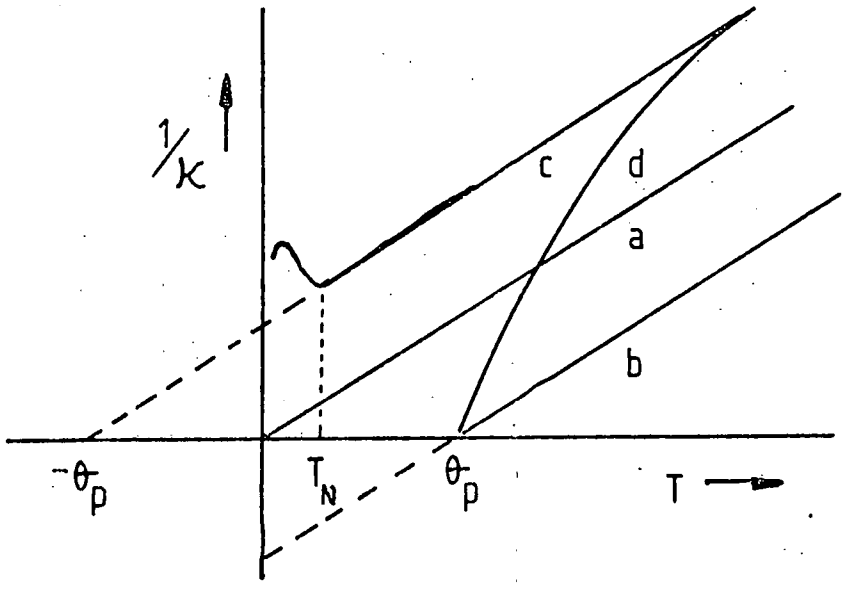

FIGURE 1.1

a Curie Paramagnet
b Curie-Weiss: - Ferromagnet
c : -Antiferromagnet
d : ¬Ferrimagnet

and replacing $\underline{H}$ by $\underline{H}_{eff}$.

$$\underline{M} = (H_{app} + N_W M) \frac{C^1}{T}$$

to give

$$K = \frac{\underline{M}}{\underline{H}_{app}} = \frac{C^1}{T - C^1 N_W}$$

$$= \frac{C^1}{(T - \theta_p)}$$

which is the Curie-Weiss Law. θ_p can be positive, giving ferromagnetic or ferrimagnetic behaviour, or negative, which corresponds to antiferromagnetism. (see Figure 1.1).

There are two other types of paramagnetism, both of which are essentially temperature independant. Van Vleck paramagnetism is a positive term in the quantum mechanical derivation of the diamagnetic susceptibility for atoms which have zero magnetic moment in the ground state but can show a magnetic moment in an excited state. When the energy gap between the states Δ, is much greater than kT only a small proportion of atoms can be in the excited state and hence the term is very small.

Pauli, or free electron, paramagnetism is found in metals and is due to conduction electrons 'flipping' their spins to align with the applied field. This effect is small due to the fact that only electrons within kT of the Fermi surface can make such a transition.

1.4 Ferromagnetism

Certain materials, for example the transition metals iron, cobalt and nickel, exhibit a large, positive value of K which is both field and temperature dependant. These materials are also observed to saturate magnetically in low fields of the order of 10^{-4} to 10^{-1} Tesla, and this saturation magnetisation is also temperature dependant. Above certain temperature T_c, the Curie temperature, this behaviour disappears and the

materials become normal paramagnets.

These characteristics can be explained by extending the Curie-Weiss Law and assuming that below Tc there exists a spontaneous Weiss molecular field. Then, using equation (1.12), when there is no applied field we have

$$\underline{H}_{eff}(T) = N_W \underline{M}(T) \qquad T < T_C$$

For a paramagnetic material, using the Brillouin treatment

$$\underline{M}(T) = \underline{M}(o) B_J(\alpha) \tag{1.13}$$

where $\alpha = g_J \mu_B \dfrac{\mu_o \underline{H}_{eff}}{k T}$

$$\underline{M}(T) = \left(\frac{g_J \mu_B \mu_o N_W}{kT}\right)^{-1}$$

$$= \frac{kT}{g_J \mu_B \mu_o N_W} \alpha \tag{1.14}$$

In theory we can plot $\underline{M}(T)$ as a function of α for equations (1.13) and (1.14). Provided Nw is large enough we will have a stable intercept as illustrated in Figure 1.2.

Experimentally it is found that the value of the molecular field is of the order of 10^3 Tesla. This large internal field cannot be due to a dipole-dipole type of interaction between the elemental magnetic moments as this would only give a field of the order of 10^{-1} Tesla. Heisenberg suggested that the internal field causing the alignment of the moments is a quantum mechanical exchange force. The exchange potential between two atoms having spins $\underline{S}_i$ and $\underline{S}_j$ is

$$W_{ij} = -2 \mathcal{J} \underline{S}_i \cdot \underline{S}_j \tag{1.15}$$

where $\mathcal{J}$ is the exchange integral. It is clear from equation (1.15) that if $\mathcal{J}$ is positive then the lowest energy configuration is one in which $\underline{S}_i$ and $\underline{S}_j$ are aligned parallel.

As this thesis deals with ferromagnetic properties, ferromagnetism will be discussed in greater detail in Chapter 2.

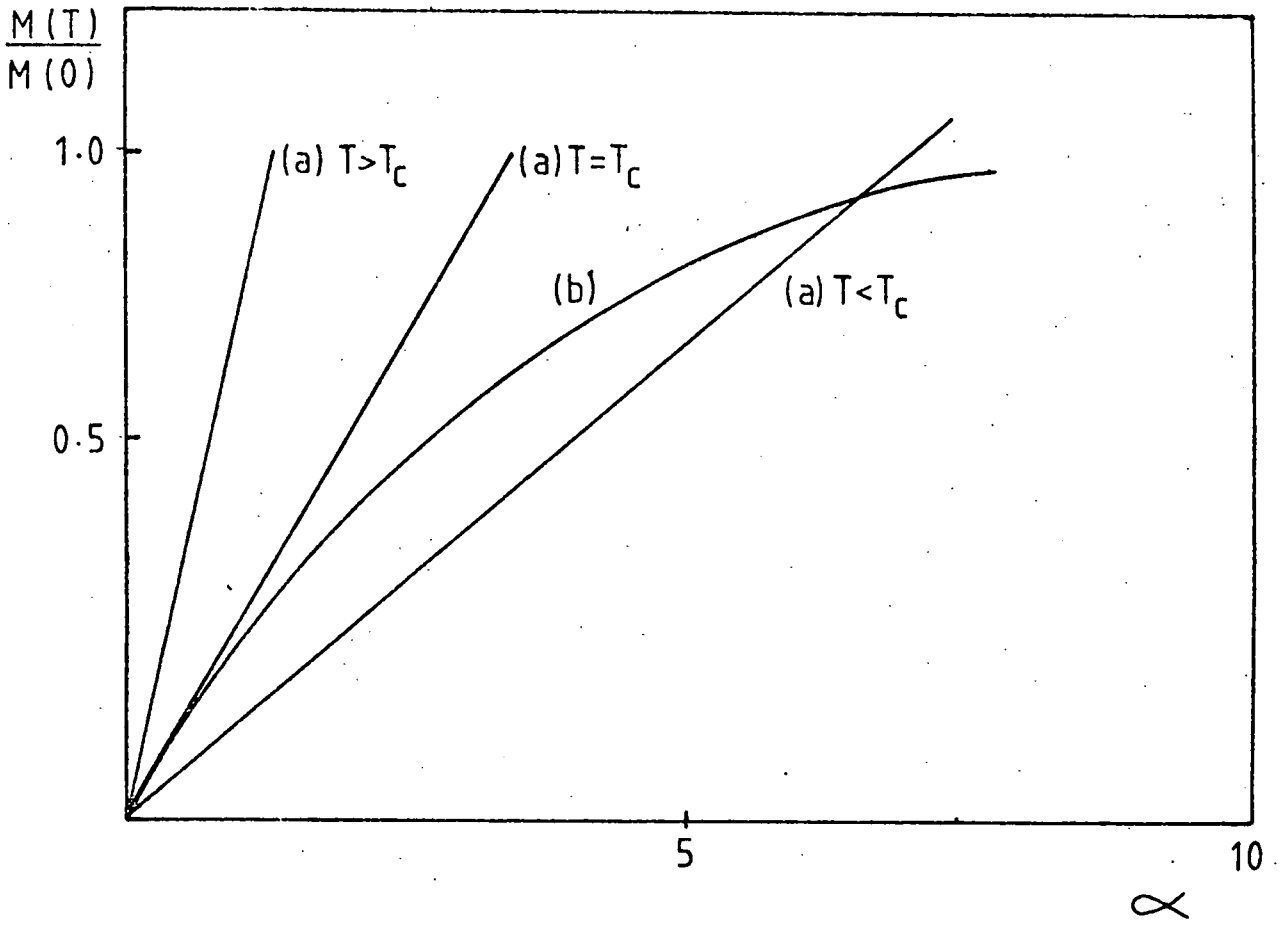

FIGURE 1.2 Condition For Spontaneous Magnetization

(a) $M(T) = \frac{kT}{g J \mu_B N_W} \propto$ for large N_W or small T

(b) $M(T) = M(0)\, B_J(\propto)$

1.5 Ferrimagnetism

In many materials which show ferromagnetic behaviour the saturation magnetisation at $T=0^{o}K$ does not correspond to parallel alignment of the constituent ions. The best known example is magnetite $Fe_3\ O_4$ which is composed of two types of Fe ions, Fe^{3+} and Fe^{2+}, whose total contribution to the magnetic moment should be $14\mu_B$. The observed value is $4.1\mu_B$. This discrepancy can be accounted for by assuming that the Fe^{3+} ions split into two groups aligned antiparallel to each other while the Fe^{2+} align parallel to one group giving a net magnetic moment. Neutron diffraction studies agree with this model.

In general for ferrimagnetic materials we have two, or more, lattice sites on which magnetic ions sit. The moments on equivalent sites order parallel to each other and antiparallel to the moments on the adjacent sites. This is illustrated schematically in Figure 1.3 for magnetite which has the inverse spinel structure. From equation (1.15) we can conclude that $\mathcal{J}$ is positive for the ions on similar sites ($\mathcal{J}_{AA}$ and $\mathcal{J}_{BB}$) and negative for the interaction between ions on different sites ($\mathcal{J}_{AB}$). In fact for magnetite it is believed that all the ions prefer antiparallel alignment but the $\mathcal{J}_{AB}$ interaction is the strongest and hence the minimum energy configuration gives the system shown in Figure 1.3. The curvature of the susceptibility against temperature curve, Figure 1.1., is characteristic of ferrimagnets and is accounted for by the interaction between different sites.

Ferrimagnets, including the commercially important ferrites, have many applications due to the fact that they have a high electrical resistivity. This reduces eddy current losses in alternating current components.

1.6 Antiferromagnetism

If we consider the case where we have negative exchange coupling between two equivalent lattice sites on which magnetic ions sit, then since

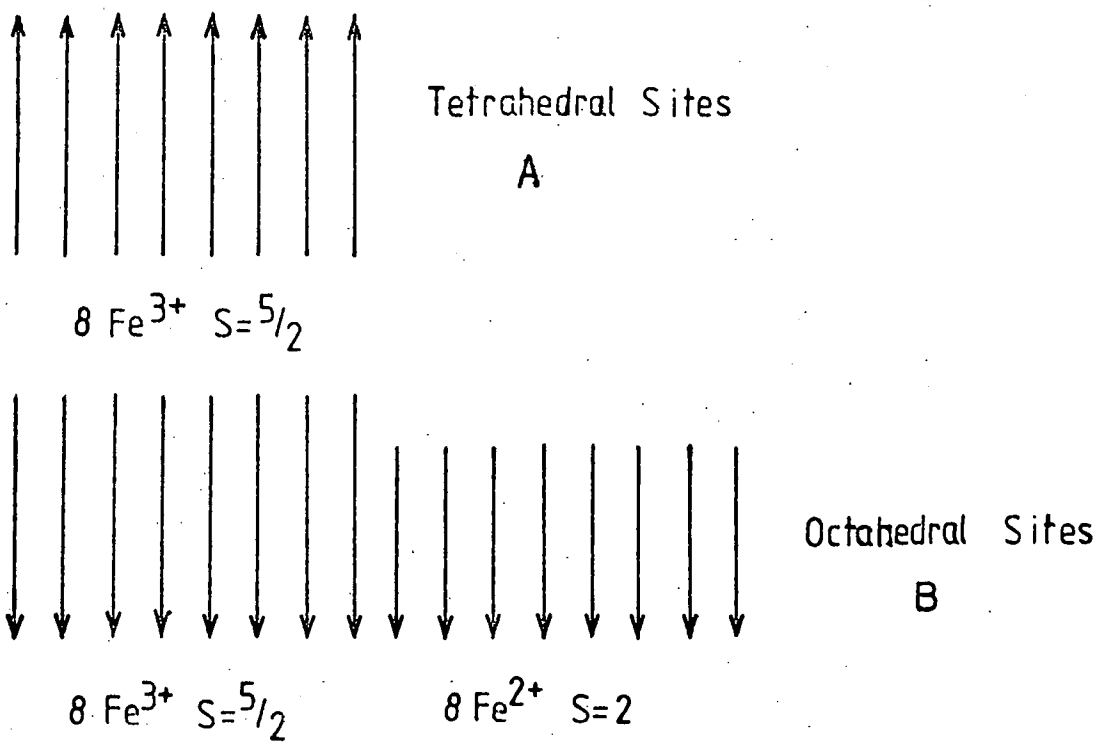

FIGURE 1.3 Ferrimagnetic Ordering in Fe_3O_4

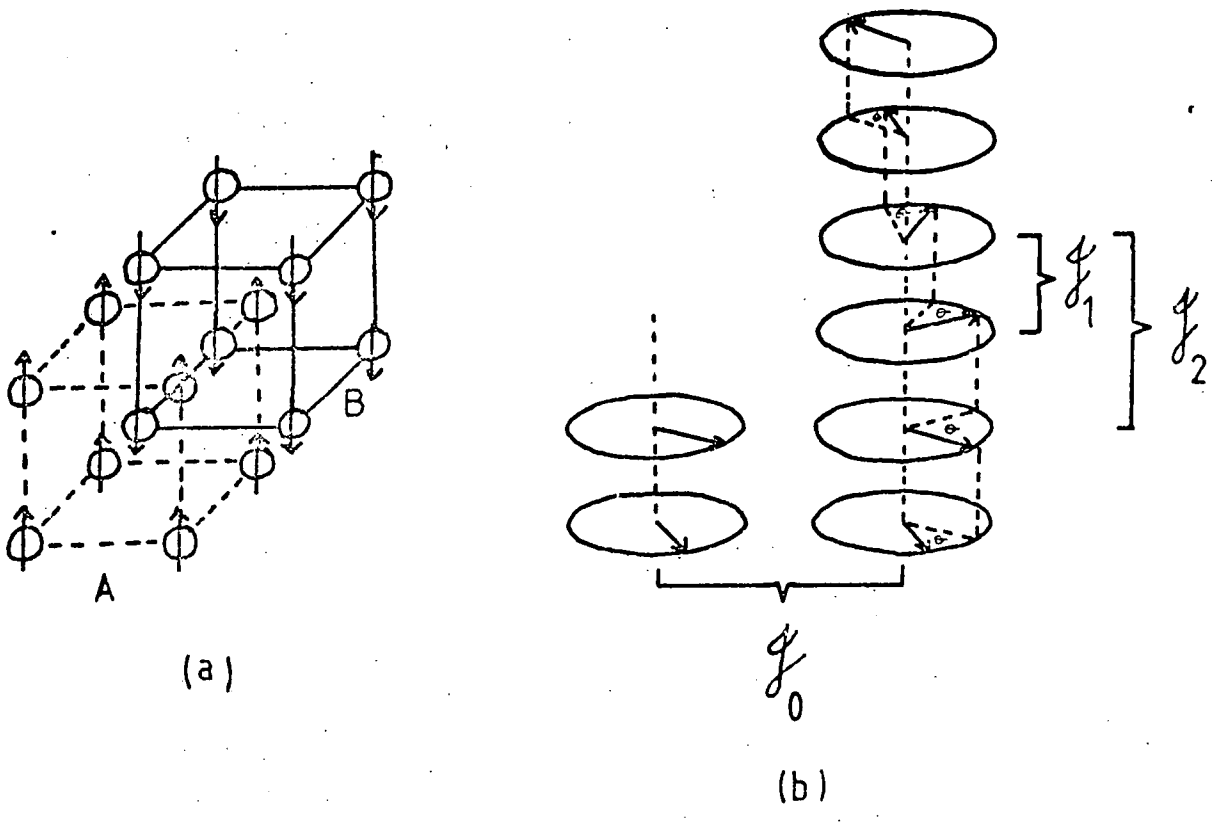

FIGURE 1.4 Types of Antiferromagnetic Ordering

the minimum energy according to equation (1.15) corresponds to antiparallel alignment, if the moments of the ions are equal there is no net magnetic moment. This phenomenon can occur in both elements, e.g. chromium below 475 K, and compounds, e.g. MnO in which antiferromagnetism was first observed. The arrangement of the spins in crystalline chromium is illustrated in Figure 1.4(a) where the body centred cubic strucutre is considered as two interlocking simple cubic lattices A and B. The negative exchange interaction between nearest neighbours gives rise to parallel alignment within the sublattices but antiparallel alignment with respect to each other. The temperature below which this type of alignment takes place is known as the Néel temperature, T_N. The Néel temperature is observed as a sharp discontinuity in the way in which the susceptibility varies with temperature (Figure 1.1). The behaviour of the susceptibility can be explained as follows. At low temperatures the exchange forces firmly hold the antiparallel spin alignment of the ions and the susceptibility is low ($\sim 10^{-4} - 10^{-3}$). As the temperature increases thermal agitation disturbs the ordering action of the exchange forces and the susceptibility rises. At the Néel temperature thermal agitation completely overcomes the exchange forces so above T_N we have normal paramagnetic behaviour. Some antiferromagnets also show a ferromagnetic phase at some temperature below T_N or above some critical value of applied field, H_c. This is known as a meta-magnetic transition.

As well as the simple arrangement of spins shown in Figure 1.4(a) some materials show complex types of antiferromagnetism. The most important of these in connection with this thesis is the type of spin structure known as helical antiferromagnetism which is exhibited by some of the rare earth elements. This type of structure may be accounted for by a simple model making use of three exchange interactions, as shown in Figure 1.4(b). The J_0 term indicates a ferromagnetic alignment within one plane of atoms. Perpendicular to this plane J_1 is the interaction between nearest

neighbours and $\mathcal{J}_2$ is the interaction between next nearest neighbours.

The arrangement is stable when

$$w = -2\,(\mathcal{J}_1\,\underline{S}_i \cdot \underline{S}_{i+1} + \mathcal{J}_2\,\underline{S}_i \cdot \underline{S}_{i+2}) \qquad (1.15)$$

is a minimum. Expressed in terms of the interplanar turn angle θ the quantity $\mathcal{J}_1 \cos\theta + \mathcal{J}_2 \cos 2\theta$ must be a minimum, which has the solution

$$\cos\theta = -\frac{\mathcal{J}_1}{4\mathcal{J}_2} \qquad (1.16)$$

For the helical structure to be stable

$$\left|\mathcal{J}_1\right| < \left|4\,\mathcal{J}_2\right|$$

and $\mathcal{J}_1$, $\mathcal{J}_2$ must be of opposite sign.

CHAPTER TWO

Ferromagnetism

2.1 The Origin of the Weiss Molecular Field and the Exchange Energy

The fundamental origin of the Weiss molecular field was first treated by Heisenberg (1928) in terms of an exchange interaction between the elemental magnetic moments. He assumed that the magnetic moment was due entirely to the spin of the electron. Experiments to determine the gyromagnetic ratio of ferromagnetic metals, using the Einstein-de Haas effect, gave foundation to this assumption. Subsequent experiments have shown that about 90% of the saturation magnetization of the 3d transition metals is due to the electron spin in incomplete shells. Heisenberg used the Heitler-London treatment of the hydrogen molecule, only the essentials of which will be presented here, as the basis for his theory.

Let $\phi_a(1)$, $\phi_b(2)$ be the wave functions for two separate hydrogen atoms, each in its lowest energy state. Applying the Schrodinger equation shows that there are two states for the composite system, a symmetrical combination of the functions $(\phi_a(1)\,\phi_b(2) + \phi_a(2)\phi_b(1))$ and an antisymmetrical combination $(\phi_a(1)\phi_b(2)-\phi_a(2)\,\phi_b(1))$, the energies of which differ by an amount dependant upon the internuclear distance. The energy values may be written as

$$E = 2\varepsilon_o \pm \mathcal{J}_o \qquad (2.1)$$

ε_o is the energy of the unperturbed separate atoms and also the energy associated with the Coulombian attractions and repulsions, and

$$\mathcal{J}_o = \iint \phi_a^*(1)\phi_b^*(2)\, V_{ab}\, \phi_a(2)\phi_b(1)\, dV_1\, dV_2 \qquad (2.2)$$

where

$$V_{ab} = \frac{e^2}{2}\left(\frac{2}{r_{ab}} + \frac{2}{r_{12}} - \frac{1}{r_{a1}} - \frac{1}{r_{b2}} - \frac{1}{r_{a2}} - \frac{1}{r_{b1}} \right)$$

in an obvious notation. The Pauli exclusion principle states that no two electrons can be in exactly the same state or, alternatively, the total wave function, including the spin state, of the electron must be anti-symmetrical. The positive sign in equation (2.1) corresponds to the singlet state, i.e. to the antisymmetrical spatial wave function and hence the spins must be antiparallel to give a total antisymmetrical wave function. For an antiparallel spin system $\mathcal{J}_o$ is negative and hence the singlet state has the lowest total energy. This is the case in the hydrogen molecule. If $\mathcal{J}_o$ is positive the triplet (antisymmetrical) state has the lowest energy, i.e. the ground state is the state in which the electrons have their spins aligned parallel. To explain ferromagnetism therefore we have to look for situations in which $\mathcal{J}_o$ can be positive.

If the wave functions ϕ_a and ϕ_b have no nodes in the region of appreciable overlap, so that $\phi_a^*(1)\,\phi_b^*(2)\,\phi_a(2)\,\phi_b(1)$ is positive, then $\mathcal{J}_o$ will be positive if the positive terms in V_{ab} exceed the negative terms. This is favoured by the wave functions being small in the neighbourhood of the nuclei and large in those regions for which r_{12} is small, i.e. midway between the atoms. Providing the inter nuclear distance is not large these theoretical considerations seem to favour d and f functions. It is therefore likely that ferromagnetism will occur in materials where there are incomplete d or f sub-shells whose diameter is less than the internuclear distance. This is illustrated schematically in Figure 2.1, where r_{al} refers to 3d electrons except in the case of gadolinium (Gd.) when it refers to the 4f electrons. The critical value of r_{ab}/r_{al} appears to be about 1.5 and although manganese (Mn) is not ferromagnetic at room temperature some of its compounds, e.g. MnAs and MnSb, which have larger lattice spacings, are ferromagnetic. This is good evidence that the above treatment is substantially correct, but some problems that arise will now be briefly discussed.

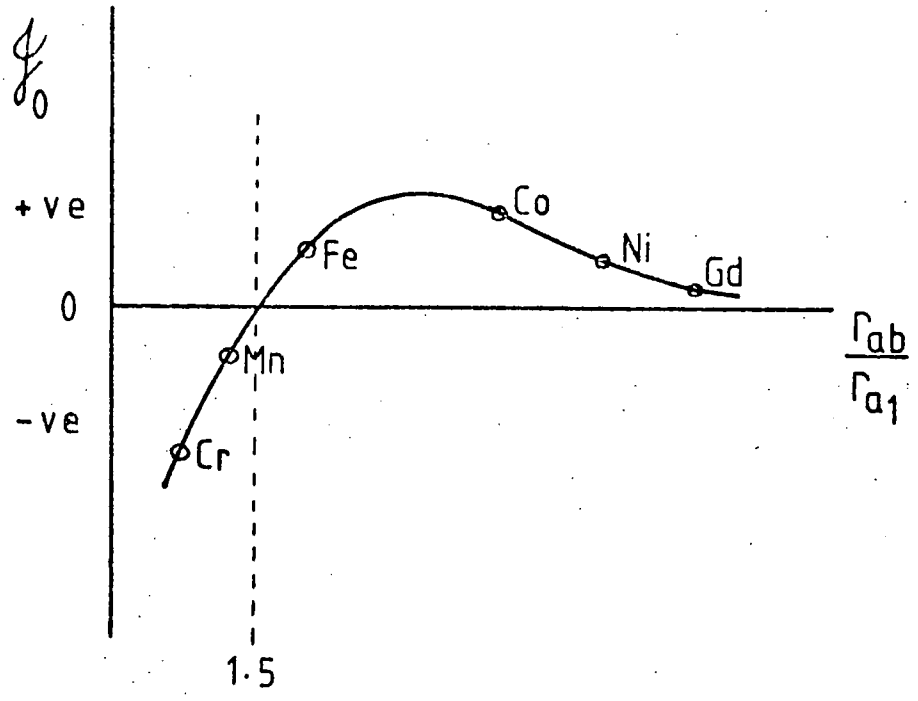

FIGURE 2.1 Variation of the Exchange Integral with Ratio of Nuclear Separation to Radius of Incomplete Shell

In Figure 2.1 we assume that the 3d electrons, in the case of the transition metals, are localised but when the solid is treated as a whole we find that the 4s and 3d wave functions overlap to form two overlapping energy bands. The wave functions of these electrons are then Bloch functions and the electrons are free to move throughout the solid. Stoner (1938) introduced a theory known as collective electron ferromagnetism which extended the initial calculations of Slater (1936) on the effect of the band structure on ferromagnetism. Essentially the 3d and 4s bands are split into 'spin-up' and 'spin down' sub-bands. The exchange interaction between electrons may be represented by a molecular field. This introduces a difference in the energy of the spin sub-bands and hence there will be a net magnetization. The molecular field acts only between electrons in the 3d band. The calculations on such a theory give good agreement with experiment, in particular the prediction of non-integral numbers of spin carriers due to the overlap of the 4s and 3d bands. Unfortunately, whereas the collective electron theory produces good results for nickel, the Heisenberg theory is better for iron.

Another theory that has been put forward on the nature of ferromagnetism involves s-d or s-f exchange. Here the d or f shells are localised at the atoms and the s(conduction) electrons are mobile. The conduction electrons are polarized by interacting with one magnetic ion then carrying its spin orientation to the next ion. The s-f interaction seems to be dominant in the rare earth metals and is known as the RKKY interaction which will be treated in greater detail later.

Whatever the origin of the exchange interation the effective coupling is equivalent to a potential energy of the form

$$V_{ij} = - 2 J_{ij} \underline{S}_i \cdot \underline{S}_j \qquad (2.3)$$

where J_{ij} is the exchange integral connecting the total spins $\underline{S}$ on atoms i and j. If we only consider the spin of a given atom and that of its

nearest neighbour, the exchange energy becomes

$$W_{ij} = -2JS^2 \sum \cos \phi_{ij} \qquad (2.4)$$

where ϕ_{ij} is the angle between the direction of the spin vectors. Assuming neighbouring spins make a small angle with each other, the exchange energy between each pair of spins is

$$W_{ij} \simeq JS^2 \phi^2 \qquad (2.5)$$

Landau and Lifshitz (1935) derived an expression of the form

$$E_{ex} = \frac{2JS^2}{a} \int [(\nabla \alpha_1)^2 + (\nabla \alpha_2)^2 + (\nabla \alpha_3)^2] dV \qquad (2.6)$$

where the α's are direction cosines and a is the lattice constant. The quantity $\frac{2JS^2}{a}$ is known as the exchange constant A and may be determined by a number of methods including ferromagnetic resonance and spin wave experiments. A simple estimate can be obtained in two ways:

a) At T_C the thermal energy becomes approximately equal to the exchange energy, therefore

$$k T_C \simeq 2JS^2 \qquad (2.6)$$

b) At low temperatures, the magnetization behaves as (Bloch (1930))

$$M = M_S (1 - CT^{3/2}) \qquad (2.7)$$

and C is directly related to the exchange constant.

These two methods are approximate and do not always agree on the value of A for a given ferromagnet.

2.2 Magnetostatic Energy

A uniformly magnetized body in an applied magnetic field has a potential energy of

$$E_s = -\mu_o \underline{H} \cdot \underline{M} \qquad (2.8)$$

The total energy of the magnetized body per unit volume is then

$$E_T = E_I - \mu_o \underline{H} \cdot \underline{M}$$

where E_I is the internal energy due to magnetocrystalline anisotropy,

magnetostriction, exchange energy and energy due to free poles. Now $\underline{H}$ is not in general equal to the applied field, $\underline{H}app$, because of the degmagnetizing field, $\underline{H}_D$, of the body. This demagnetizing field is present even when there is no applied field and is due to the dipole field of the magnetic body.

$$\underline{H}_D = - N \underline{M} \tag{2.9}$$

N is the demagnetizing factor and is determined by the geometry of the body. The self energy of the body due to the interaction of the free pole and the demagnetizing field is then

$$\begin{aligned} E_D &= {}^1/_2 \quad \underline{H}_D \cdot \underline{M} \\ &= {}^1/_2 \quad N M^2 \end{aligned} \tag{2.10}$$

The factor of 1/2 is introduced so that each dipole is not introduced twice.

Demagnetizing factors (N_a, N_b and N_c) for ellipsoids have been calculated by Stoner (1945) and Osborne (1945), as these shapes have uniform magnetization, with reference to the major semi-axes, a, b and c. It was found that

$$N_a + N_b + N_c = 1$$

and

$$N = N_a \alpha_1^2 + N_b \alpha_2^2 + N_c \alpha_3^2 \tag{2.11}$$

where the α's are the direction cosines of the magnetization with respect to the major semi-axes. For a sphere, $N_a = N_b = N_c = 1/3$, and for a disc the demagnetizing factor parallel to the plane of the disc is

$$N_a = N_b = \frac{1}{2}\left[\frac{k^2}{(k^2-1)^{3/2}} \sin^{-1}\frac{\sqrt{k^2-1}}{k} - \frac{1}{k^2-1} \right] \tag{2.12}$$

where k is the ratio of the diameter to the thickness.

2.3 Anisotropy Energy

When the magnetization is measured as a function of magnetic field it is found that it is 'easier' to saturate the sample in certain directions than in others. These directions are known as 'easy' directions with respect to other 'hard' directions where a larger applied field is required

to produce saturation. The difference in energy required to magnetize a sample along a hard direction with respect to an easy direction is known as the anisotropy energy, E_A.

2.3.1 Magnetocrystalline Anisotropy

This is an anisotropy due to the symmetry of the crystal lattice and is therefore observed in pure crystals and orientated polycrystals. The simplest form of magneto-crystalline anisotropy is uniaxial anisotropy. In this case one particular crystallographic direction is easy with all other directions being hard. This is often found in hexagonal crystals with the C axis usually being easy. Cubic materials are more complex due to the existence of equivalent directions, such as<100>, <110> or <111>, in the crystal which may be easy or hard with respect to each other. Magnetocrystalline anisotropy will be discussed in detail in Chapter 4.

2.3.2 Shape Anisotropy

If we consider equations (2.10) and (2.11) it is apparent that if $N_a \neq N_b \neq N_c$ different amounts of energy will be required to magnetize the sample along a, b, and c directions. As the N's are geometric factors they depend on the shape of the body to be magnetized and hence we have a shape anisotropy. As indicated above the N's can only be calculated exactly for certain shapes.

2.3.3 Magnetostrictive Anisotropy

Magnetic anistotropy can be produced by applying mechanical stress to the material. This type of anisotropy can be induced in a number of ways, for example, by heat treating the material or introducing strain in the growth process of single crystals. Growth induced anisotropy is used to produce uniaxial anisotropy perpendicular to the plane of thin films to overcome the shape anisotropy which favours the plane of the film being easy. Such thin films are used in magnetic bubble devices.

2.4 Magnetostriction and Magnetoelastic Energy

It is found experimentally that when ferromagnetic materials are magnetized they undergo small changes in their dimensions. This is called magnetostriction. Two types of magnetostriction are involved in the magnetization process. An anisotropic magnetostriction is associated with the process up to the state of technical saturation and beyond this point an isotropic volume magnetostriction occurs. The anisotropic magnetostriction is closely linked with the magnetocrystalline anisotropy. We denote the deformation in a particular direction by $\lambda = dl/l$, and if there is also a tensile stress σ present then the magnetoelastic energy is given by

$$E_\sigma = -\frac{3}{2} \lambda \sigma \cos^2 \theta \qquad (2.13)$$

where θ is the angle between the stress direction and the magnetization. Comprehensive reviews of magnetostriction have been given by Lee (1955) and Birss (1959).

2.5 The Magnetization Process and the Domain Hypothesis

A typical magnetization curve for a ferromagnet is shown in Figure 2.2. It was the fact that a ferromagnet could exist in a demagnetized state that presented an early problem to the Weiss molecular field theory. Further problems arose from the existence of hysteresis in the cyclic magnetization leading to a remanent magnetization, M_r, and coercive field, B_c. The saturation magnetization, M_s, is produced when the applied magnetic field B_o is sufficient to align all the elemental moments.

Weiss (1907) was the first to suggest that ferromagnets are subdivided into small regions which are each magnetized to saturation by the internal molecular field. Because these regions are magnetized in different directions the net magnetization can be zero. This hypothesis has subsequently been confirmed experimentally and the regions of

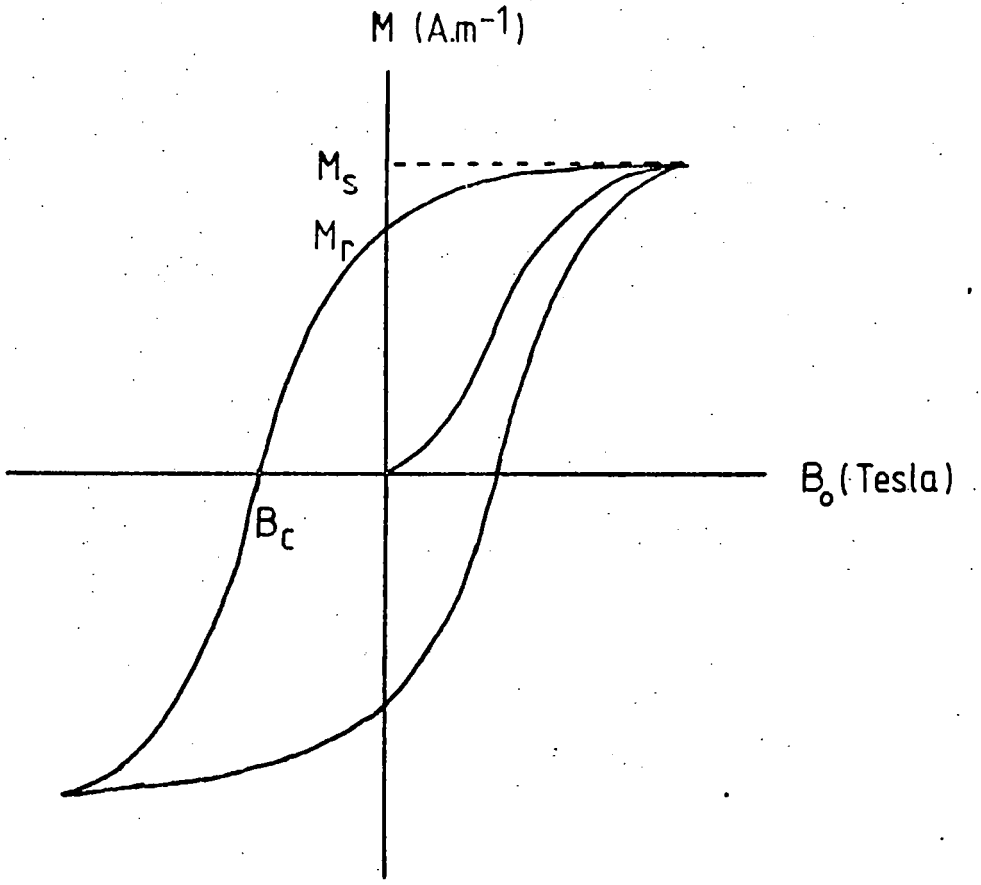

FIGURE 2.2 A Typical Magnetization Curve

magnetization have become known as magnetic domains. The domain hypothesis also leads to an explanation of the magnetic hysteresis curve. If an external magnetic field is applied to a demagnetized sample then initially there is a growth of domains preferentially orientated with respect to the applied field. For small displacements such changes are reversible and the initial part of the magnetization curve shows no hysteresis. As the applied field is increased the preferred domains grow rapidly and also some rotation of the magnetization within other domains can take place until the state of saturation is reached. When the applied field is reduced various conditions within the ferromagnet, such as crystal defects, grain boundaries or inclusions, prevent the domains returning to their original state. This produces a remanent magnetization and also gives rise to the coercive field, which is the reverse field required to produce a new equilibrium state where the magnetizations of the domains again cancel. The theory of magnetic domains will be discussed in Chapter 6.

In technology ferromagnets are broadly classified into soft and hard materials. Basically, soft materials have a small remanent magnetization and coercive field and therefore a narrow hysteresis loop. As the area contained by the hysteresis loop represents the energy disipated in a magnetization cycle, soft magnetic materials are used in applications such as transformer cores. Hard materials have high remanent magnetization and coercive fields and are used for permanent magnets. Reviews of the basic properties of soft and hard magnetic materials were given by Lee (1959) and Wohlfarth (1959) respectively.

2.6. Micromagnetics

In the present chapter the basic energy contributions to ferromagnetism have been discussed. We are therefore in a position to write an equation for the total energy of a ferromagnet.

$$E_T = E_S + E_D + E_A + E_\sigma + E_{ex} + E_o \qquad (2.14)$$

where the E's are defined above and E_o represents any other contributions

to the total energy. For a particular ferromagnetic specimen we can, in theory predict its magnetic state by determing the minimum free energy. The process is known as micromagnetics (Brown (1963)). Such calculations in practice are extremely difficult but micromagnetics can be useful in certain cases. Even a simple calculation leads naturally to the formation of a magnetic domain structure where a large magnetostatic energy can be reduced dramatically with only small increases in other energy contributions, essentially E_k and E_{ex}.

CHAPTER THREE

The Rare Earth Metals

3.1 General Properties

There are fifteen rare earth elements; the first is Lanthanum (atomic number 57) and the series progresses to lutetium (atomic number 71). These elements are also often known as the lanthanides after the first member. All these elements show very similar chemical properties, which are also shared by the elements scandium (atomic number 21) and yttrium (atomic number 39). These two elements are often included in discussions on the rare earths. The rare earths, scandium and yttrium are members of group IIIa of the periodic table. Due to the similarity of their chemical properties extracting the rare earths in a pure form was very difficult before the development of the ion-exchange method. Preparation of pure single crystals for experimental work has also been a problem with the rare earths maninly due to their affinity for the gases oxygen, hydrogen and helium. The first single crystals were produced in the early 1960's at the Ames Laboratory U.S.A. Recent techniques for producing good quality crystals have been reviewed by McEwen and Touborg (1973), Jordan (1974) and Jones et al (1977).

The common chemical properties of the rare earths are due to their electronic structure which has the form

$$(1s^2\ 2s^2\ 2p^6\ 3s^2\ 3p^6\ 3d^{10}\ 4s^2\ 4p^6\ 4d^{10})4f^n(5s^2\ 5p^6)\ 5d^{(1)}6s^2$$

This is a xenon core (in brackets) with the addition of 4f and 6s electrons, and in some cases a 5d electron. The 5d electron (if present) or a 4f electron and the two 6s electrons usually form the conduction electrons to give a normal valancy of 3. There are exceptions to this and these are noted in Table 3.1 which gives an outline of the electronic and structural properties of the rare earths and also scandium and yttrium. In all the

The Rare Earth Metals, Scandium and Yttrium,
General Data

Element		Z	Atomic volume cm^3/mole	Crystal structure	Electronic structure of the neutral atom	Normal valency	Normal ion	Lattice Parameters: hcp and d-hex 'c' nm	hcp and d-hex 'a' nm	hcp and d-hex c/a or c/2a	fcc 'a' nm	bcc 'a' nm	Transition temperatures: fcc above °C	Transition temperatures: bcc above °C	Radius of atom in metal nm	Radius of 3+ ion nm	Density gm cm^{-3}	Melting point °C
Lanthanum	La	57	22.55	d-hex	(Xe) - $5d^1\ 6s^2$	3	(Xe)	1.2144	0.3772	1.61	0.530	0.426	310	861	0.1877	0.122	6.166	920
Cerium	Ce	58	20.69	fcc	$(Xe)4f^2$ - $6s^2$	3/4	$(Xe)[4f^1]$	1.1802	0.3675	1.607	0.516*	0.412	-70	762	0.1824	0.118	6.771	798
Praseodymium	Pr	59	20.81	d-hex	$(Xe)4f^3$ - $6s^2$	3	$(Xe)\ 4f^2$	1.1833	0.3672	1.611		0.413		795	0.1828	0.116	6.772	931
Neodymium	Nd	60	20.60	d-hex	$(Xe)4f^4$ - $6s^2$	3	$(Xe)\ 4f^3$	1.1799	0.3659	1.612		0.413		855	0.1822	0.115	7.003	1018
Promethium	Pm	61		d-hex	$(Xe)4f^5$ - $6s^2$	3	$(Xe)\ 4f^4$	1.165	0.365	1.60							7.26	
Samarium	Sm	62	19.95	Sm type	$(Xe)4f^6$ - $6s^2$	3	$(Xe)\ 4f^5$	2.6178	0.3626	1.605		0.407		924	0.1802	0.113	7.537	1072
Europium	Eu	63	28.95	bcc	$(Xe)4f^7$ - $6s^2$	2	$(Xe)\ 4f^7$	-	-			0.458		stable	0.1983	0.113	5.255	822
Gadolinium	Gd	64	19.91	hcp	$(Xe)4f^7\ 5d^1\ 6s^2$	3	$(Xe)\ 4f^7$	0.5781	0.3634	1.591		0.405		1260	0.1801	0.111	7.898	1311
Terbium	Tb	65	19.30	hcp	$(Xe)4f^9$ - $6s^2$	3	$(Xe)\ 4f^8$	0.5698	0.3604	1.581		0.402		1287	0.1783	0.109	8.234	1360
Dysprosium	Dy	66	19.03	hcp	$(Xe)4f^{10}$ - $6s^2$	3	$(Xe)\ 4f^9$	0.5655	0.3593	1.574		0.398		1384	0.1775	0.107	8.54	1409
Holmium	Ho	67	18.78	hcp	$(Xe)4f^{11}$ - $6s^2$	3	$(Xe)\ 4f^{10}$	0.5626	0.3578	1.572		0.396		1428	0.1767	0.105	8.781	1470
Erbium	Er	68	18.49	hcp	$(Xe)4f^{12}$ - $6s^2$	3	$(Xe)\ 4f^{11}$	0.5595	0.3560	1.572					0.1758	0.104	9.045	1522
Thulium	Tm	69	18.14	hcp	$(Xe)4f^{13}$ - $6s^2$	3	$(Xe)\ 4f^{12}$	0.5558	0.3537	1.571					0.1747	0.104	9.314	1545
Ytterbium	Yb	70	24.82	fcc	$(Xe)4f^{14}$ - $6s^2$	2	$(Xe)\ 4f^{14}$	-	-		0.5485	0.444		792	0.1938	0.100	6.972	824
Lutetium	Lu	71	17.79	hcp	$(Xe)4f^{14}\ 5d^1\ 6s^2$	3	$(Xe)\ 4f^{14}$	0.3553	0.3505	1.584					0.1735	0.099	9.835	1656
Scandium	Sc	21	15.04	hcp	(A) - $3d^1\ 4s^2$	3	(A)	0.5268	0.3309	1.592				1335	0.1641	0.081	2.989	1539
Yttrium	Y	39	19.95	hcp	(Kr) - $4d^1\ 5s^2$	3	(Kr)	0.5741	0.3650	1.575		0.408		1479	0.1803	0.106	4.457	1523

* Ce has another fcc phase below 77K (approximately) with a = 0.485 nm

TABLE 3.1 (AFTER WELFORD(1974))

ions the outermost electrons are the two 5s and six 5p electrons. The rare earths conveniently split up into two groups, the light rare earths (La to Eu) with the 4f shell having zero to seven electrons and the heavy earths (Gd to Lu) with seven to fourteen 4f electrons.

The atomic radius of the rare earths in metallic form shows a linear decrease as we proceed through the series from lanthanum to lutetium. This is known as the lanthanide contraction and can be explained in terms of the increase in nuclear charge not being effectively screened by the increase in the number of 4f electrons. Most of the rare earths crystallize in the hexagonal close packed structure, the double hexagonal close packed, d.h.c.p., for the light elements (exceptions are Ce, Sm and Eu) and the simple hexagonal close packed, h.c.p., for the heavy elements (the exception is Yb). The h.c.p. structure is illustrated in Figure 3.1 with the notation used for describing directions and planes in the crystal lattice

The physical properties of gadolinium will be discussed in section 3.3. The reader is referred to Taylor (1970) and Taylor and Darby (1972) for a dicussion of the general properties of all the rare earth elements.

3.2 Magnetic Properties

Since Urbain et al (1935) discovered that gadolinium is ferromagnetic the magnetic properties of the rare earths have been intensively studied. They have been found to exhibit a wide variety of magnetic behaviour. The basic magnetic properties common to all the rare earths and the properties of gadolinium in detail will be discussed here. For a study of each element the following books and review articles can be referred to: Cooper (1968), Elliott (1972), Taylor and Darby (1972) and Coqblin (1977) Rhyne and McGuire (1972) gave a review of the magnetic properties of the rare earth elements, alloys and compounds. Taylor (1971) has reviewed intermetallic rare earth compounds.

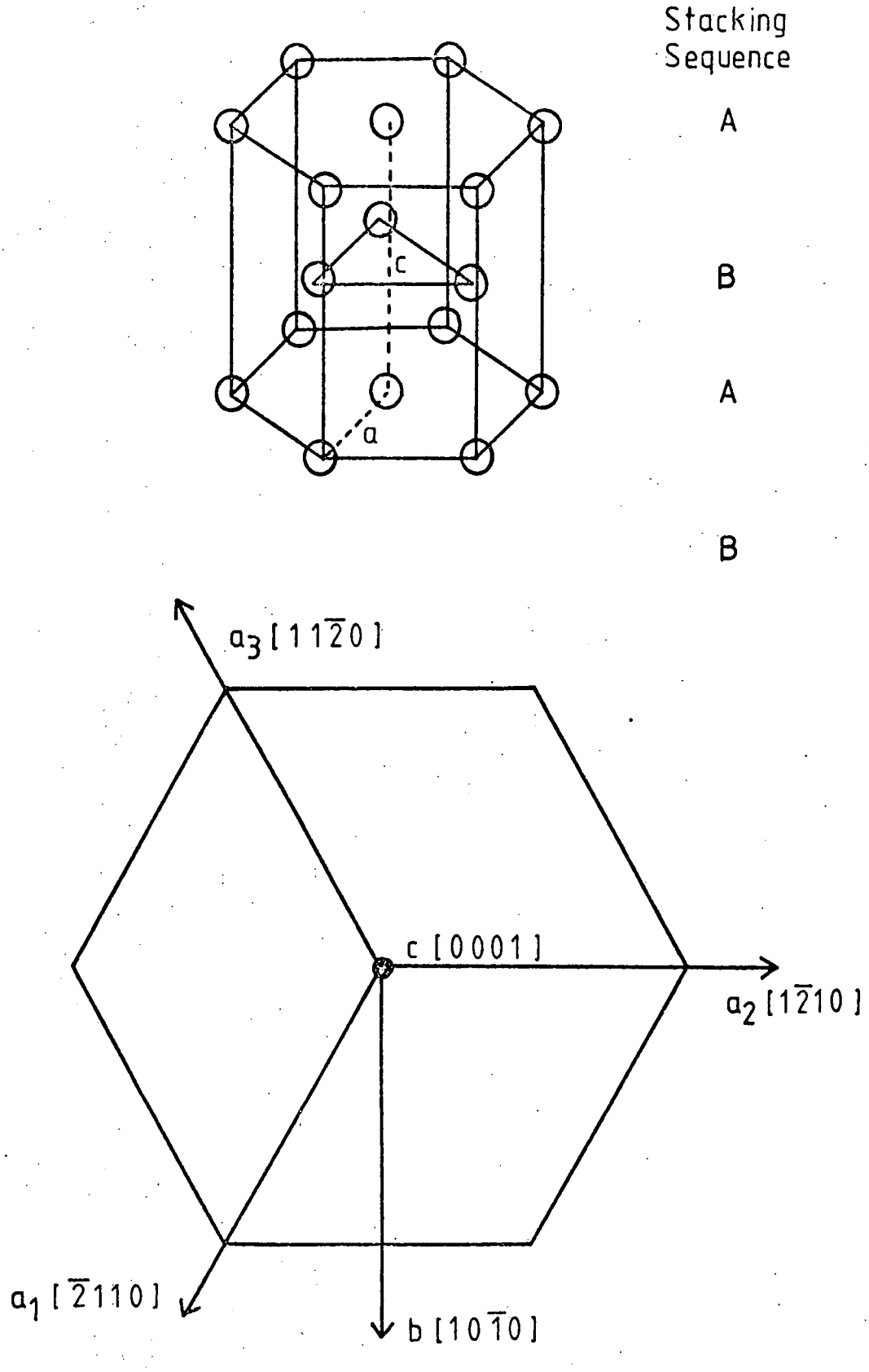

FIGURE 3.1 The Hexagonal Close Packed Structure (h.c.p.)

The magnetic properties of the rare earths arise from the highly localised incomplete 4f shell. The filling of the 4f shell is in accordance with Hund's Rules which state;

a) The electron spin moments (S) are arranged to give a maximum total moment ($S = \sum s$) consistent with the Pauli exclusion principle.

b) The orbital moments align to give a maximum angular moment L consistent with (a).

c) The total angular moment J is given by

$J = L - S$ for a less than half-full shell

$J = L + S$ for a more than half-full shell

Using equation (1.11) we can calculate the effective number of Bohr magnetons, P_{eff}, and hence the paramagnetic susceptibility for the rare earth ions. The values of S, L, J and μ are given in Table 3.2 for the trivalent ions. For most of the rare earths, the magnetic moment of the metal is very close to the theoretical value of the trivalent ion. The small discrepancies are accounted for by conduction electron polarization. This is important when considering the exchange interaction. The large discrepancies in the case of Eu^{3+} and Sm^{3+} can be understood in terms of the excitation process proposed by Van Vleck and Frank (1929) where the ground and 1st excited state are mixed at room temperature. Ytterbium is not magnetic as it has a closed 4f shell with a valency of 2. Europium shows a moment that is close to the predicted value for the Eu^{2+} ion when in the metallic state.

All the rare earths, except Lanthanium, ytterbium and lutetium, show some sort of magnetic ordering at low temperatures and of these only gadolinium does not have an antiferromagnetic phase. The types of ordering are given in Table 3.3 for the heavy rare earths. Figure 3.2. gives a schematic representation of the types of ordering noted in Table 3.3. These magnetic structures have been established mainly through neutron diffraction techniques, notably at the Oak Ridge Laboratory, Tennesse, U.S.A.

Magnetic moments of rare earth metals

	La	Ce	Pr	Nd	Pm	Sm	Eu	Gd	Tb	Dy	Ho	Er	Tm	Yb	Lu
S	0	1/2	1	3/2	2	5/2	3	7/2	3	5/2	2	3/2	1	1/2	0
L	0	3	5	6	6	5	3	0	3	5	6	6	5	3	0
J	0	5/2	4	9/2	4	5/2	0	7/2	6	15/2	8	15/2	6	7/2	0
Theoretical magnetic moment at 0 K (eqn 1.51)	0	2.54	3.58	3.62	2.68	0.84	0	7.94	9.7	10.6	10.6	9.6	7.6	4.5	0
Theoretical magnetic moment at room temperature (from Van Vleck and Franck)	0	2.56	3.62	3.68	2.83	1.60	3.45	7.94	9.7	10.6	10.6	9.6	7.6	4.5	0
Experimental magnetic moment	0	Ce_{γ}^{β}: 2.51 Ce α: 0	3.56	3.3	—	1.74	7.12	7.95	9.7	10.64	10.89	9.5	7.62	0	0

TABLE 3.2 (AFTER COQBLIN(1977))

Summary of the magnetic structures of heavy rare earth metals. The different notations of the table are: (1) Metal. (2) Paramagnetic Curie temperature of polycrystals. (3) Paramagnetic Curie temperature of single crystals with the magnetic field applied along the $\vec{c}$-axis. (4) Paramagnetic Curie temperature of single crystals with the magnetic field in the basal plane. (5) Temperatures of the specific heat anomalies. (6) Neel temperature. (7) Structure below the Neel temperature. (8) Intermediate ordering temperature T_H (for Erbium only). (9) Structure below T_H (for Erbium only). (10) Ferromagnetic Curie temperature. (11) Structure below the Curie temperature. (12) Saturation magnetization parallel to the easy magnetization axis (in μ_B). (13) Theoretical values of the magnetic moment for the trivalent rare earths ion (in μ_B).

(1) Metal	(2) θ_p(K)	(3) $\theta_\parallel$(K)	(4) $\theta_\perp$(K)	(5) T_λ(K)	(6) T_N(K)	(7) Structure	(8) T_H(K)	(9) Structure	(10) T_c(K)	(11) Structure $T = 4.2$ K	(12) μ_{sat} (μ_B)	(13) $g_J J$ (μ_B)
Gd	317	317	317	291.8	$T_N = T_C$ 293.2	Ferromagnetic (g): ($\vec{\mu}$, $\vec{c}$) angle variable with T					7.55	7.0
Tb	237	195	239	227.7 221	229	Helix (e): $\vec{\mu}\perp\vec{c}$ $\omega_i = 20.5°$ $\omega_{f'} = 18°$			221	Ferro (f): $\vec{\mu}\perp\vec{c}$	9.34	9
Dy	153	121	169	174 83.5	179	Helix (e): $\vec{\mu}\perp\vec{c}$ $\omega_i = 43°$ $\omega_{f'} = 26.5°$			87	Ferro (f): $\vec{\mu}\perp\vec{c}$	10.2	10
Ho	87	73	88	131.6 19.4	133	Helix (e): $\vec{\mu}\perp\vec{c}$ $\omega_i = 51°$ $\omega_{f'} = 33°$			20	Cone (d) $\omega = 30°$ $\omega_f = 30°$	10.34	10
Er	40	61.7	32.5	84 53.5 19.9	80	$\vec{c}$-axis modulated with occurrence of harmonics. $\vec{\mu} \parallel \vec{c}$ (b). $\omega_i = 51.4°$	$T_H = 53$ $\omega = 51.4$	$\vec{c}$-axis modulated with occurrence of harmonics. Helix for $\mu_\perp(c)$. $\omega_{f'} = 45°$	20	Cone (d) $\omega = 45°$ $\omega_f = 45°$	8	9
Tm	20			55	56	$\vec{c}$-axis modulated: $\vec{\mu} \parallel \vec{c}$($b$) $\omega_i = 51.4°$ $\omega_{f'} = 51.4°$			38	Antiphase Ferro. 3–4 (a) $\omega_f = 51.4°$	3.4	7

TABLE 3.3 (AFTER COQBLIN(1977))

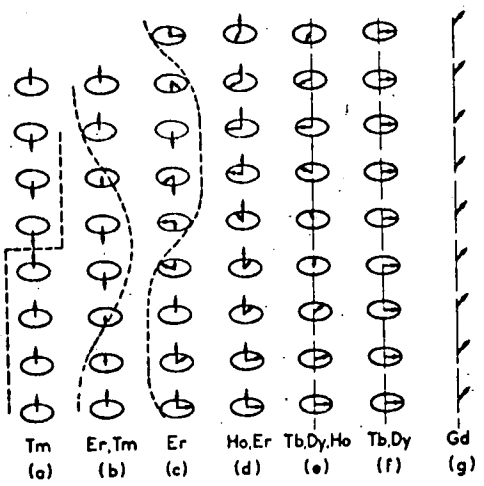

Schematic representation of the magnetic structures of heavy rare earth metals. The magnetic moments are assumed to be parallel to each other in a given hexagonal layer and the propagation axis is the $\vec{c}$-axis.

FIGURE 3.2 (AFTER COQBLIN(1977))

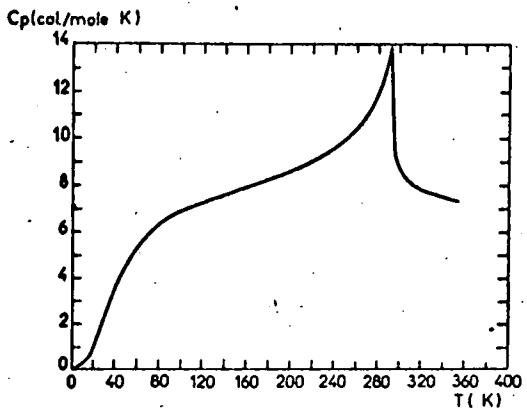

Thermal dependence of the specific heat of Gadolinium.

FIGURE 3.3 (AFTER GIFFEL et. al.(1954))

(Koehler 1972). The diverse and exotic structures are a result of the interplay of strong fundamental interactions which also manifest themselves in the large magnetocrystalline anisotropy (of the order of 10^6 J m^{-3}) and magnetostriction (of the order of 10^{-2}) found in the heavy rare earths.

3.3 Interactions Causing Magnetic Ordering

As the 4f shell is highly localised and well screened by the 5s 5p electrons there is little possibility of a direct Heisenberg type exchange interaction as described in section 2.1. To explain the magnetic structures observed in the rare earth metals the exchange interation must have the following properties. It must;

a) have a long range

b) vary in magnitude and decrease with separation

c) change sign between nearest and next nearest neighbour.

Such an interaction theory was developed by Rudermann and Kittel (1954), Kasuya (1956) and Yosida (1957) and has since become known as the R.K.K.Y. interaction. This theory assumes that the exchange coupling between the 4f orbitals is an indirect one which involves the polarization of the conduction electrons.

Phenomenologically we can write the interaction between the conduction electrons and the 4f shell (the s-f interaction) as

$$H_i = - \Gamma \, \underline{S} \cdot \underline{s} \qquad (3.1)$$

in analogy with equation (1.15) where S is the total spin of the 4f shell and s the spin of the conduction electron. Γ is the interaction constant dependent upon the separation of the ion and the conduction electron. The effect of the interaction is to favour conduction electrons with spin parallel to the ion. Such an electron will distort its wave function so it will be larger in the vicinity of the ion. This is brought about by a mixing of wave functions with spin parallel to the ion to interfere constructively about the ion. The result is as though only states above

the Fermi level are added and we have an electron polarization about the ion

$$P_i(\underline{r}) = \frac{9\pi Z^2 \Gamma}{4 V^2 E_F} S \cdot F(2\underline{k}_F \cdot \underline{r}) \qquad (3.2)$$

where Z is the number of conduction electrons

V is the atomic volume

E_F is the Fermi energy

$\underline{k}_F$ is the wave vector of the conduction electrons at the Fermi surface

Since the wave functions must correspond to a range of wavevectors and therefore a range of wavelengths they must begin to interfere destructively as the distance from the ion increases. An inverse process occurs with the antiparallel wavefunctions. $F(2\underline{k}_F \cdot \underline{r})$ is a function which describes the overall effect of the interference on the spin density distribution. The R.K.K.Y. interaction assumes a spherical Fermi Surface and free conduction electrons which leads to $F(2\underline{k}_F \cdot \underline{r}) \equiv F(x)$ having the form

$$F(x) = \frac{\sin x - x \cos x}{x^4} \qquad (3.3)$$

The interaction of the conduction electron polarization with a second ion has the same form as equation (3.1) and this leads to an interaction between the two ions of the form

$$H_{ij} = \frac{-9\pi Z^2 \Gamma^2}{4 V^2 E_F} \sum F(2\underline{k}_F \cdot \underline{r}_{ij}) \underline{S}_i \cdot \underline{S}_j \qquad (3.4)$$

A detailed review of this type of indirect exchange has been given by Kittel (1968). de Gennes (1962) showed that in order to take account of the spin-orbit coupling in the rare earths it is necessary to replace S_i and S_j by $(g-1)J_i$ and $(g-1)J_j$, the projections of the spins on the direction of J, the total angular momentum. Equation (3.4) then becomes

$$H_{ij} = -\mathcal{J}(g-1)^2 J(J+1) \qquad (3.5)$$

where $G = (g-1)^2 J(J+1)$ is known as the deGennes factor.

One of the most essential features of the R.K.K.Y. interaction is the polarization of the conduction electrons and this should give an extra magnetic moment. This excess moment was mentioned in section 3.2. in connection with Table 3.2 which shows that such an excess moment occurs in the heavy rare earths. The R.K.K.Y. theory makes two major simplifications in assuming that the Fermi surface is spherical and that the conduction electrons are of a pure s character. Fermi surfaces of the rare earths have been calculated using non-relativistic and relativistic augmented-plane-wave methods and they are reviewed by Cracknell (1971). The Fermi surface has also been charted experimentally using the de Haas-Van Alphen effect, notably in gadolinium (Schirber et al (1977) and Mattocks and Young (1977)) and using position annihilation experiments (Gupta and Loucks (1968)). Both theory and experiment have shown the Fermi surface to be different from the free electron sphere. Temple et al (1977) have used a simple non-spherical surface in magnetic structure calculations in the rare earths and compared these to the structures obtained using a spherical surface. A notable result of these calculations is that the exchange interaction is no longer isotropic. Campbell (1972) has put forward an alternative indirect exchange interaction involving 4f-5d positive exchange on the same ion and 5d-5d direct exchange between different ions. Eagles (1975) has also considered the effect of the 5d electrons in the heavy rare earths and the influence of the f-d interaction. Account must also be taken of the scattering of the conduction electrons which tends to damp the oscillations of R.K.K.Y. interaction. These considerations lead to some modifications, but the R.K.K.Y. interaction is still accepted as the main contribution to the magnetic ordering in the heavy rare earths.

3.4. Gadolinium

3.4.1 General Properties

Gadolinium is the first member of the heavy rare earths and has a half full 4f shell (7 electrons). It forms a tri-positive ion with the

$5d^1\ 6s^2$ electrons forming the conduction band. The band structure and Fermi surface have been investigated both theoretically (Batallon and Sommers (1977)) and experimentally (Mattocks and Young (1977)). The latter used the high quality crystals being produced at the Centre for Materials Science, University of Birmingham (Jordan et al (1974)) using the solid state electrotransport process. The availability of such material has lead to many of the properties of gadolinium being re-measured, as in the present investigation. Other recent experiments using this high quality material have been performed by Wells et al (1974) on the specific heat which shows a large anomaly at the Curie temperature. This is shown in Figure 3.3 which is taken from Griffel et al (1954). Robinson and Lanchester (1978) have investigated the critical thermal expansion. The crystal structure and lattice parameters of gadolinium have been measured by Banister et al (1954) and Darnell (1963), and show that gadolinium remains h.c.p. at low temperatures. The five single crystal elastic constants of gadolinium in the temperature range 4.2K to 300K have been studied by Palmer et al (1974).

3.4.2 Magnetic Properties

In this section the magnetic properties of gadolinium will be discussed with the exception of the magnetocrystalline anistotropy and the magnetic domain structure which will be reviewed later. Gadolinium is the only heavy rare earth which shows only ferromagnetic and paramagnetic behaviour. The essential single crystal magnetization data for gadolinium was obtained by Nigh et al (1963). They determined the Curie temperature to be 293.2K and found a saturation magnetic moment of $7.55\,\mu_B$ per atom. The magnetization data is shown in Figure 3.4. The saturation manetization has also been measured by Graham (1967) who also obtained a value of $7.55\mu_B$ per atom but recent measurements by Roeland et al (1975) on high quality single crystals gave a value of $7.63\,\mu_B$ per atom. The results of Graham (1967) and Roeland et al (1975) are compared in Figure 3.5. The value of

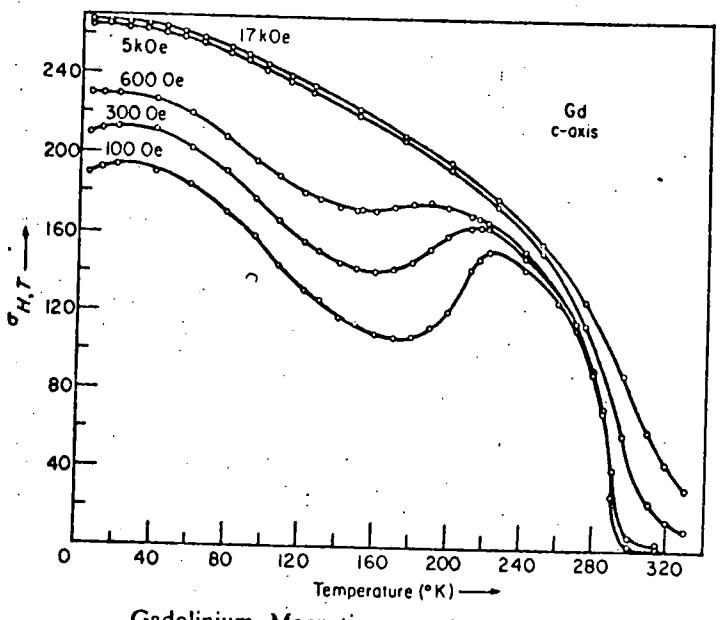

Gadolinium. Magnetic moment per gram *vs.* temperature for the *c*-axis crystal. Internal magnetic fields are indicated (Nigh *et al.*, 1963).

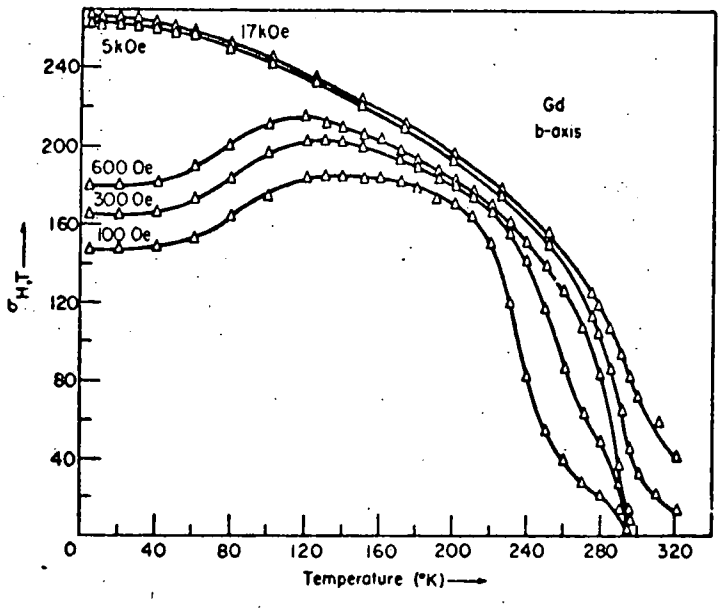

Gadolinium. Magnetic moment per gram *vs.* temperature for the *b*-axis crystal. Internal magnetic fields are indicated (Nigh, Legvold and Spedding, 1963).

FIGURE 3.4

FIGURE 3.5 The Saturation Magnetization of Gadolinium

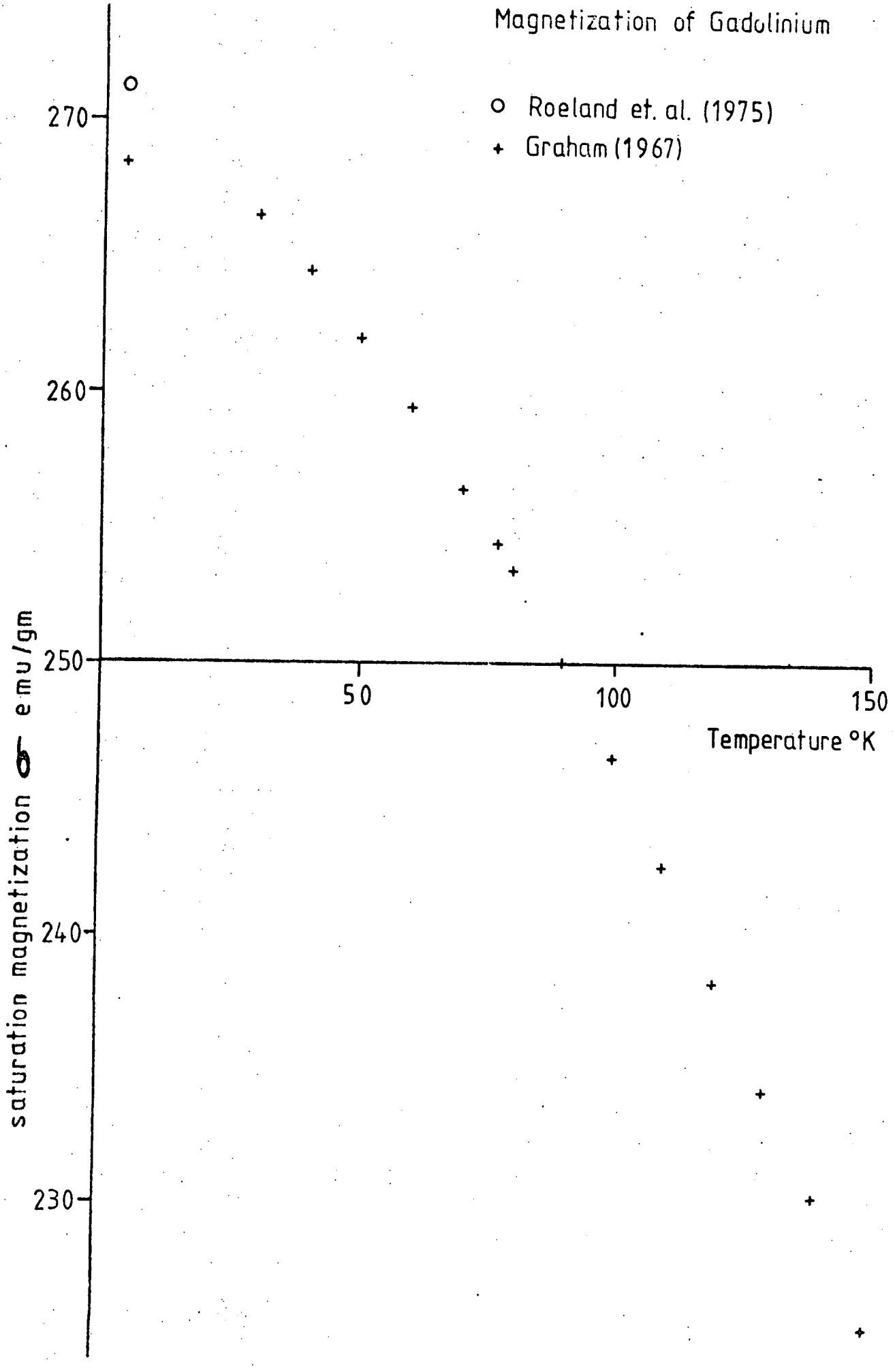

Roeland et al (1975) is the more reliable result at 4.2K due to the quality of the material used and a doubt about the temperature measurements of Graham (1967).

Belov and Pedko (1962) reported a low field antiferromagnetic phase in gadolinium but extensive neutron diffraction studies (Will et al (1964), Cable and Wollen (1968), Kuchin et al (1969), and Moon et al (1972)) have shown that no such phase exists. The probable cause of the anomaly observed by Belov and Pedko (1962) is the very low anisotropy and the change of easy direction in that temperature region. Neutron diffraction studies on gadolinium require samples enriched in the Gd^{160} istope due to the large cross section of natural gadolinium to thermal neutrons (1800 barns).

Gadolinium, in constract to the other heavy rare earths, has only a small magnetostriction of the order of 10^{-4} compared to 10^{-2} for terbium. A complete theoretical treatment of magnetostriction has been given by Birss (1964). The magnetostriction of gadolinium has been the subject of several studies by Bozorth and Wakiyama (1963), Coleman and Pavlovic (1964), Alstad and Legvold (1965) and Mishima (1976). The latter two results are in good agreement and the values of Alstad and Legvold (1965) are illustrated in Figure 3.6. They use an expression for the magnetostriction of the form

$$\frac{\delta l}{l} = \lambda_A[(\alpha_1\beta_1+\alpha_2\beta_2)^2 - (\alpha_1\beta_1+\alpha_2\beta_2)\alpha_3\beta_3]$$

$$+ \lambda_B[(1-\alpha_3^2)(1-\beta_3^2) - (\alpha_1\beta_1+\alpha_2\beta_2)^2]$$

$$+ \lambda_C[(1-\alpha_3^2)\beta_3^2 - (\alpha_1\beta_1+\alpha_2\beta_2)\alpha_3\beta_3]$$

$$+ 4\lambda_D[(\alpha_1\beta_1+\alpha_2\beta_2)\alpha_3\beta_3] \qquad (3.6)$$

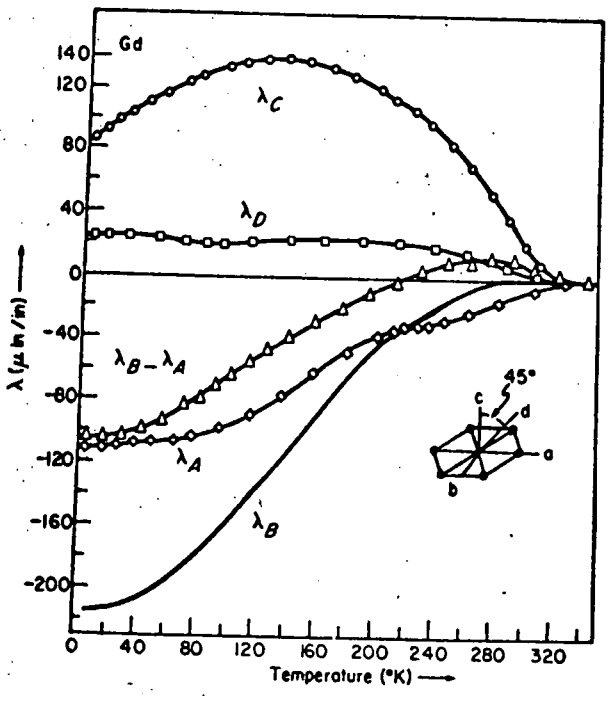

The magnetostriction constants of gadolinium as a function of temperature (Alstad and Legvold, 1964).

FIGURE 3.6

where the α_i and β_i are, respectively, the direction cosines of the magnetization and the linear strain direction with respect to the hexagonal a, b and c axes. The λ_i are the saturation magnetostriction constants. Callen and Callen (1965) have investigated the origin of the magnetostriction and its temperature dependence in terms of one-ion and two-ion interactions. The experimental values for gadolinium indicate a two-ion interaction and this would be expected from the s-state character of the Gd^{3+} ion. Tonegawa (1964) has theoretically investigated the forced magnetostriction and anomalous thermal expansion by calculating the strain dependence of the indirect exchange interaction via the conduction electrons and some agreement was found with the experimental data of Bozorth and Wakiyama (1963).

The magnetic properties of gadolinium as a technological material have received some investigation. Swift (1973) has investigated magnetic losses in textured gadolinium sheet at 77K and Sydney et al (1976) have measured the A.C. and D.C. susceptibilities around the Curie temperature. Brown (1976) has proposed taking advantage of the unique Curie temperature, $18^{o}C$ (about normal room temperature), by using gadolinium as a magnetic heat pump. Gadolinium can be used in transition metal compounds to produce magnetic materials with a wide range of Curie temperatures for specialised applications (Salmons et al (1968)).

CHAPTER FOUR

Magnetocrystalline Anisotropy

4.1 Introduction.

In section 2.3 magnetocrystalline anisotropy was introduced as giving rise to a term in the total free energy of a crystalline magnetic body. In a given crystal this contribution to the free energy depends only on the direction of the spontaneous magnetization. The magnetocrystalline anisotropy energy, E_a, is the difference in the energy of the magnetization along an arbitary direction and its value along a selected crystallographic axis. The direction of spontaneous magnetization within a ferromagnetic domain is along an easy axis if there is no applied magnetic field. This corresponds to a minimum in the magnetocrysatlline anisotropy energy.

4.2 Phenomenology of Magnetocrystalline Anisotropy.

The free energy,F, analogous to the Helmholz free energy of ordinary materials, is defined by

$$F = U - TS \tag{4.1}$$

giving, in the case of a magnetic crystal,

$$dF = -SdT + \underline{B}_o \cdot d(V\underline{M}) + V^o \sigma_{ij}\, de_{ij} \tag{4.2}$$

(sum over repeated indices)

σ_{ij} are the components of the symmetric stress tensor

e_{ij} are the components of the symmetric strain tensor

V^o refers to the unstrained volume, a hypothetical state where the lattice assumes the state it would have if the magnetic interactions were not present.

For constant strain and temperature, de_{ij} is zero and dT is zero, then

$$dF = \underline{B}_o \cdot d(V\underline{M})$$

$$F = V\int_{M_o}^{M} \underline{B}_o \cdot d\underline{M} + \text{constant} \qquad (4.3)$$

where M_o and M are some initial and final magnetization states respectively. We can expand the free energy, F, into a series in powers of direction cosines, α_i, of the magnetization with respect to a set of rectangular cartesian co-ordinates as,

$$E_a = \frac{F}{V} = \bar{b}_i \alpha_i + \bar{b}_{ij}\alpha_i\alpha_j + \bar{b}_{ijk}\alpha_i\alpha_j\alpha_k + \bar{b}_{ijkl}\alpha_i\alpha_j\alpha_k\alpha_l + \text{- - - -} \qquad (4.4)$$

where the $\bar{b}_i$, $\bar{b}_{ij}$ etc. are property tensors dependant entirely on the crystal symmetry. As we are only interested in h.c.p. crystals in this thesis we shall only consider this symmetry case. Other crystal types have been treated by Mason (1951, 1954). For the h.c.p. structure the energy density becomes

$$E_a = \frac{F}{V} = K_o + K_1 \sin^2\theta + K_2 \sin^4\theta + K_3 \sin^6\theta + K_4 \sin^6\theta \times \cos 6\phi + \text{- - - - -} \qquad (4.5)$$

where the K's are the anisotropy constants at constant strain. θ is the angle between the magnetization and the c[0001] axis and ϕ is the angle between the magnetization and the b[$10\bar{1}0$] axis. (ϕ is often defined with respect to the a[$\bar{2}110$] axis but the b axis is preferred here to give a positive value of K_4 for gadolinium). The K's have units of energy per unit volume (J m^{-3}).

It is often found in theoretical work that F/V is expanded in terms of an orthogonal set of functions such as surface spherical harmonics

$$\frac{F}{V} = \sum_{l=0}^{\infty} \sum_{m=-l}^{l} k_{l,m}\, Y_l^m(\theta,\phi)$$

$$= k_{0,0} + k_{2,0} Y_2^0 + k_{4,0} Y_4^0 + k_{6,0} Y_6^0 + k_{6,6} Y_6^6 + \text{- - - - -} \qquad (4.6)$$

The $k_{l,m}$ are known as the anisotropy coefficients and the Y_l^m are normalized to unity for $\theta = \phi = 0$. Then $k_{l,m}$ are related to the K's by

$$\begin{aligned} K_0 &= k_{0,0} + k_{2,0} + k_{4,0} + k_{6,0} \\ -K_1 &= \tfrac{2}{3} k_{2,0} + 5k_{4,0} + \tfrac{21}{2} k_{6,0} \\ K_2 &= \tfrac{35}{8} k_{4,0} + \tfrac{189}{8} k_{6,0} \\ K_3 &= -\tfrac{231}{16} k_{6,0} \\ K_4 &= 10395 k_{6,6} \end{aligned} \qquad (4.7)$$

The analysis of the anisotropy energy in terms of spherical harmonics has several advantages (Birss and Keeler (1974)). The coefficients are numerically in proportion to their contribution to the total energy and the orthogonality of the spherical harmonics means that the lower order coefficients are independent of the (arbitrary) stage at which the series is terminated. Also, as mentioned above, theoretical work tends to be carried out using spherical harmonics. In this thesis the expansion of equation (4.5) is used to analyse results in terms of the anisotropy constants. This is the traditional method and leads to a much simpler analysis of the experimental data. It also has the advantage that the anisotropy constants are used directly in calculations on such properties as domain wall width and energy. The anisotropy constants give a physical, macroscopic insight in to the anisotropy energy whereas the anisotropy coefficients give a more fundamental, microscopic view.

The meaning of K_0 (or $k_{0,0}$) in the energy expansion has not been given much attention in the past. Most authors tend to ignore it completely. Darby and Taylor (1964) used the energy required to magnetize the crystal along the easy direction as a value for K_0.

This procedure would seem to be dubious for a number of reasons. The magnetization energy would contain contributions from domain wall movement, magnetostatic energy and magnetostriction energy. In this thesis it is proposed to define K_0 as a normalization parameter to produce zero anisotropy energy along the easy direction of magnetization. To illustrate this consider a simple uniaxial crystal with anisotropy energy

$$E_a = K_0 + K_1 \sin^2\theta \tag{4.8}$$

If the c axis is easy, then K_0 is zero and the anisotropy energy is zero along the c axis. If K_1 is negative then the basal plane will be easy,

$$E_a = K_0 - K_1$$

and in this case K_0 would be made equal to K_1 to give zero anisotropy energy in the basal plane.

The easy direction of magnetization can be determined from the K values, equation (4.5), by finding the position of minimum energy with respect to θ and ϕ.

$$\frac{\delta E_a}{\delta \theta} = 2K_1 \sin\theta\cos\theta + 4K_2 \sin^3\theta\cos\theta + 6K_3 \sin^5\theta\cos\theta$$
$$= 0 \tag{4.9}$$

(neglecting the last term of equation (4.5)).

This has the solutions;

$\theta = 0^\circ$ and 90°, corresponding to the c axis and basal plane respectively, and

$$\theta = \sin^{-1}\left[\frac{K_2 \pm (K_2^2 - 3K_1K_3)^{1/2}}{3K_3}\right]^{1/2} \tag{4.10}$$

The easy direction is the direction of minimum energy corresponding to $\frac{\delta^2 E_a}{\delta \theta^2} > 0$.

The easy direction within the basal plane is given by

$$\frac{\delta E_a}{\delta \phi} = -6K_4 \sin 6\phi$$

$$= 0$$

$$\frac{\delta^2 K_a}{\delta \phi^2} > 0$$

Then if K_4 is positive the a[11$\bar{2}$0] axis is easy and if K_4 is negative the b[10$\bar{1}$0] axis is easy.

The definition of E_a, equation (4.4), is for constant strain, whereas experimental measurements are usually performed under the conditions of constant external stress, (i.e. under a constant pressure). Under these conditions the appropriate thermodynamic potential is the Gibbs function, G.

$$G = F - V^o \sigma_{ij} e_{ij} \qquad (4.11)$$

and

$$dG = -SdT + \underline{B}_o \cdot d(V\underline{M}) - V^o e_{ij} d\sigma_{ij} \qquad (4.12)$$

The anisotropy constants, K_n^1, derived using this expression are different from those derived from dF, equation (4.2). The difference arises from the magnetostriction. The observed anisotropy energy density is thus composed of two parts, an intrinsic part appropriate to zero lattice strain and a magnetoelastic contribution of magnitude, (Birss (1964) Pg.198)

$$\tfrac{1}{2} V^o{}_{ij} e_{ij}^* = -\tfrac{1}{2} C_{ijkl} e_{ij}^* e_{kl}^*$$

where e_{ij}^* are the equilibrium values of the strain components e_{ij} and C_{ijkl} are the elastic stiffness constants. Following Birss (1964) we can obtain expressions for the magnetoelastic correction to the anisotropy constants in terms of the magnetostriction.

$$\Delta K_0 = -R_o^2 (C_{11} + C_{12}) - 2C_{13} R_o(R_o+R_1) - \tfrac{1}{3} C_{33}(R_o+R_1)^2$$

$$\Delta K_1 = -(C_{11}+C_{12})R_o(2R_2+R_5) - C_{13}\,[2R_o(R_2 + R_3)+(R_o+R_1)(2R_2+R_5)]$$

$$\Delta K_2 = -1/2\, C_{11}(2R_2^2 + 2R_2R_5 + R_5^2) - C_{12}R_2(R_2+R_5) - C_{13}(R_2+R_3)$$
$$(2R_2+R_5) - 1/2\, C_{33}(R_2+R_3)^2 + 1/2\, C_{44}R_4^2 \qquad (4.14)$$

The R_n are the saturation magnetostriction constants and the C's are the experimentally determined elastic constants. The R_n are related to the experimentally determined magnetostriction constants, equation (3.6) by

$$\begin{aligned} R_2 &= \lambda_B \\ R_3 &= \lambda_C - \lambda_D \\ R_4 &= 4\lambda_D - \lambda_A - \lambda_C \\ R_5 &= \lambda_A - \lambda_B \end{aligned} \qquad (4.15)$$

R_o is the thermal expansion parallel to the c axis.

$(R_0 + R_1)$ is the thermal expansion perpendicular to the c axis.

The values of R_0 and $(R_0 + R_1)$ are associated with the volume strain which is due to the presence of the spontaneous magnetization and gives rise to the thermal expansion anomaly. The actual values of R_0 and $(R_0 + R_1)$ are therefore dependent on the choice of the state of zero strain. This makes estimating their values difficult. Recently the importance of the magnetoelastic contribution has been discussed for the cases of nickel, Fujiwara et.al.(1977), and cobalt and cobalt-nickel alloys, Takahaski et.al. (1978). They concluded that the correction was important in the former case and negligible in the latter. Brooks and Goodings (1968) have estimated ΔK_1 for gadolinium, their result is shown in Figure (4.1) and is of the order of $10^4 Jm^{-3}$ at 170K. Unfortunately they do not indicate how they estimated R_0 and $(R_0 + R_1)$. Using the data of Palmer et.al. (1973) and Alstad and Legvold (1964) the value of ΔK_2 was calculated and found to be $7 \times 10^2 Jm^{-3}$ at 170K.

Another possible correction to the measured anisotropy constants

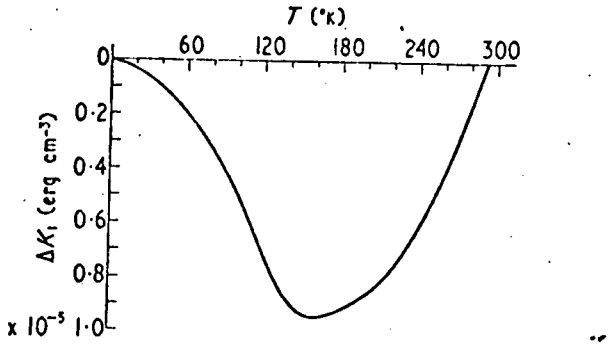

Strain-dependent contribution to $K_1(T)$ in gadolinium

FIGURE 4.1 (AFTER BROOKS and GOODINGS (1968))

is due to the anisotropy of the spontaneous magnetization. This contribution is only important in high anisotropy materials where the measuring field $\underline{B}_o$ is of the order of the exchange field (Callen and Callen (1960)).

4.3 The Theory of Magnetocrystalline Anisotropy.

4.3.1 Introduction.

The Heisenberg exchange is the major contribution to the total magnetic energy but in the form,

$$E_{ex} = \mathcal{J} \underline{S}_i \cdot \underline{S}_j$$

it is an isotropic contribution and therefore cannot be responsible for magnetocrystalline anisotropy.

The first interaction to be considered as the cause of the anisotropy was the dipole-dipole interaction between two magnetic moments which has the form

$$E_{dipole} = -\frac{1}{4\pi\mu_o r_{12}^3} [(\underline{M}_1 \cdot \underline{M}_2) - \frac{3}{r_{12}^2}(\underline{M}_1 \cdot \underline{r}_{12})(\underline{M}_2 \cdot \underline{r}_{12})] \quad (4.16)$$

where $\underline{M}_1$, $\underline{M}_2$ are the magnetic moments and $\underline{r}_{12}$ is the vector connecting them. This interaction is too small to explain the observed magnetocrystalline anisotropies. Van Vleck (1956) introduced the concept of a pseudo-dipole and pseudo-quadrupole coupling of the form of equation (4.16) but with ad-hoc large coupling constants. A possible cause of the large coupling constants could be the spin-orbit interaction which would couple the elemental magnetic moments to the symmetry of the crystal lattice. This idea is now central to theories on magnetocrystalline anisotropy. For localized moment systems two types of mechanism are considered, one-ion anisotropy and two-ion anisotropy which are not mutually exclusive. For iron transition metals other theories have to be utilized due to the band nature of

the ferromagnetism. These will not be considered here and for reviews of such theories reference can be made to Furey (1967) and Darby and Isaac (1974). Since the moments are localized in the rare earth metals the anisotropy observed is usually explained in terms of the one or two-ion theories but Eagles (1975) has presented some work which claims to show the effect of the 5d bands on the anisotropy in the heavy rare earths.

4.3.2 Single-Ion Model.

In the single-ion model we assume that the microscopic anisotropy is determined by the quantum states of one ion only. In no applied field the electronic charge cloud, which is anisotropic except for an S state ion, will mimimize its energy by taking up a particular orientation with respect to the electrostatic crystalline field. The spins are coupled to the orbital state by the spin-orbit interaction and will therefore align in a particular direction with respect to the crystal lattice. This will define the easy direction. If the spins are re-orientated by the application of a magnetic field then the electron clouds will have to distort to accomodate the change and work will be done on the system. This gives rise to the anisotropy energy.

If we represent the exchange interaction by an isotropic Weiss molecular field the major terms of the Hamiltonian are

$$\mathcal{H} = g\mu_B \underline{B}_{o_w} \cdot \underline{S} + V_c(\underline{r}) + \mathcal{H}_{S.L} + \mu_B \underline{B}_o \cdot (\underline{L} + 2\underline{S}) \qquad (4.17)$$

where $V_c(\underline{r})$ is the crystalline field which can be represented as

$$V_c(\underline{r}) = \sum_{l,m} r^l A_l^m Y_l^m(\theta,\phi) \qquad (4.18)$$

In principle we are in a position to calculate the ionic quantum

states in the presence of an applied magnetic field using equation (4.17). The A_l^m of equation (4.18) are functions of the distance to the neighbouring ions, the screening effect of the conduction electrons and the valency. They can be determined from electron spin resonance (E.S.R.) experiments and are temperature dependent. When evaluating the matrix elements of the energy equation it is more useful to write the crystalline field as

$$V_c(\underline{r}) = \sum_{l,m} B_l^m \, O_l^m \qquad (4.19)$$

where $B_l^m = \langle r^l \rangle A_l^m \alpha_l$

$\langle r^l \rangle$ is the average of the radial wave function

α_l is the l^{th} pole moment of the charge distribution, the Stevens factors, Stevens (1952).

O_l^m are the operator equivalents of the spherical harmonics. In the rare earth metals the large angular moment of the 4f shell (except for the S state ions Gd^{3+} and Eu^{3+}) leads to a strong spin-orbit coupling and we can label the quantum state by the total angular moment J. Then;

$$V_c(\underline{r}) = B_2^0 O_2^0(J) + B_4^0 O_4^0(J) + B_6^0 O_6^0(J) + B_6^6 \times [O_6^6(J) + O_6^{-6}(J)] \qquad (4.20)$$

and $V_c \gg H_{S.L}$. V_c is then considered as a perturbation on the energy system and using $\underline{B}_{ow}$ as the polar axis for the Y_l^m we can obtain (Rhyne (1972))

$$\begin{aligned} k_{2,0} &= 2\alpha_2 A_2^0 \langle r^2 \rangle J(J-1/2) \\ k_{4,0} &= 8\alpha_4 A_4^0 \langle r^4 \rangle J(J-1/2)(J-1)(J-3/2) \\ k_{6,0} &= 16\alpha_6 A_6^0 \langle r^6 \rangle J(J-1/2)(J-1)(J-3/2)(J-5/2) \\ k_{6,6} &= \alpha_6 A_6^6 \langle r^6 \rangle J(J-1/2)(J-1)(J-3/2)(J-5/2) \end{aligned} \qquad (4.21)$$

The $A_l^m \langle r^n \rangle$ show only relatively small variations for the heavy rare earths and therefore the anisotropy is dominated by the value of the Stevens factors. The anisotropy in most of the heavy rare earths is explained in terms of the single ion model although recently a debate has been in progress as to whether there is a large two ion contribution. This was proposed by Jensen (1976, 1977) and refuted by Lindgård (1976(a), 1976(b), 1978). For the s state ions Gd^{3+} and Eu^{2+} the crystal field can produce no splitting in the energy levels because it acts only upon the orbital part of the wavefunction, and this is non-degenerate. Consequently the observed anisotropy is frequently accounted for phenomenologically by a single-ion spin Hamiltonian

$$Vc = \sum_{l,m} B_l^m \; O_l^m (S) \qquad (4.22)$$

with effective spin S = 7/2.

4.3.3 The Two-Ion Model

In the two-ion model we assume that there is an anisotropic coupling between spins on separate ions. Van Vleck (1956) considered a pseudodipole-dipole interaction, H_D,

$$H_D = \sum_{i<j} D_{ij} \; [\underline{S}_i . \underline{S}_j - 3 \, (\underline{S}_i \cdot \underline{R}_{ij})(\underline{S}_j \cdot \underline{R}_{ij}) \, R_{ij}^{-2})] \qquad (4.23)$$

(c.f. equation (4.16))

and also a pseudo quadrupole-quadrupole interaction, Hq.

$$Hq = \sum_{i<j} Q_{ij} \, (\underline{S}_i \cdot \underline{R}_{ij})^2 \, (\underline{S}_j \cdot \underline{R}_{ij})^2 \qquad (4.24)$$

The D_{ij} and Q_{ij} are empirical constants. These two interactions, equations (4.23), (4.24), are considered as pertubations on the isotropic exchange interaction. Qualitatively the origin of the two-ion effect is the interaction between the charge clouds which

depends upon their shape. The spin is linked to the shape of the charge clouds via the spin-orbit coupling, and hence to the charge cloud of another ion. The interactions between the charge clouds are the Coulomb interaction, H_c, which is independent of the spins, and the exchange interaction, H_{ex}, which is spin dependent. To give an anisotropic contribution the lowest order of perturbation required involving H_c is the fifth. This gives a pseudo quadrupole-quadrupole interaction of the form of equation (4.24). Using third order perturbation theory with H_{ex} will give an anisotropic contribution of the pseudo dipole-dipole form, equation (4.23). The anisotropic exchange arises from a high order perturbation on the isotropic exchange but in the rare earths, as we have an indirect s-f exchange, the exchange can be anisotropic in itself. Smith (1976) has considered anisotropic versions of the R.K.K.Y. interaction in the s-d exchange case. He considered two mechanisms, dipole coupling and the higher orders of perturbation with the conduction electron spin-orbit coupling. Calculations on the two-ion model are extremely complex and only qualitative interpretation is possible from the temperature dependence of the anisotropy.

4.3.4 The Temperature Dependence of Magnetocrystalline Anisotropy.

The basis of all theories on the temperature dependence of the anisotropy was given by Akulov (1936). He assumed that at zero temperature there is an intrinsic anisotropy (due to any of the mechanisms above) and at higher temperatures the elemental moments sample the anisotropy energy surface due to their thermal energy. This immediately predicts that the anisotropy should be smaller at higher temperatures, which is a well established experimental fact. This process is illustrated in Figure 4.2.

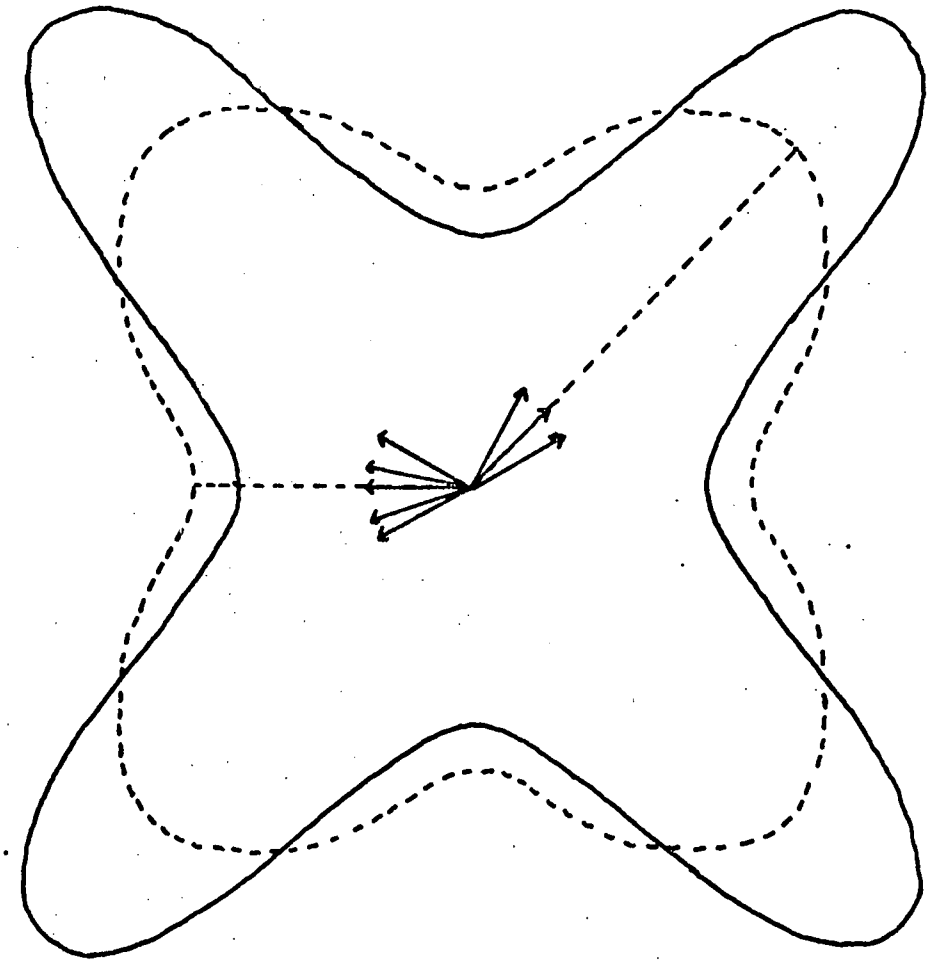

FIGURE 4.2 —— Anisotropy Surface at 0 K

----- Anisotropy Surface at T>0 K

Zener (1954) used a random walk function to describe the thermal fluctuation process and obtained the now well known power law in terms of the reduced magnetization, m_T.

$$\frac{K_n(T)}{K_n(0)} = m_T^{\frac{n(n+1)}{2}}, \quad m_T = \frac{M_s(T)}{M_o(0)} \tag{4.25}$$

Callen and Callen (1966) have reviewed the history of the power law and have generalized the treatment for the case of single-ion anisotropy. They obtained,

$$k_l(T) = k_l(0)\,\hat{I}_{l+1/2}(X) \tag{4.26}$$

where $\hat{I}_{l+1/2}(X)$ is a reduced hyperbolic Bessel function and X is a parameter defined by the relationship

$$m_T = \hat{I}_{3/2}(X) \tag{4.27}$$

Reduced hyperbolic Bessel functions are related to normal Bessel functions by the relationship

$$\hat{I}_{l+1/2}(X) = \frac{I_{l+1/2}(X)}{I_{3/2}(X)} \tag{4.28}$$

From equation (4.27) it can be seen that $\hat{I}_{3/2}(X)$ can be identified with the Langevin function L(X), equation (1.9).

At low temperatures equation (4.26) reduces to

$$k_l(T) = k_l(0)\, m_T^{\frac{l(l+1)}{2}} \tag{4.29}$$

which is the Zener power law. At high temperatures (i.e. $T \rightarrow Tc$) equation (4.26) also predicts that

$$k_l(T) = k_l(0)\, m_T^{l} \tag{4.30}$$

but it is found experimentally that this is not a good approximation, probably due to the various anomalies that occur around the Curie temperature.

For the two-ion case we have to consider pairs of spins on

separate ions fluctuating thermally from the anisotropy surface. This will depend on the degree of correlation of the two spins, i.e. to what extent they remain parallel. At low temperatures we would expect a high degree of correlation and hence would treat the two spins effectively as one. This would give the Zener power law. The correlation between the spins breaks down as the temperature increases due to the excitation of thermal spin waves. When the wavelengths of the thermal spin waves are of the same order of magnitude as the range of the two-ion mechanism there will be zero correlation and equation (4.30) would apply. Varying degrees of correlation can be included in spin-wave theory and such calculations have been carried out by Brooks and Goodings (1968) for the case of gadolinium and Brooks and Egami (1973) for highly anisotropic ferromagnetics. Yang (1971) has obtained expressions for the temperature dependence of k_1 and k_2 (equation 4.5) which includes terms representing two-ion interactions with no correlation as well as single-ion interaction terms. For hexagonal close packed crystals these were

$$\frac{K_1(T)}{K_1(o)} = a^1 \hat{I}_{5/2}(X) + b^1 \hat{I}_{9/2}(X) + a^{11}(m_T)^2 + b^{11}(\hat{I}_{5/2}(X))^2 \quad (4.31)$$

$$\frac{K_2(T)}{K_2(0)} = c^1 \hat{I}_{9/2}(X) + c^{11}(\hat{I}_{5/2}(X))^2 \quad (4.32)$$

with $X = \hat{I}^{-1}_{3/2}(m_T)$. $\hat{I}_{9/2}(X)$ and $\hat{I}_{5/2}(X)$ are the single ion contributions (c.f. Callen and Callen (1966)) and $(\hat{I}_{5/2}(X))^2$ and $(\hat{I}_{3/2}(X))^2 = m_T^2$ are the two-ion contributions. a^1, b^1, c^1, a^{11}, b^{11}, c^{11} are constants which are not known and are used as variable parameters by Yang (1971). Good fits with experimental data can be obtained for gadolinium and cobalt but with so many variable parameters the test is not very critical. Some theoretical basis for the constants will have to be

developed before the results of Yang (1971) can be applied effectively.

4.4 Techniques for Determining the Anisotropy Constants.

4.4.1 Magnetization Measurements.

The work done in magnetizing a specimen in a particular direction [h k l] is given by

$$W_{[h\ k\ l]} = \int_o^m \underline{B}_o \cdot d\underline{M} \tag{4.33}$$

If the specimen is symmetrical, unstrained, magnetized to saturation and $\underline{B}_o$ is corrected for demagnetizing effects and irreversible processes (e.g. domain wall movement) then $W_{[h\ k\ l]}$ is the anisotropy energy $E_{a_{[h\ k\ l]}}$. Using the definition of K_o in section 4.2 and considering the simple uniaxial case for hexagonal crystals, equation (4.8) with K_1 positive becomes

$$W_{[0001]} = \int_0^M \underline{B}_o \cdot d\underline{M}$$

$$= K_o = 0 \tag{4.34}$$

$$W_{[basal]} = K_o + K_1 \tag{4.35}$$

$$= K_1$$

The situation is more complicated for other than the simple uniaxial case, requiring one more magnetization curve than the number of anisotropy constants to be determined.

This method has several disadvantages. The specimen demagnetizing factor and orientation must be known precisely. In some materials the hysteresis energy (i.e. irreversible processes) can be as large as the anisotropy energy so that this method could not be used in these cases. Also in some magnetic materials, particularly the rare earths, the magnetic fields available are not high enough to saturate the specimen in the hard direction. In such cases a theoretical

magnetization curve can be predicted and made to agree with the experimental curve by varying the appropriate values of the anisotropy constants. This requires an even more detailed knowledge of the specimen and its properties. Such measurements have been made on the rare earths by Feron (1969(a), 1969(b)) for Gd, Tb, Dy and Ho. Recently Birss et.al (1976(a), 1976(b)) have developed a rotating sample magnetometer, for use in a high field super conducting magnet, to measure anisotropy constants.

4.4.2 Torque Measurements.

Following the argument of Warnock (1975), if $F = E_B + E_a$ is the total free energy of a crystal in a saturating magnetic field, the torque on the magnetization in an applied field $\underline{B}_o$ is

$$L = - \frac{\delta F}{\delta (\psi - \theta)} \qquad (4.36)$$

where θ and ψ are the angles that $\underline{M}_s$ and $\underline{B}_o$ respectively make with the easy axis, Figure 4.3. Now $\frac{\delta F}{\delta \theta} = 0$ as the magnetization is in an equilibrium position and therefore

$$\frac{\delta E_B}{\delta \theta} + \frac{\delta E_a}{\delta \theta} = 0 \qquad (4.37)$$

The anisotropy energy is a function of θ only, $E_a = f(\theta)$, and θ and ψ are not explicilty related so $\frac{\delta E_a}{\delta \psi} = 0$

Then $$L = -\frac{\delta F}{\delta (\psi - \theta)} = -\frac{\delta E_B}{\delta \psi}$$

Now $$E_B = - M_s B_o \cos (\psi - \theta)$$

$$\frac{\delta E_B}{\delta \psi} = Ms\ Bo \sin (\psi - \theta)$$

$$= - \frac{\delta E_B}{\delta \theta}$$

Using equation (4.37) gives

$$L = - \frac{\delta E_a}{\delta \theta} \qquad (4.38)$$

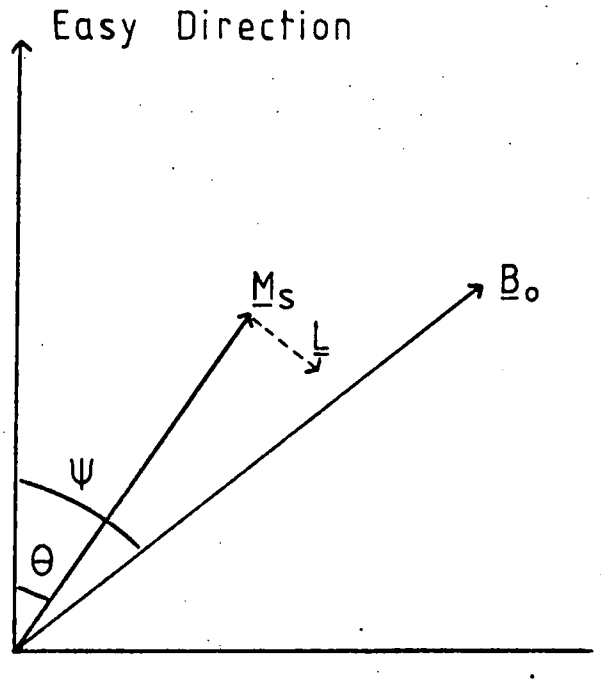

FIGURE 4.3 $L = M_s B_o \sin(\Psi - \theta)$

$= - \frac{\partial E_a}{\partial \theta}$

Hence by measuring the torque produced by a magnetic field acting on a magnetic crystal we can determine the anisotropy constants. The apparatus used for such measurements is known as a torque magnetometer and can exist in many forms. Torque magnetometry will be discussed in detail in section 4.5.

4.4.3 Ferromagnetic Resonance.

In an applied magnetic field the angular momentum of the electrons precesses at a rate depending on the field strength. A second, oscillating, applied field can be made to resonate by varying its frequency (in the GH_z region) with the electron's angular momentum, i.e. the electron absorbs energy from the oscillating field. The resonance field is found to vary with the angular position of the crystal with respect to the applied magnetic field and Kittel (1948) has shown that this is a result of the magnetocrystalline anisotropy. It is apparent from equation (2.11) that shape effects will also contribute to the change in the resonance condition. Bagguley and Liesegang (1967) give expressions for the resonance frequency in terms of the applied field, anisotropy constants, demagnetizing factors and saturation magnetization for h.c.p. crystals.

In an experimental determination the crystal is shaped so that the demagnetizing factors can be easily calculated (usually a sphere). It is mounted in a resonant cavity between the poles of an electromagnet so that the applied field and the radio frequency field are mutually perpendicular. The cavity is fed with microwaves of fixed frequency while the applied magnetic field is altered to obtain the resonance condition. Gadsden and Heath (1978) have used this technique to determine the first three anisotropy constants of nickel-vanadium alloys. They found good agreement with the torque measurements of Amighian

and Corner (1976) for K_1.

4.4.4 Inelastic Neutron Scattering.

Anisotropy constants can be determined by exciting spin waves in a crystal by bombarding it with monoenergetic neutrons. Using a neutron spectrometer the wave vectors of the incident and scattered neutrons can be measured and hence the wave vector of the spin wave deduced. From this magnon (spin wave) dispersion relation can be determined and the anisotropy constants obtained from the energy of the zero wave vector spin wave. The excitation of spin waves by neutron scattering was discussed by Kittel (1971).

4.5 Torque Magnetometry.

The most straightforward method of determining anisotropy constants is torque magnetometry. This was the method used in the present work. The apparatus used was an automatically balancing counter torque magnetometer of the type first used by Penoyer (1959) and it will be described in Chapter 5. The magnetometer produces a continuous curve of the counter torque against the degree of rotation of the electomagnet; this is known as a torque curve. A review of the history of torque magnetometry has been given by Warnock (1975). The principles on which a counter torque system works are as follows. The rotation of the electromagnet is regarded as the positive direction. The applied field causes a positive torque (+L) on the magnetization which, as it moves to follow the field direction, then experiences a counter torque (-L) due to the anisotropy energy trying to maintain the magnetization along the easy direction. The anisotropy couples the crystal lattice to the magnetization and so the crystal as a whole experiences a positive torque (+L) and therefore to hold the crystal

stationary a negative torque (-L) is applied by the counter torque system. Therefore, measurement of the counter torque required to hold the crystal stationary in a rotating megnetic field is a measure of the torque due to the anisotropy energy, ($\frac{\delta E_a}{\delta \theta}$).

For h.c.p. crystals the anisotropy energy is expressed as, equation (4.5)

$$E_a = K_o + K_1 \sin^2\theta + K_2 \sin^4\theta + K_3 \sin^6\theta + K_4 \sin^6\theta \cos 6\varphi$$

Consider two separate cases,

a) Anisotropy in a (0001) plane

In this case equation (4.5) reduces to

$$E_a = K_o + K_1 + K_2 + K_3 + K_4 \cos 6\varphi \qquad (4.39)$$

and the torque, Γ_c, is given by

$$\frac{\delta E_a}{\delta \varphi} = -\Gamma_c = -6K_4 \sin 6\varphi \qquad (4.40)$$

b) Anisotropy in a $(10\bar{1}0)$ plane

In this case equation (4.5) reduces to

$$E_a = K_o + K_1 \sin^2\theta + K_2 \sin^4\theta + K_3 \sin^6\theta \qquad (4.41)$$

and the torque, Γ_B, is given by

$$\frac{\delta E_a}{\delta \theta} = -\Gamma_B = 2K_1 \sin\theta\cos\theta + 4K_2 \sin^3\theta\cos\theta + 6K_3 \sin^5\theta\cos\theta \qquad (4.42)$$

Equation (4.42) can alternatively be expressed as

$$\frac{\delta E_a}{\delta \theta} = (K_1 + K_2 + \frac{15}{16} K_3) \sin 2\theta - (\frac{K_2}{2} + \frac{3}{4} K_3) \sin 4\theta + \frac{3K_3}{16} \sin 6\theta \qquad (4.43)$$

Equations (4.40) and (4.43) are readily analysed by Fourier analysis techniques. Examples of torque curves produced in cases b) and a) are shown in Figures (4.4) and (4.5) respectively. In general the torque curves will have other periodic components due to misalignments in the magnetometer. An analysis of these components was given by

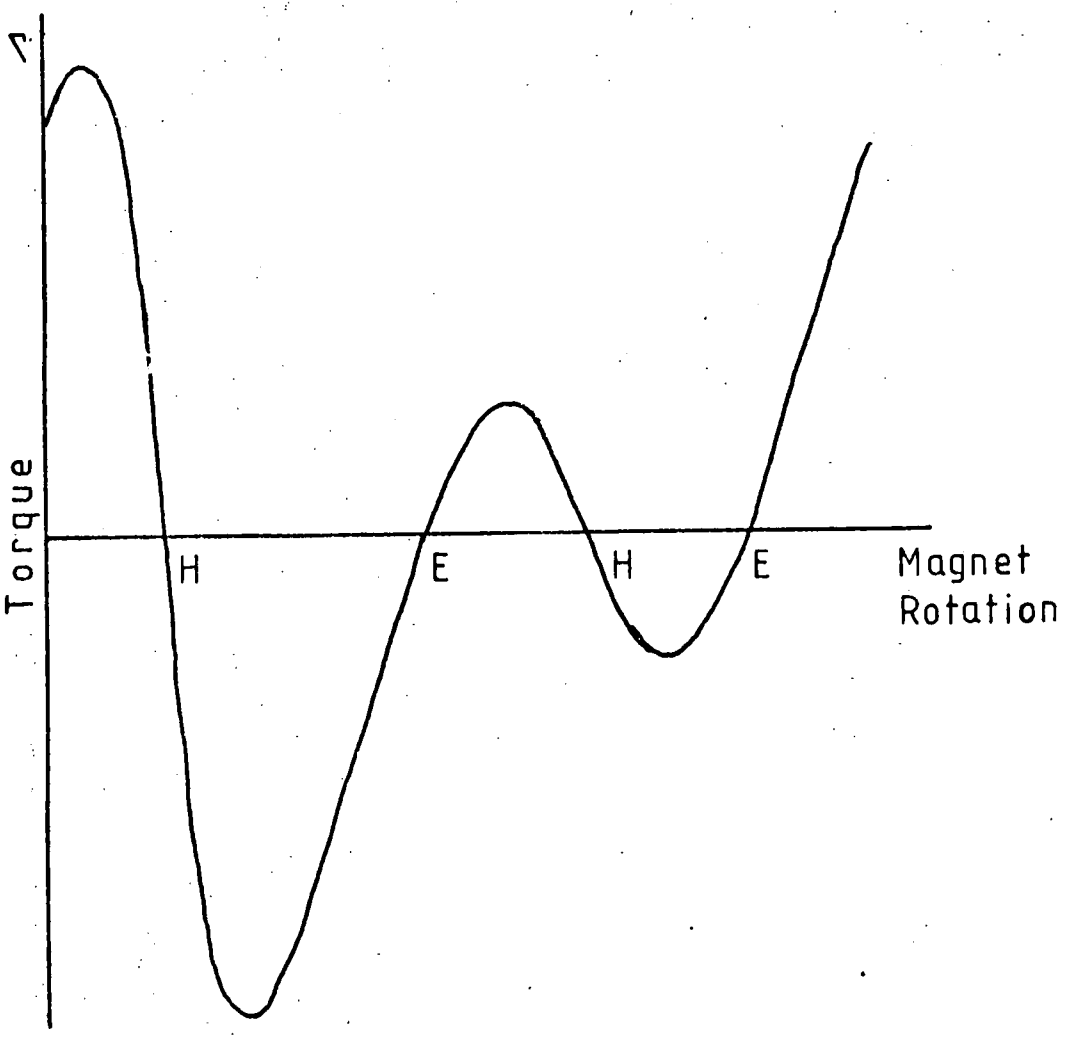

FIGURE 4.4 b Plane Torque Curve

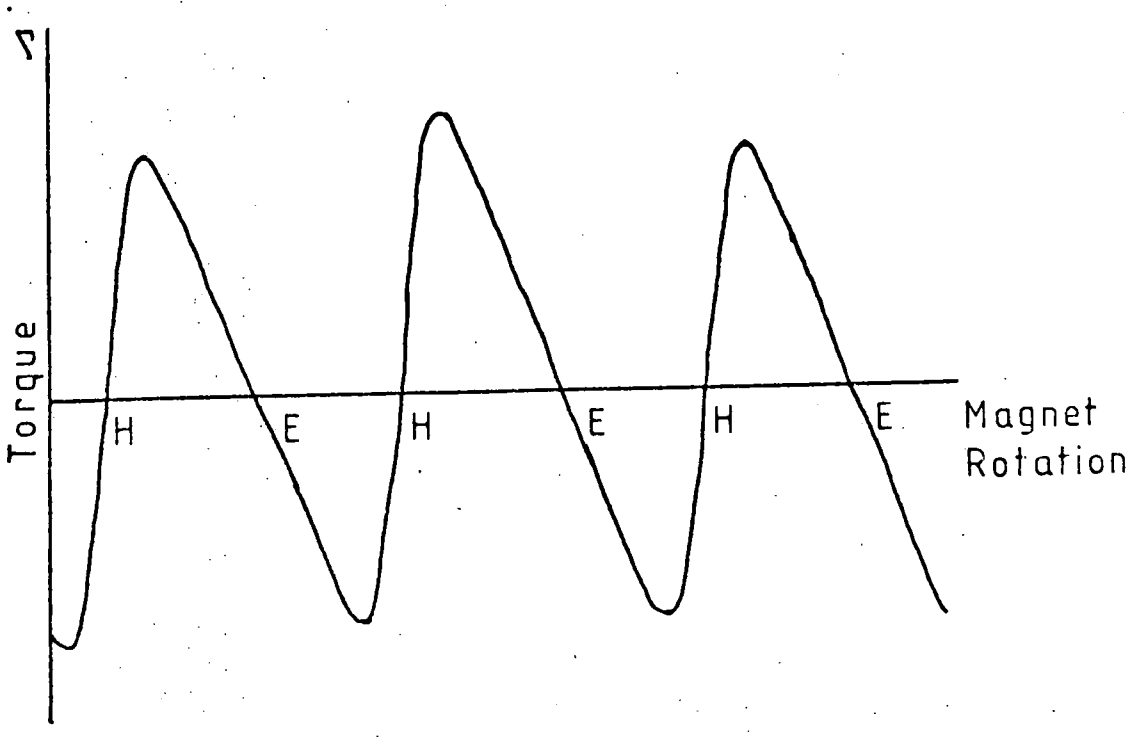

FIGURE 4.5 Basal Plane Torque Curve

Welford (1974). The symbols E and H denote the easy and hard directions in the crystal and it can be seen that the curves are sheared from a pure sinusoidal variation away from the easy axis. The cause of this shearing is the fact that in finite magnetic fields the magnetization vector in the crystal does not lie parallel to the applied field, except at zero torque, but is always directed between the applied field and the nearest axis. The angle, Θ , by which the torque ordinate is displaced is given by,

$$\sin \Theta = \frac{L}{B_0 M_s} \qquad (4.44)$$

and it can be seen that the amount of correction is proportional to the torque on the crystal. For gadolinium the torques expected would be of the order of 5×10^4 Nm m^{-3} in an applied field of 1T (for case (b)). The saturation magnetization is approximately 2×10^6 A m^{-1} which gives a value for Θ of approximately 1.5°. The corrections needed are therefore of the order of a few degrees, a larger correction required for low fields. When analysing a large number of torque curves some automatic form of correction needs to be applied. The correction was obtained in this work by the use of an inclined graticule. This method will be discussed in Chapter 5.

CHAPTER FIVE

The Magnetocrystalline Anisotropy Constants of Gadolinium

5.1 Previous Work

The magnetocrystalline anisotropy of gadolinium has been investigated by a number of authors. Torque magnetometry has been used by Corner et al. (1962), Graham (1962, 1967) and Darby and Taylor (1964). Feron (1969) has determined the anisotropy constants from the analysis of magnetization curves. Tajima (1971), Tohyama and Chikazumi (1973), Ito (1973) and Fujii et al. (1976) have studied the effect on the anisotropy of adding small quantities of other rare earth metals to gadolinium. The theory of the magnetic anisotropy of rare earth impurities in gadolinium metal has been discussed by Asada (1973).

The easy direction of magnetization was determined directly by Birss and Wallis (1964), Corner and Tanner (1976) and Franse and Mihai (1977) using zero torque magnetometry. Neutron diffraction measurements on the easy direction have been made by Cable and Wollen (1968) and Kuchin et al. (1969) and an investigation using positive muons to look at the local magnetic field in polycrystalline gadolinium has been carried out by Graf et al. (1977).

These investigations dealt with the temperature dependence of the anisotropy constants and easy direction. The effects of pressure on the anisotropy constants have been studied by Birss and Hegarty (1976) and Tayama et al.(1969). The effect of pressure on the easy direction has been investigated by Milstein and Robinson (1969) using magnetization measurements.

The agreement in the case of the unaxial constants is not satisfactory especially when the easy direction of magnetization is calculated and compared with the direct measurements. In gadolinium the direction of the magnetic moment with respect to the c axis changes with temperature. Above

about 240 K there is general agreement that the magnetic moment is parallel to the c axis and below this temperature the magnetic moment makes an angle to the c axis which varies with temperature. According to the work of Graham (1962), Birss and Wallis (1964) and Franse and Mihai (1977) this angle has a maximum of 90^{o} (i.e. the magnetization enters the basal plane) over a temperature range of 100 K to 240 K. There is no agreement between these authors on the exact temperature regions where the basal plane is easy. Corner et al. (1962), Feron (1969) and Corner and Tanner (1976) give an easy direction which makes an easy cone below 240 K of varying angle, which is always less than 90^{o}. The easy directions of Corner and Tanner (1976) and Franse and Mihai (1977) are compared in Figure 5.1. The investigations using neutron diffraction and muon techniques both lead to an easy cone of angle less than 90^{o}. In particular the work of Cable and Wollen (1969) is in good agreement with that of Corner and Tanner (1976), Figure 5.1(a).

The investigations of the basal plane anisotropy of gadolinium (K_4 of equation 4.5) by Darby and Taylor (1964) and Graham (1967) are in reasonable agreement in the temperature range 65 K to 90 K but there are differences at higher temperatures. Graham (1967) extended the investigation down to 4.2 K and this is the only previous work on K_4 at temperatures below 65 K.

It is possible that the variations in the values of the anisotropy constants could be due to the varying quality of the material used in these experiments. Except for that used by Corner and Tanner (1976) the material was typically of 2N to 3N purity with respect to metallic impurities, but usually contained substantial numbers of inclusions. The application of solid state electrotransport to rare earth metals had led to single crystals of very high quality becoming available and it seemed desirable to attempt to obtain reliable values of the uniaxial and basal plane anisotropy constants

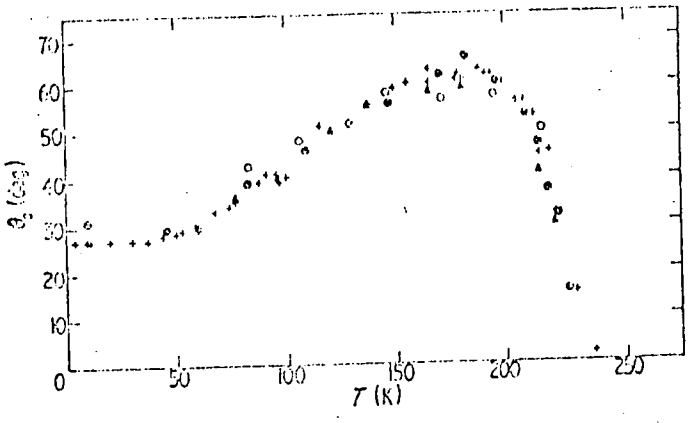

Plot of the angle between the magnetization and c axis as a function of temperature. +, present experimental points at 0·35 T; ▲, our extrapolated values; ○, ◐, taken from neutron diffraction data of Cable and Wollan (1968) (○ from 100 reflections, ◐ from 002 reflections).

(AFTER CORNER AND TANNER (1976))

(a)

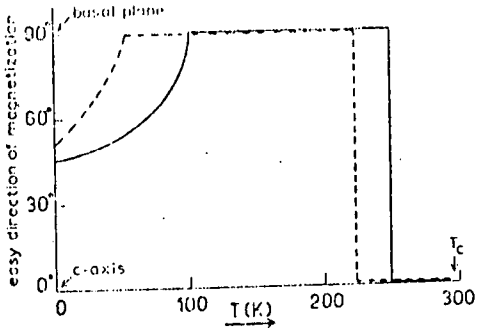

The easy direction of magnetization in gadolinium as a function of temperature; full curve: 1 bar; broken curve: 3 kbar.

(AFTER FRANSE AND MIHAI(1977))

(b)

FIGURE 5.1

using such crystals of gadolinium.

The theoretical aspects of the temperature dependence of the magnetocrystalline anisotropy of gadolinium have been discussed by Brooks and Goodings (1968) and Yang (1971). Their results were discussed in section 4.4 and will be assessed with respect to the present work in section 5.6.

5.2 The Apparatus

The apparatus used to investigate the magnetocrystalline anisotropy of gadolinium was a torque magnetometer, the principles of which were described in sections 4.4.2 and 4.5. The torque magnetometer was of the automatically balanced type where a servosystem is employed to hold the crystal stationary while the applied magnetic field is rotated about it. The magnetometer was originally constructed by Roe (1961) and several modifications had been made by Bly (1967), Welford (1974) and Amighian (1975). For the present work the apparatus was completely overhauled and some modifications introduced. These will be described in the following sections. The principles of the apparatus are shown in Figure 5.2.

5.2.1 The Electromagnet

The electromagnet was first constructed by Roe (1961) and is a conventional water cooled magnet with soft iron pole pieces and copper coils. The magnet face plates had become warped with age and these were replaced. The cooling system was also improved using lightweight plastic tubing which allowed greater rotational freedom of the magnet. The maximum possible rotation was then increased to 270^{o} as compared with the 200^{o} obtained by Welford (1974). A second heat exchanger was added to the cooling system and this allowed currents of 100 A to be used for long periods without the magnet overheating. Currents of up to 150 A could be used for short

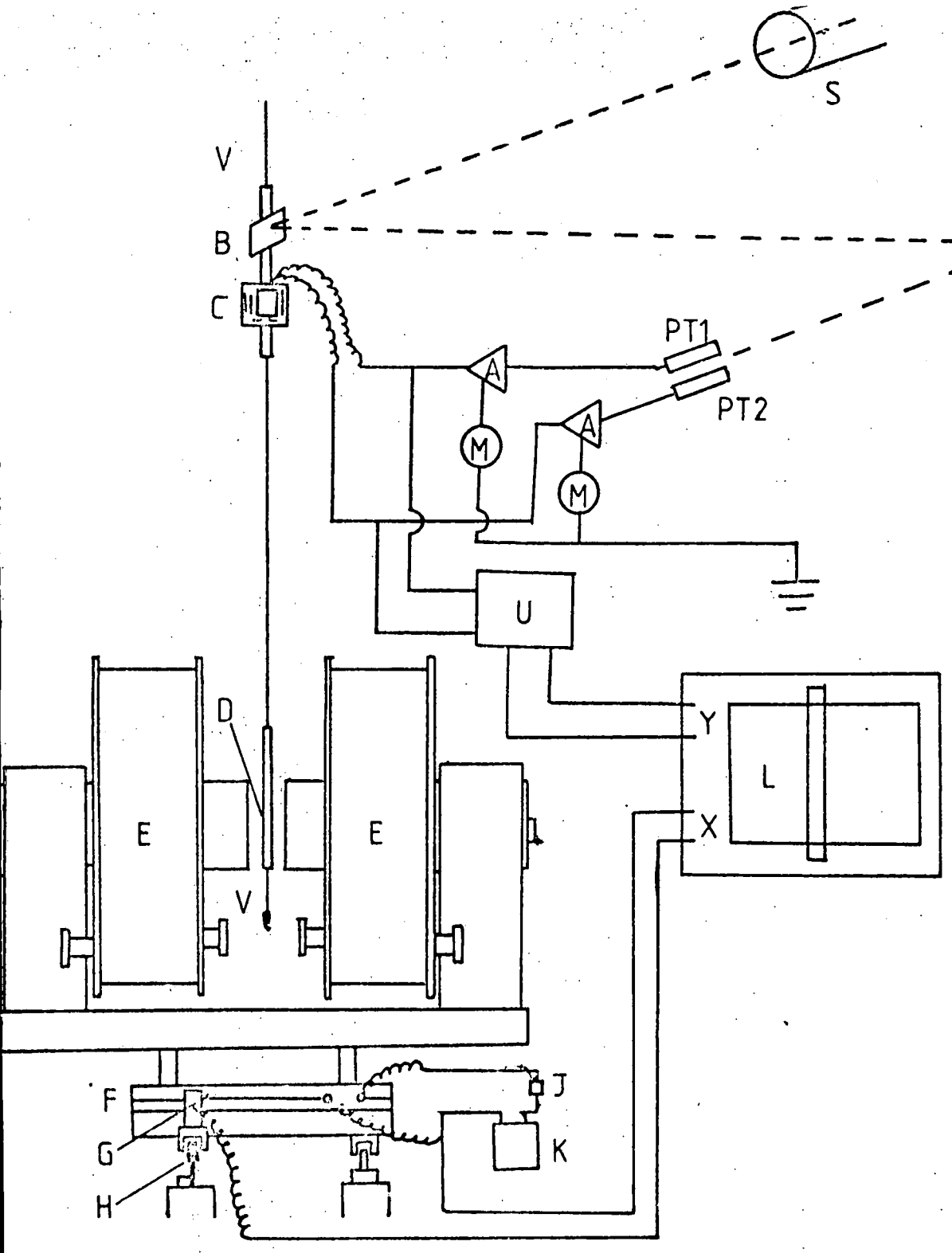

A-Amplifier B-Plane Mirror C-Counter Torque Coil
D-Crystal E-Electromagnet F-Slide Wire Potentiometer
G-Sliding Contact H-Magnet Rails J-Resistor
K-Voltage Supply L-X-Y Recorder M-Warning Meters
PT1, PT2-Phototransistors S-Projector Light Source
T-Concave Mirror f= 30cm. U-Output Potentiometer
V-Suspending Ligaments

FIGURE 5.2 The Torque Magnetometer

periods. The magnet coils have a nominal resistance of 1 ohm when connected in series. The maximum current supplied by the power unit is 200 A at 200 V. This is unsmoothed D.C. rectified from the mains supply.

Due to the modifications of the cryostat system the pole face separation was increased to 5.1 cm from the 5.07 cm used by Amighian (1975). The magnet was carefully recalibrated to ensure that its performance had not been greatly impaired. The pole pieces are circular and 10 cm in diameter with flat faces. Calibration was carried out with a Hirst FM75 combined fluxmeter and Hall probe meter with a type H 22e/T 101 Hall probe which has linear output characteristics up to 1.5 Tesla. The Hall probe was calibrated with a standard permanent magnet, nominally of 0.17 Tesla $\pm$ 2%. The permanent magnet was checked using a small search coil of 25 turns (0.75 ohm) and cross section of 0.82 cm^2. This gave a calibration of 0.166 $\pm$ 0.001 Tesla, within the nominal value given. The electromagnet calibration curve is shown in Figure 5.3; the magnet current was read from the power supply control box. Readings taken with the current increasing and decreasing show that there was negligible hysteresis. The magnet calibration was also checked with two different search coils in conjunction with the fluxmeter and gave good agreement with the Hall probe calibration. The uniformity of the field within the pole pieces was also checked using the Hall probe by scanning horizontally and vertically from one edge of the pole piece to the other. The results are shown in Figures 5.4 and 5.5 and show that the electromagnet produces a field uniform to 1% over a volume of 30 cm^2 about the centre of the magnet. On the magnet base is a slide wire potentiometer which provides a direct reading of the magnet rotation on the X-Y recorder. By suitable adjustment of J, K (Figure 5.2) and the scale on the x axis on the x-y recorder a deflection of 1 cm per 10 degrees of rotation was obtained. This setting was checked regularly.

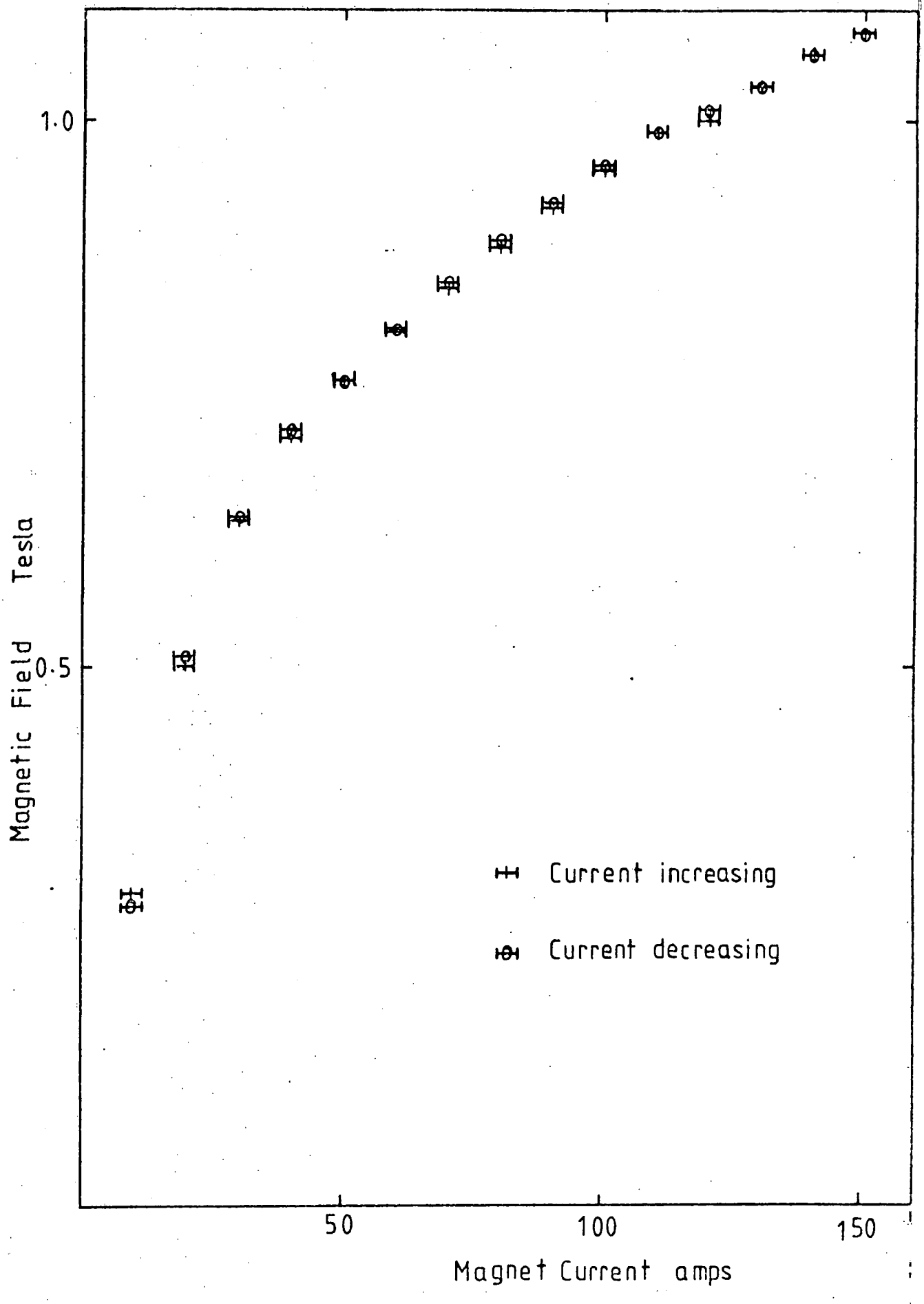

FIGURE 5.3 The Electromagnet Calibration

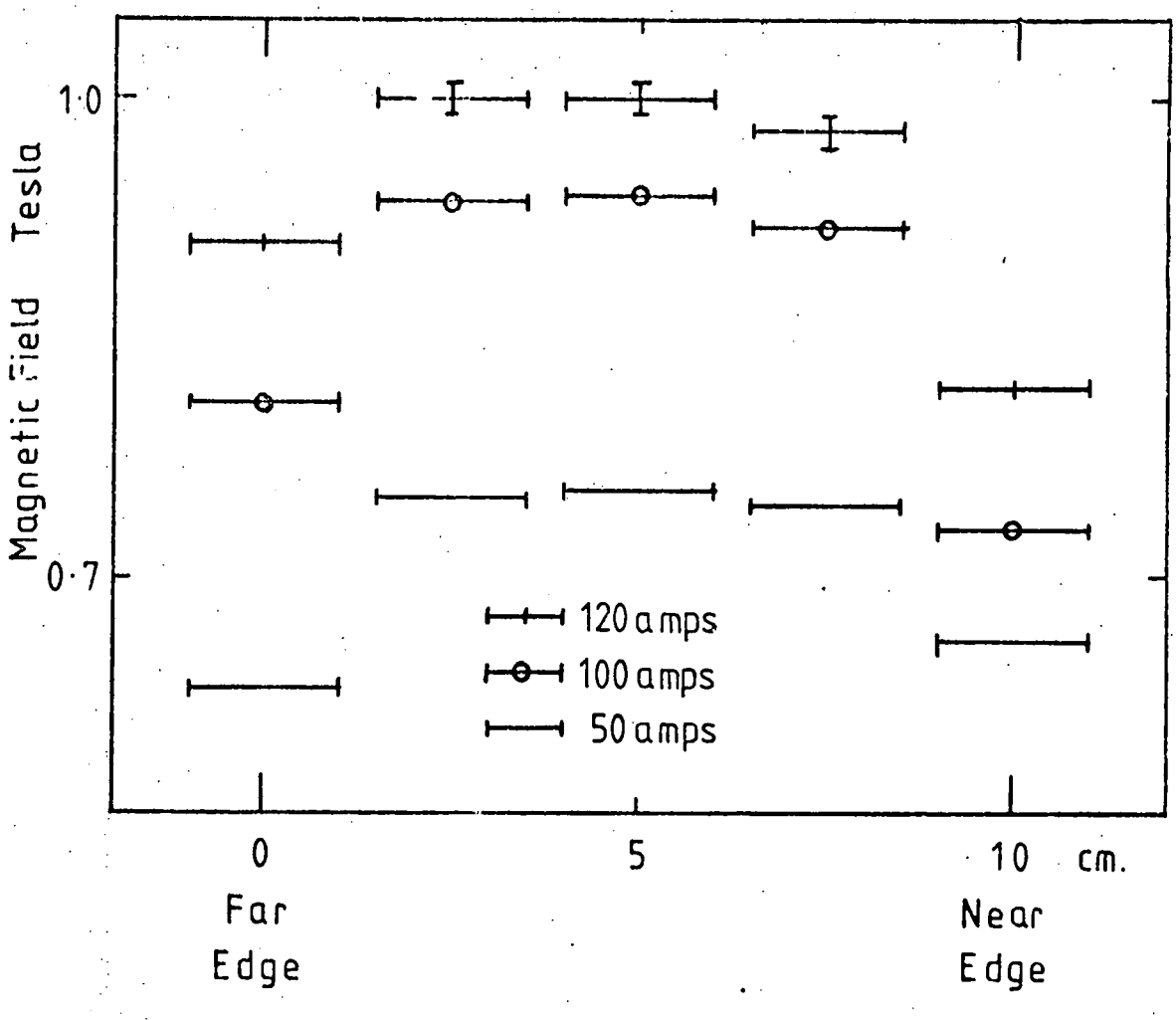

FIGURE 5.4 Horizontal Calibration of the Electromagnet

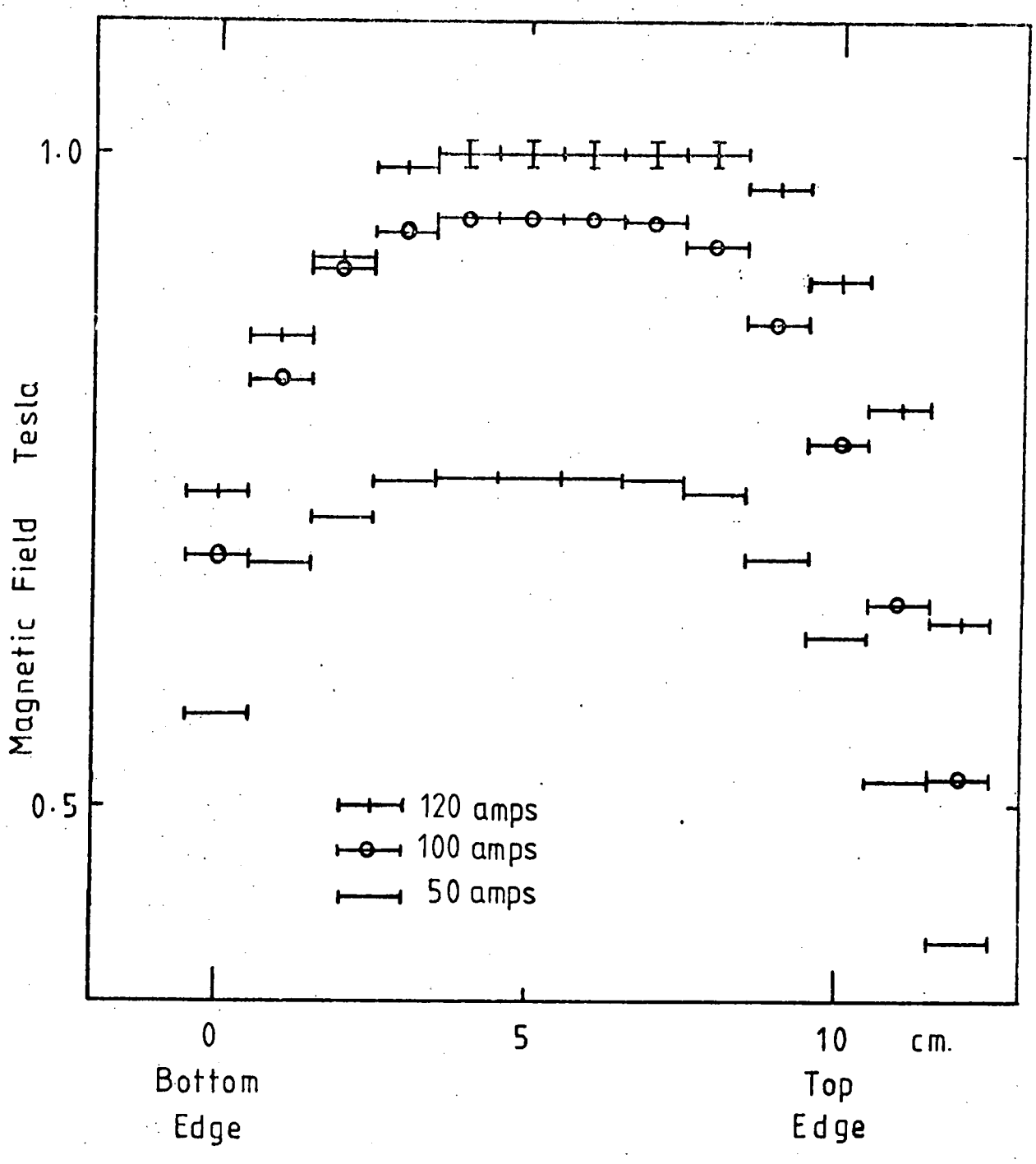

FIGURE 5.5 Vertical Calibration of the Electromagnet

5.2.2 The Magnetometer

The magnetometer was essentially the same as that described by Welford (1974) with some improvements. The most important of these was the re-design of the optical system. The original lamp, slit, lens and mirror system (Welford (1974), Figure 6.8) was replaced by a projector (using an Atlas lamp 21.5 V, 150 W), a small plane mirror (ground to 2.5 x 2.0 x 0.6 cm thick) mounted on the torsion head and a concave mirror (10 cm dia. 30 cm focal length). The principle of the new system is to image the small plane mirror on the phototransistors by use of the concave mirror (Figure 5.2). The mirror must have well defined edges and be small enough to reflect through the window in the torsion head cover. This system proved to be very successful.

The electronics of the magnetometer are the same as described by Welford (1974). The output of the counter torque coil was fed to the Y terminals of a Philips PM 8120 X-Y recorder via a potentiometer network shown in Figure 5.6. All the work reported here was carried out using the most sensitive output (Range 5) and varying the sensitivity of the X-Y recorder as required.

Other slight modifications were the adjustment of the lower suspension to place the sample in the centre of the electromagnet and a reconstruction of the vacuum system.

5.2.3 Temperature Measurement

Amighian (1975) had modified the magnetometer to allow it to be used at liquid helium temperatures using glass dewars. A new glass helium dewar was designed with thinner walls to give greater clearance around the tail of the magnetometer. This allowed more liquid helium to surround the tail and provide greater temperature stability. This was only partially successful as temperatures of only 20 K could be easily maintained. Lower

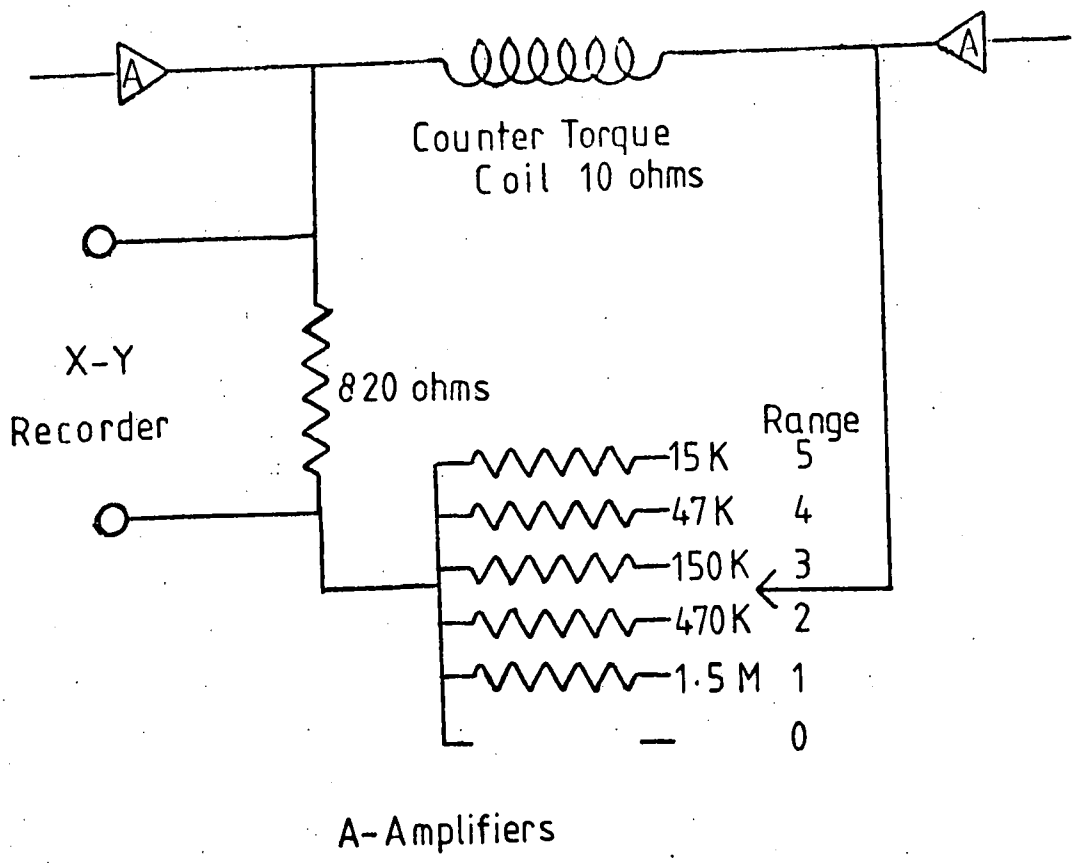

FIGURE 5.6 Output Potentiometer

temperatures could be reached with difficulty. It was therefore decided to design a stainless steel dewar which would enable even thinner walls and smaller wall spacing to be used. The dewar design is shown in Figure 5.7 and it was constructed by Allbon-Saunders Ltd., Oxford. This dewar allowed liquid helium temperatures to be reached.

Previously (Amighian (1975)) a completely glass helium syphon had been used but this was found to be extremely difficult to use as it could not tolerate any strain and hence the alignment of the liquid helium transport dewar was critical. The glass part of the syphon within the magnetometer was retained and a glass adaptor designed to fit a Thor Cryogenics, Oxford, stainless steel transfer line for use with the helium transport dewar. The inner glass part of the syphon only extended as far as the neck of the helium dewar and so a piece of heat shrinkable plastic tubing was added to ensure that the liquid helium entered the bottom of the dewar.

The temperature of the crystal was measured using a copper-constantan thermocouple situated just above it. The reference junction was immersed in liquid nitrogen and the thermal e.m.f. was measured with a Schlumberger A200 digital voltmeter, capable of reading to 1μV, or a Pye portable potentiometer, capable of reading to 10μV. A standard copper-constantan calibration chart was used to determine the temperature. This arrangement gave a temperature sensitivity of $\pm$1 K over the range 4 K to 300 K.

5.2.4 Calibration of the Magnetometer

Welford (1974) described three methods of calibration, using a flux meter, a torsion fibre and a current carrying coil. The first method was found to give inconsistent results. In the present investigation the method of the current carrying coil was used as it is capable of giving very accurate results.

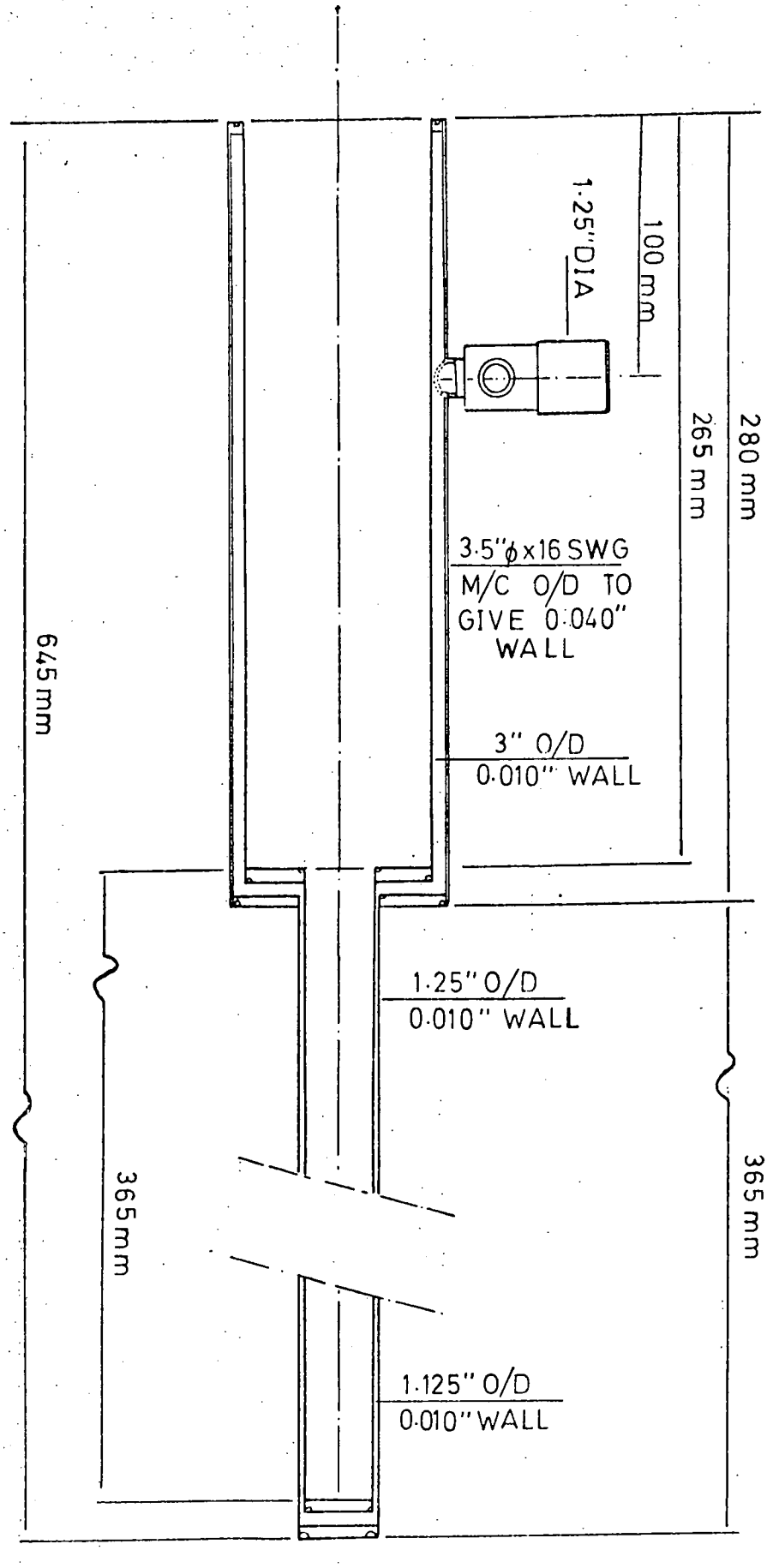

FIGURE 5.7 The Stainless Steel Dewar

A small coil was constructed on a brass former of square cross section, similar to the one used by Welford (1974). This coil gave very erratic results especially in high magnetic fields. The reason for this was that the brass former was found to be ferromagnetic or superparamagnetic, probably due to impurities in the brass.

A coil of 30 turns (N) of 42 s.w.g. copper wire was wound on a circular section Tufnol former, drilled and fitted with a grub screw so that the coil could be fastened to the specimen holder at the level normally occupied by the specimen. The diameter of the coil was 1.807 cm and it had a nominal resistance of 9 ohm. The axis of the coil was set perpendicular to the magnetic field of the electromagnet. The lower suspension wire of the magnetometer movement was fastened to a heavy support which rested on the yoke of the magnet. The lead in wires to the coil were made as long as possible and were twisted together and then loosely coiled around the magnetometer suspension. The current was measured using a Cambridge Electrodynamic AC/DC sub-standard ammeter and a current reversing switch was also included in the circuit. The magnetometer output, on range 5, was measured on the X-Y recorder for currents flowing in both directions for each magnetic field value. Currents between 0.1 and 0.5 amp. were passed through the coil and magnetic fields up to 1 Tesla were used. The quantity B_oAIN/V was calculated for each value of current, I, and magnetic field, B_o, where V is the voltage obtained from the X-Y recorder. A is the cross sectional area of the coil.

The mean of 22 readings was found to be

$$1.24 \pm 0.01 \times 10^{-5} \text{ Nm (mV)}^{-1}$$

This corresponds to the sensitivity on range 5 of the output potentiometer. The absolute sensitivity (i.e. the voltage applied to the counter torque coil) was

$$6.44 \pm 0.05 \times 10^{-4} \text{ Nm (mV)}^{-1}$$

The value obtained by Welford (1974) was $7.47 \pm 0.055 \times 10^{-4}$ Nm $(mV)^{-1}$ and Amighian gave $7.32 \pm 0.02 \times 10^{-4}$ Nm $(mV)^{-1}$ for the absolute sensitivity. Subsequent values obtained by Edwards (1977) and Jackson (1978) were 6.68×10^{-4} Nm $(mV)^{-1}$ (no error quoted) and $6.5 \pm 0.2 \times 10^{-4}$ Nm $(mV)^{-1}$ respectively. From an analysis of the calibration data the maximum torque measurable by the magnetometer is approximately 3×10^{-3} Nm.

5.3 The Specimens

The two specimens required were cut by Dr. B. K. Tanner using electrospark erosion from a single crystal of gadolinium. The crystal had been grown at the Centre for Materials Science, University of Birmingham, using the solid state electrotransport technique by Drs. R. G. Jordan and D. W. Jones. The single crystal produced was without observable inclusions, with the oxygen content reduced to 10^2 atomic p.p.m. and resistance ratio greater than 90. One disc (A) was cut with the c axis lying in the plane of the disc, with the b axis parallel to the axis of the cylinder, $(10\bar{1}0)$, and was the sample used by Corner and Tanner (1976) while the other (B) was cut with the c plane, (0001), as the plane of the disc. The dimensions and masses of the two specimens are shown in Table 5.1 as well as the demagnetizing factor, N_{11}, for magnetization parallel to the plane of the disc (equation 2.12). The two discs were polished mechanically and then chemically polished in 50% nitric acid, 50% acetic acid, followed by a thorough wash in methanol, to remove the surface strain. They were mounted with 'Durofix' cement and back reflection Laue X-ray photographs taken to check the orientation. The photographs showed sharp clear spots and these proved the orientation to be correct to within approximately one degree.

5.4 Analysis of Results

The magnetometer produces on the X-Y recorder a continuous trace of

The Crystals

Crystal	Diameter mm	Thickness mm	Mass mg	Demagnetizing Factor N_{11}
A	2.62 ± 0.01	0.68 ± 0.01	30.8 ± 0.2	0.152
B	2.82 ± 0.01	0.36 ± 0.01	16.0 ± 1.0	0.085

TABLE 5.1

the voltage, via the output potentiometer, across the counter torque coil (torque) against the angular rotation of the electromagnet. Typical torque curves obtained for crystals A and B are shown in Figures 5.8 and 5.9 respectively. The curves show three distinct features: symmetry, hysteresis and shearing. The symmetry arises from the magnetocrystalline anisotropy, equation 4.5. The hysteresis and shearing effects are due to the applied field not being large enough to keep the magnetization exactly parallel to it, section 4.5. Welford (1974) has discussed fully the two effects and the methods used to correct for them. As the angle of shearing was found to be small (section 4.5), of the order of a few degrees, an inclined graticule was used to correct for it. The use of the inclined graticule restores the symmetry of the curves about the axis of the graticule and the curves are analysed with respect to this axis. Welford (1974) conducted a series of tests on this shearing correction as applied to 6 fold symmetry curves, e.g. Figure 4.5, and showed that even a rough correction for shearing gave a great improvement in the accuracy of the results. To test if the same conditions applied to a curve of the form of Figure 4.4 an artificial curve was constructed using the function

$$\Gamma = 4.5 \sin 2\theta - 6.0 \sin 4\theta + 0.5 \sin 6\theta \qquad (5.1)$$

Starting at an arbitrary value of θ this curve was deliberately sheared and the sheared curve was then analysed as an experimental curve with the inclined graticule. The Fourier analysis program produced an equation for the curve,

$$\Gamma = 1.11 + 4.834 \sin 2\theta - 5.903 \sin 4\theta + 0.5087 \sin 6\theta \qquad (5.2)$$

in good agreement with equation 5.1. The constant 1.11 is due to the arbitrary choice of the zero on the vertical scale for the horizontal axis. If the sheared curve was analysed without being corrected the following

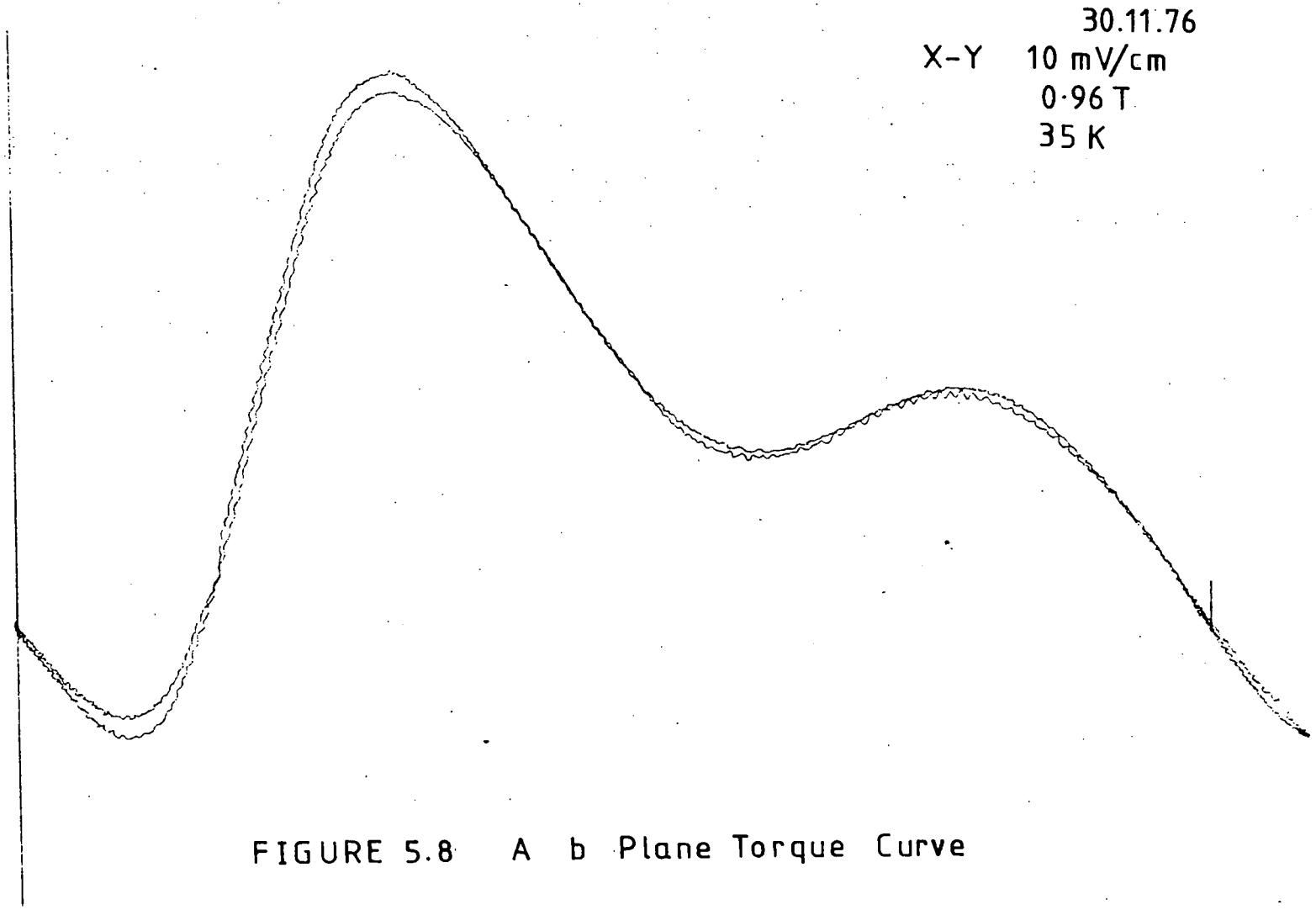

FIGURE 5.8 A b Plane Torque Curve

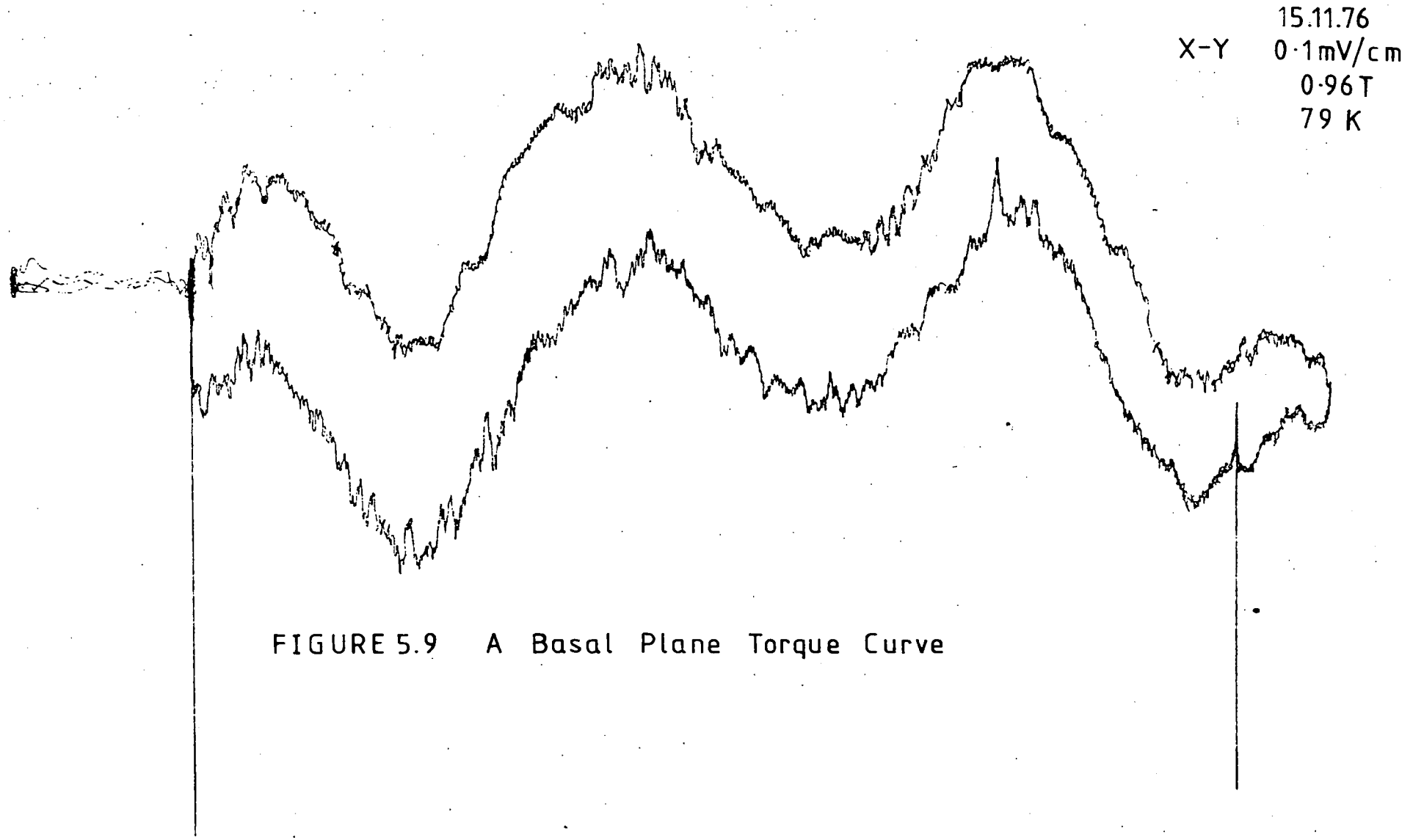

FIGURE 5.9 A Basal Plane Torque Curve

equation was derived by the analysis program.

$$\Gamma = 3.16 + 3.99 \sin 2\theta - 4.99 \sin 4\theta + 1.44 \sin 6\theta \qquad (5.3)$$

As the shearing has most effect on the higher order terms the correction should aim to minimize the errors in their coefficients when determining the anisotropy constants (equation 5.4).

To determine the anisotropy constants from the torque curves a Fourier analysis of the curves was carried out in terms of the series

$$\Gamma = A_o + \sum_n A_n \sin 2n (\theta + \varphi_n)$$

If we truncate the series at the 6θ term then the anisotropy constants are expressed as

$$\begin{aligned} -K_1 &= A_1 + 2A_2 + 3A_3 \\ K_2 &= 2A_2 + 8A_3 \qquad (5.4) \\ K_3 &= -\frac{16}{3} A_3 \quad , \end{aligned}$$

if we are analysing a torque curves of the type in Figure 5.8, and

$$K_4 = \frac{A3}{6} \qquad (5.5)$$

if we are analysing a torque curve of the type in Figure 5.9.

The Fourier analysis was carried out numerically using the basic program developed by Welford (1974). The values of the torque (in cm) were measured at 5^o intervals for both clockwise and anticlockwise curves from 0^o to 175^o with respect to the inclined graticule axis. These values, along with the date of the curve, its number, the scale of the X-Y recorder, the inclination of the graticule, the magnetic field and the temperature, formed the data from which the program computed the anisotropy constants. The calibration factor of the magnetometer, the mass of the crystal and its density were also required to give the final values of the anisotropy constants in $J\ m^{-3}$. The program for the analysis of the basal plane (K_4) curves is given in Appendix I. As this program did not give the signs of

the components due to the summation process used a least squares procedure was added to derive the relative signs of the components by comparison with the original torque curve. This new program could be used to determine K_1, K_2 and K_3 and it is given in Appendix II. Both of these programs are written in the language P.L.1. Typical output data from the programs are given in Tables 5.2 and 5.3. All the computing was carried out on the N.U.M.A.C. (Northumbrian Universities Multi Access Computer) system.

The errors involved in the determination of the anisotropy constants may be summarized as follows:

(a) Mass of the specimens A 0.65%
B 6.0%

(b) Calibration of the magnetometer 0.8%

(c) Reading the torque curves; the torque ordinates were read to an accuracy of 0.5 mm on the inclined graticule. A typical ordinate would be 2.5 cm and as the K values were computed from 72 such readings the error is of the order of 0.2%. The X-Y recorder has an error of 0.25% f.s.d.

(d) The error due to the Fourier analysis summation process is negligible. This was determined by calculating a series of values of equation 5.1 and then analysing them. The error due to the shear correction is difficult to estimate but from consideration of equations 5.1, 5.2 and 5.3 it can be seen that the use of the shear correction is vital and will reduce what would have been an extremely large error down to single figure percentage. The shear correction will also be field dependent. The result of equation 5.2 represents a shearing considerably larger than that found in any experimental curve.

(e) The density of gadolinium was treated as a constant over the temperature range 4 K to 300 K to convert the constants from J Kgm^{-1} to J m^{-3}. From an analysis of the lattice parameters as determined by Darnell (1963) this would produce a maximum error of 0.03%.

30 NCVEMBER 197 NUMBER 25 SCALE 0.01000 V/CM DY= 1.50 LL= 17.50
MAG.FIELC=1.01T TEMP=37 K

MEASURED VALUES

CW.RDGS.	4.50	3.35	2.30	1.30	0.60	-0.10	-0.50	-0.80	-0.85	-0.80	-0.60	-0.35
	-0.20	-0.10	-0.15	-0.40	-0.90	-1.65	-2.70	-3.80	-4.90	-5.90	-6.70	-7.00
	-6.90	-6.20	-4.90	-3.50	-2.00	-0.60	0.90	2.30	3.40	3.90	3.85	3.10
ACW.RDGS	4.35	3.35	2.30	1.30	0.40	-0.25	-0.70	-0.90	-0.95	-0.90	-0.70	-0.45
	-0.30	-0.20	-0.30	-0.60	-1.15	-1.90	-2.90	-4.00	-5.10	-6.15	-6.90	-7.30
	-7.15	-6.40	-5.10	-3.70	-2.20	-0.80	0.75	2.10	3.30	3.70	3.60	3.10

VALUES CORRECTED FOR SHEAR

CW.RDGS.	4.47	3.38	2.39	1.45	0.81	0.17	-0.17	-0.42	-0.41	-0.31	-0.06	0.25
	0.45	0.60	0.61	0.41	-0.03	-0.72	-1.71	-2.75	-3.79	-4.73	-5.47	-5.72
	-5.56	-4.81	-3.47	-2.02	-0.48	0.97	2.51	3.96	5.11	5.66	5.66	4.97
ACW.RDGS	4.32	3.38	2.39	1.45	0.61	0.02	-0.37	-0.52	-0.51	-0.41	-0.16	0.15
	0.35	0.50	0.46	0.21	-0.28	-0.97	-1.91	-2.95	-3.99	-4.98	-5.67	-6.02
	-5.81	-5.01	-3.67	-2.22	-0.68	0.77	2.36	3.76	5.01	5.46	5.41	4.97

VALUES CALC FRCM 2,4,6 FOLD CCMPCNENTS

CW.RDGS.	4.49	3.56	2.55	1.57	0.73	0.09	-0.32	-0.51	-0.50	-0.33	-0.08	0.20
	0.44	0.58	0.55	0.32	-0.14	-0.82	-1.69	-2.68	-3.69	-4.59	-5.25	-5.55
	-5.42	-4.81	-3.76	-2.33	-0.66	1.07	2.70	4.07	5.04	5.55	5.59	5.21
ACW.RDGS	4.58	3.69	2.68	1.68	0.79	0.08	-0.39	-0.64	-0.68	-0.54	-0.30	-0.01
	0.25	0.41	0.41	0.21	-0.22	-0.88	-1.74	-2.73	-3.74	-4.67	-5.37	-5.74
	-5.68	-5.15	-4.17	-2.80	-1.17	0.57	2.24	3.67	4.74	5.36	5.51	5.22

	MEAN	2FOLC	4FOLD	6FOLD	8FOLD	10FOLD	12FCLD
AMPS(CW)	1.334E-01	-1.364E+01	1.170E+01	-1.063E+00	3.549E-01	3.217E-01	2.175E-01
AMPS(ACW)	-5.C59E-01	-1.390E+01	1.173E+01	-9.596E-01	2.930E-01	2.856E-01	2.600E-01

HYSTERESIS ESTIMATE= -4.017E+00 JKG-1 PERREV

MEAN K3= 5.395E+00 JKG-1 K3V= 4.259E+04 J M-3
MEAN K2= 1.534E+01 JKG-1 K2V= 1.211E+05 J M-3
MEAN K1= -6.628E+00 JKG-1 K1V= -5.233E+04 J M-3
RMS ERROR= 1.500E-01 2.254E-01

TABLE 5.2 Analysis of b Plane Torque Curve

23 JUNE 1976 NUMBER 6 SCALE 0.00020 V/CM DY= 0.75 LL= 17.50

MAG.FIELD=1.0 T TEMP=79K

MEASURED VALUES

CW.RDGS.	-2.70	-2.70	-1.50	0.00	1.50	2.30	2.80	3.40	3.60	3.60	3.40	2.90
	1.80	0.40	-0.90	-1.60	-1.90	-1.50	-1.60	-1.70	-1.40	-1.00	-0.80	-1.00
	-1.40	-2.20	-2.80	-2.90	-2.90	-2.50	-2.00	-1.10	-0.30	0.40	0.90	1.00
ACW.RDGS	-3.30	-2.80	-2.90	-1.90	-1.40	-2.10	-2.00	-2.10	-2.00	-2.20	-2.60	-3.30
	-4.80	-5.50	-6.10	-6.90	-7.30	-7.30	-7.10	-6.80	-6.50	-6.40	-6.60	-7.00
	-7.50	-8.00	-8.20	-8.00	-8.00	-7.70	-6.80	-5.90	-5.00	-4.10	-3.40	-3.20

VALUES CORRECTED FOR SHEAR

CW.RDGS.	-2.65	-2.63	-1.41	0.11	1.63	2.45	2.97	3.59	3.81	3.83	3.65	3.08
	2.10	0.72	-0.56	-1.23	-1.41	-1.09	-1.17	-1.25	-0.93	-0.51	-0.29	-0.46
	-0.84	-1.62	-2.20	-2.23	-2.26	-1.83	-1.31	-0.39	0.43	1.15	1.67	1.73
ACW.RDGS	-3.25	-2.73	-2.81	-1.79	-1.27	-1.95	-1.83	-1.91	-1.78	-1.96	-2.34	-3.52
	-4.50	-5.17	-5.75	-6.53	-6.91	-6.89	-6.47	-6.34	-6.02	-5.90	-6.08	-6.46
	-6.94	-7.41	-7.59	-7.37	-7.33	-7.03	-6.11	-5.19	-4.27	-3.35	-2.63	-2.40

VALUES CALC FROM 2,4,6,12FOLD COMPONENTS

CW.RDGS.	-0.09	1.35	2.20	2.41	2.35	2.39	2.53	2.47	2.05	1.46	1.19	1.52
	2.21	2.66	2.40	1.45	0.27	-0.69	-1.35	-1.95	-2.43	-3.19	-3.17	-2.34
	-0.98	0.22	0.72	0.49	-0.08	-0.57	-0.91	-1.33	-1.93	-2.48	-2.45	-1.57
ACW.RDGS	-2.48	-1.58	-1.06	-0.85	-0.80	-0.91	-1.30	-2.04	-2.97	-3.81	-4.27	-4.37
	-4.32	-4.41	-4.72	-5.13	-5.49	-5.81	-6.20	-6.77	-7.41	-7.93	-7.83	-7.42
	-6.87	-6.45	-6.26	-6.18	-6.04	-5.83	-5.67	-5.63	-5.62	-5.37	-4.69	-3.62

	MEAN	2FOLD	4FOLD	6FOLD	8FOLD	10FOLD	12FOLD
AMPS(CW)	1.283E-01	3.059E-01	1.481E-01	2.222E-01	8.907E-02	7.519E-02	7.168E-02
PHASE(CW)		7.106E+00	-2.144E+01	9.651E-01	5.074E+00	4.650E+00	1.090E+00
AMPS(ACW)	-4.467E+00	4.319E-01	8.395E-02	1.262E-01	1.847E-02	2.330E-02	3.407E-02
PHASE(ACW)		2.214E+01	3.505E+00	-9.780E-01	1.110E+01	5.136E+00	5.138E+00

HYSTERESIS ESTIMATE= -4.670E+00 JKG-1 PERREV

MEAN K4= 2.903E-02 JKG-1

RMSERROR= 1.791E+02 -6.990E-77

K4V= 2.292E+02 J M-3

TABLE 5.3 Analysis of Basal Plane Torque Curve

(f) Temperatures were measured to an accuracy of 1 K.

(g) The magnetic field was measured to 2% at 1 T. The error was almost entirely due to reading the ammeter on the control box of the power supply.

The total error for K_4 values estimated as above was $\pm$ 9%. From the scatter of the experimental values, Figure 5.12, this would seem to be a reasonable estimate. The total error on K_1, K_2 and K_3 was estimated at about $\pm$ 4% which is reflected in the smooth variation obtained for these constants, Figure 5.11.

5.5 The Results

5.5.1 The Anisotropy Constants

Torque curves were plotted for both crystals A and B over the temperature range 4.2 K to 300 K. For each temperature a series of measurements were taken at applied magnetic fields of 0.64 T, 0.76 T, 0.85 T, 0.96 T and 1.01 T. The torque curves from crystal A changed character from a simple 2θ curve (uniaxial anisotropy) to the curve illustrated in Figure 5.8 at about 240 K. Crystal B only gave recognisable torque curves of the type illustrated in Figure 5.9 below 120 K. The signs of the constants K_1, K_2 and K_3 were determined by comparison with the temperature region where there is uniaxial anisotropy and K_1 is therefore positive. The computer program only gives the relative signs of the constants. There was no change of sign, and therefore of easy direction, in the case of K_4. For the determination of K_1, K_2 and K_3 a total of 98 torque curves were analysed and 154 curves were analysed for K_4. The curves for K_4 were in general more difficult to analyse due to the small value of K_4 and also the small crystal disc used. Most curves for K_4 were plotted on the most sensitive scale of the X-Y recorder (0.05 mV cm^{-1}) and were extremely

susceptible to noise, mainly from vibrations in the magnetometer producing a spurious response in the optical system. A table of results is given in Table 5.4 which gives all the complete sets of values of K_1, K_2 and K_3 obtained.

From Table 5.4 it can be seen that the anisotropy constants still have a magnetic field dependence and some type of extrapolation procedure is required to remove this dependence. The magnetic field dependence has been discussed by Corner and Tanner (1976) in terms of the presence of magnetic domains, as it was shown by Kouvel and Graham (1957) that domains could still be present in crystals at fields well above the expected saturation field. Empirically the field dependence of the anisotropy constants may be expressed, Corner et al. (1962), as

$$K_1' = K_1 \left(1 + B B_o^2 + \frac{b}{B_o} \right)$$

$$K_2' = K_2 \left(1 + A B_o^2 + \frac{a}{B_o} \right) \qquad (5.6)$$

A, B, a, and b are temperature dependent parameters. A and B represent a paramagnetic contribution and at low temperatures they should be negligible and extrapolation to $B_o^{-1} = 0$ should give a true value of the anisotropy constant. The extrapolations of K_1, K_2 and K_3 are shown in Figure 5.10 at 79 K. A least squares straight line fit was carried out to determine the extrapolated values. The program used to carry out the least squares fitting is given in Appendix III and is written in the language Fortran IV. Above 200 K the extrapolation was carried out with respect to B_o^2, i.e. to zero field, but this was found to have negligible effect on the K_1 values. The K_1, K_2 and K_3 values are shown in Figure 5.11 at 1.01 Tesla and the extrapolation is indicated by the dashed line.

For K_4 the extrapolation procedure was found to be unreliable due to the large errors involved in the determination of K_4, especially in low

Temperature °K	B_o Tesla	Anisotropy Constants Jm^{-3} K_1	K_2	K_3
12	0·64	$-6·09\times10^4$	$18·1\times10^4$	$-2·26\times10^4$
	0·76	-5·58	14·7	2·18
	0·85	-5·81	15·7	1·86
	0·95	-5·90	14·7	3·02
	1·01	-6·36	16·8	1·55
20	0·64	-5·58	15·7	-3·23
	0·76	-4·71	11·8	4·25
	0·85	-4·48	10·8	4·33
	0·95	-5·76	14·2	3·35
	1·01	-5·95	14·6	3·33
37	0·64	-4·54	12·6	1·50
	0·76	-4·40	10·5	4·78
	0·85	-4·65	11·7	4·14
	0·95	-5·13	12·9	3·48
	1·01	-5·23	12·1	4·26
60	0·64	-5·31	13·7	-5·34
	0·76	-4·43	9·59	3·74
	0·85	-4·08	7·33	4·85
	0·95	-4·52	8·24	4·35
	1·01	-4·66	8·18	4·36
90	0·64	-3·72	5·27	1·74
	0·76	-4·40	5·28	2·10
	0·85	-4·68	5·91	1·79
	0·95	-5·06	5·98	1·91
	1·01	-5·06	6·08	1·85
110	0·64	-3·99	4·12	1·60
	0·76	-4·69	4·67	1·45
	0·85	-4·90	4·75	1·49
	0·95	-5·23	5·24	1·24
	1·01	-5·25	5·06	1·37
150	0·64	-5·34	2·95	1·01
	0·76	-5·47	2·84	1·22
	0·85	-5·61	2·97	1·20
	0·95	-5·85	3·30	1·04
	1·01	5·78	3·02	1·22

TABLE 5.4 The Anisotropy Constants

Temperature °K	B_o Tesla	Anisotropy Constants $J m^{-3}$ K_1	K_2	K_3
170	0·64	$-4·57 \times 10^4$	$2·24 \times 10^4$	$0·78 \times 10^4$
	0·76	−4·63	2·20	0·84
	0·85	−4·78	2·38	0·76
	0·95	−4·64	2·07	0·91
	1·01	−4·89	2·36	0·80
195	0·64	−2·98	2·64	−0·69
	0·76	−3·14	2·73	−0·70
	0·85	−2·63	0·95	0·59
	0·95	−2·75	1·08	0·11
	1·01	−2·84	1·09	0·57
220	0·64	−1·29	0·81	0·25
	0·76	−1·30	0·78	0·23
	0·85	−1·37	0·83	0·26
	0·95	−1·41	0·79	0·29
	1·01	−1·45	0·86	0·21
240	0·64	0·44		
	0·76	0·36		
	0·85	0·92		
	0·95	0·72		
	1·01	1·36		
250	0·64	1·49		
	0·76	1·06		
	0·85	1·16		
	0·95	1·01		
	1·01	0·91		
273	0·64	2·20		
	0·76	2·19		
	0·85	2·17		
	0·95	2·04		
	1·01	2·02		
282	0·64	1·80		
	0·76	1·88		
	0·85	1·87		
	0·95	1·86		
	1·01	1·88		

TABLE 5.4 (cont.)

Temperature °K	B_o Tesla	Anisotropy Constant K_1 J m^{-3}
289	0·64	$1·62 \times 10^4$
	0·76	1·67
	0·85	1·66
	0·95	1·84
	1·01	1·73
300	0·64	1·09
	0·76	1·15
	0·85	1·17
	0·95	1·20
	1·01	1·54

TABLE 5.4 (cont.)

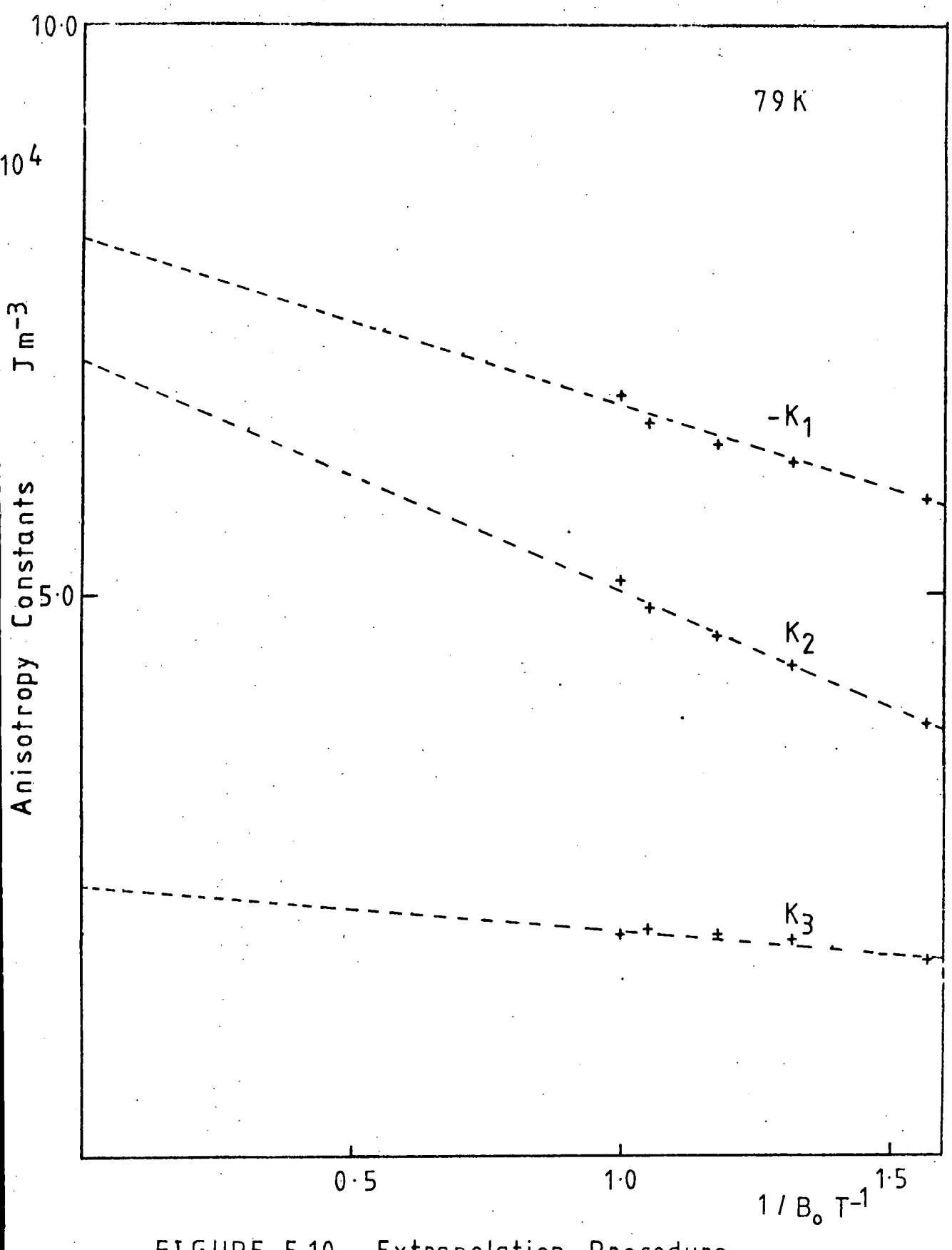

FIGURE 5.10 Extrapolation Procedure

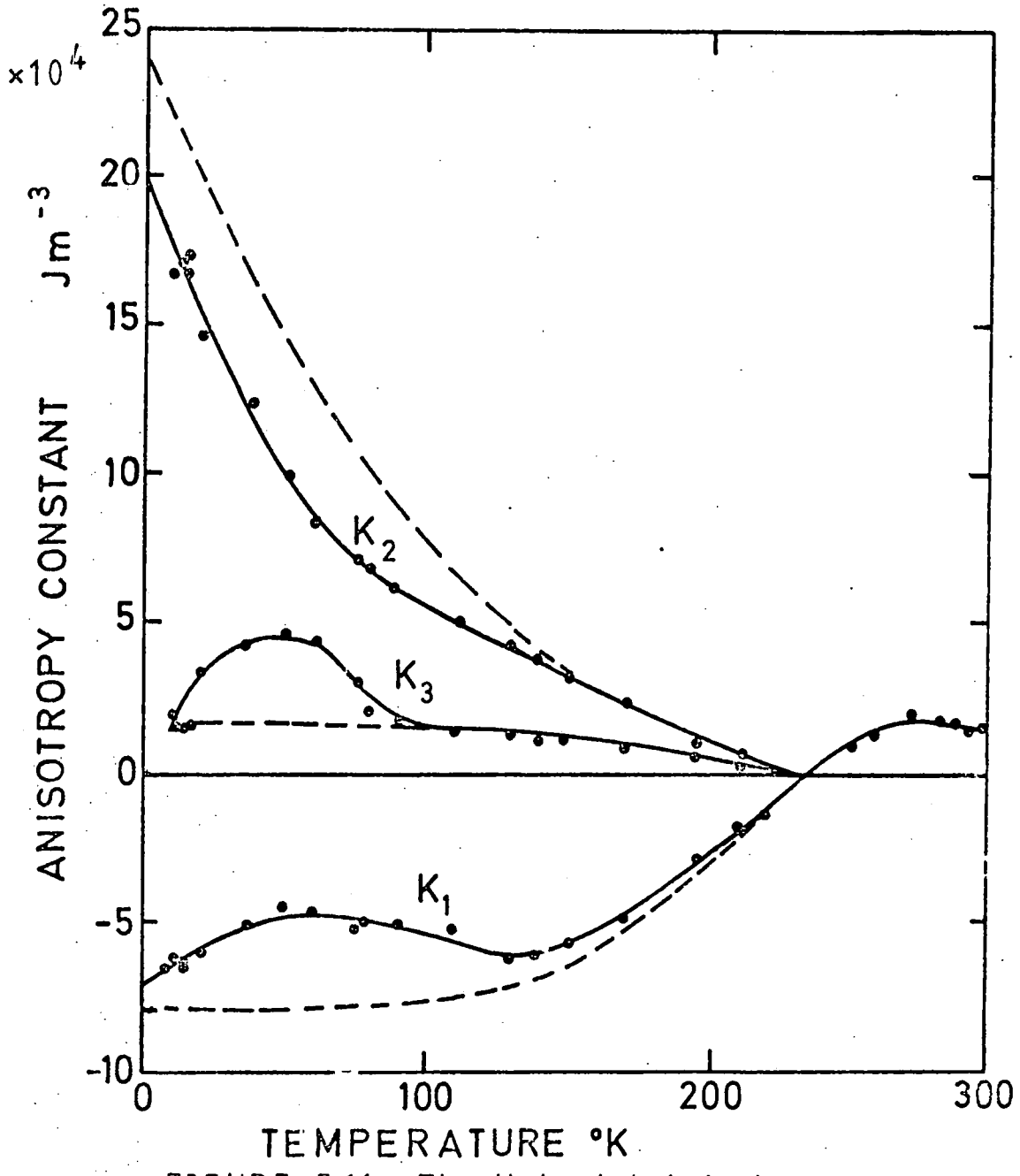

FIGURE 5.11 The Uniaxial Anisotropy Constants of Gadolinium

magnetic fields. The values of K_4 are plotted in Figure 5.12 for an applied field of 1.01 Tesla and compared with the values of Darby and Taylor (1964) and Graham (1967) which were obtained using applied fields of 1.25 Tesla and 2.5 Tesla respectively. The agreement is found to be generally good within the experimental errors. A significantly higher value for K_4 at 4.2 K than that of Graham (1967) was obtained. Referring to Figure 3.5 we see that the value of the saturation magnetization of gadolinium obtained by Graham (1967) was also significantly lower than the value of Roeland et al. (1975). By extrapolation the values of Graham (1967) for the saturation magnetization and K_4 both correspond to a temperature of 20 K. This leads to the suggestion that the values for these two quantities as determined by Graham (1967) are correct but that the temperature was in fact 20 K rather than the 4.2 K quoted. The method of temperature measurement was not quoted in the paper of Graham (1967).

The values obtained for K_1, K_2 and K_3 (Figure 5.11) do not give good agreement with any of the previously determined values. The general shape of the K_1 and K_2 curves are similar to that determined by Corner et al. (1962) and Graham (1962). This behaviour would be expected if the cause of the disagreement in the previously determined values was the quality of the crystals used. Useful comparisons with the results of Tajima (1971) and Tohyama and Chikazumi (1973) are difficult for, although the material each used appeared to be of common origin and quality and measurements had been made using the same apparatus, their results are significantly different from each other and there appears to have been no correction made for shearing effects in either case.

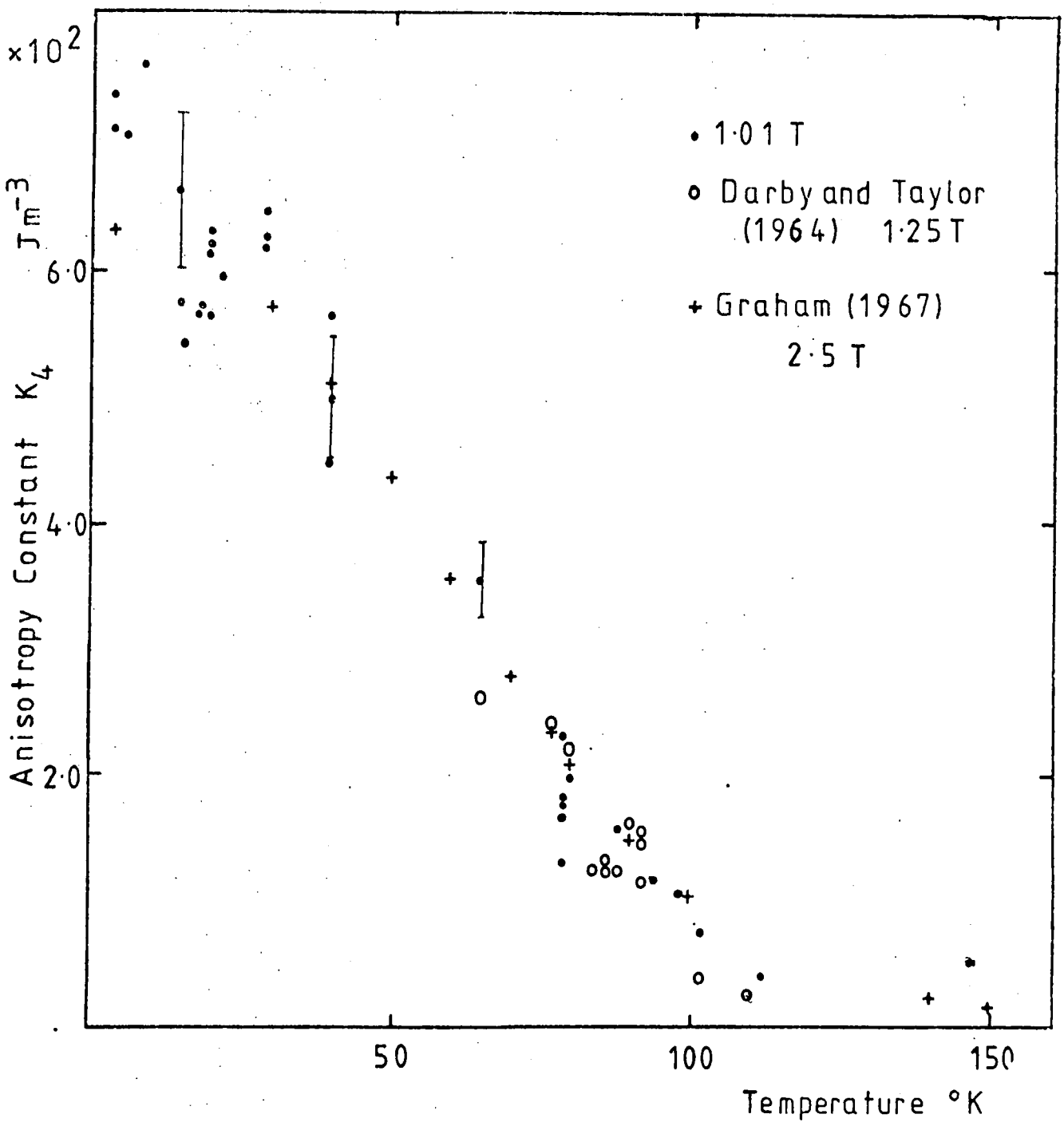

FIGURE 5.12 The Temperature Dependence of K_4 of Gadolinium

5.5.2 The Easy Direction of Magnetization

The easy direction of magnetization was determined in two ways from the anisotropy data. The first was by direct inspection of the torque curves. For each torque curve analysed the easy direction was determined by observing the effect of the shearing on the curve as in Figures 4.4 and 4.5. Below 240 K two easy directions were observed corresponding to an easy cone. The easy direction was also obtained by using equation 4.10 and the values of K_1, K_2 and K_3 determined at 1.01 Tesla and also from the extrapolated values of the anisotropy constants. The calculated values are in good agreement with those measured directly and are shown in Figure 5.13 along with the direct measurements of Corner and Tanner (1976). The agreement is again found to be very good and from reference to Figure 5.1(a) the calculated values also agree with the neutron diffraction measurements of Cable and Wollen (1968). The maximum angle that the easy cone makes with the c axis is 65^{o} and this is in sharp diagreement with the results of Franse and Mihai (1977), Figure 5.1(b).

A possible explanation for the discrepancy in the determination of the easy direction could be that strain had been introduced into the crystal when it had been mounted. Usually this is with an adhesive; 'Durofix' was used in the present work. This could also introduce stress into the crystal as it was cooled down due to the differential expansion of the adhesive and the crystal. To test this explanation crystal A was carefully mounted on a torque magnetometer specimen holder using four strips of 'Sellotape' crossed over the top of the crystal and down the sides of the specimen holder. A fifth strip was wrapped round the specimen holder and over the ends of the other strips to secure them. This should provide a firm attachment which is immune to thermal cycling and differential thermal expansion. The crystal was placed in

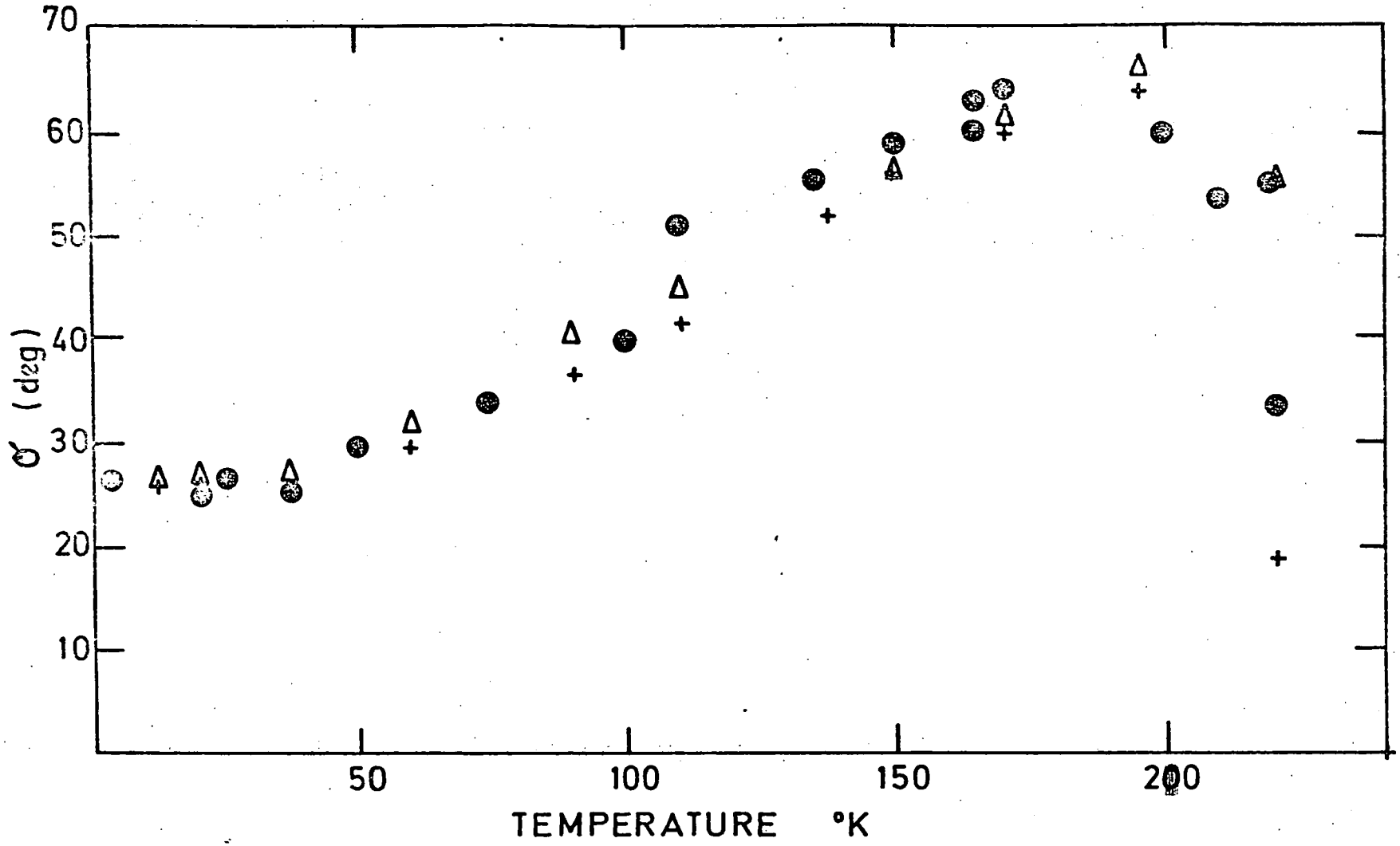

FIGURE 5.13 The Easy Direction of Magnetization
+ at 1 T
Δ extrapolated values
● at 0·85 T (AFTER CORNER and TANNER (1976))

the torque magnetometer and the experiment of Corner and Tanner (1976) was repeated. This involved the disconnection of the servo-system to the counter torque coil and the phototransistors were replaced by a translucent screen. The concave mirror was replaced by a plane mirror and a small slit was introduced between the condenser and projector lenses in the projector lamp. This slit was then imaged on the translucent screen, with no magnetic field applied to the crystal, and its position marked. The easy direction in the crystal was then located by applying a magnetic field of 0.85 Tesla. As the crystal could rotate freely the easy direction aligned itself with the magnetic field, and then by rotating the magnet to bring the slit image back to the mark on the translucent screen the easy direction was located precisely. This is the position of zero torque. This procedure was carried out while the ambient room temperature was below the Curie temperature of gadolinium, 18°C. The rotation of the magnet could be read to $\frac{1}{2}^{o}$. The crystal was then cooled to liquid nitrogen temperature and the magnet continuously rotated to maintain the easy direction in the initial position. The crystal was then warmed up gently and the rotation of the magnet recorded as a function of temperature. The results are shown in Figure 5.14 along with the corresponding results of Corner and Tanner (1976). The agreement is found to be excellent except in the temperature region 200 K to 240 K where the easy direction is varying rapidly. This could be due to thermal hysteresis. It is also worth noting that the experiment of Corner and Tanner (1976) was quasi-static with the temperature being stabilized for each measurement. The present experiment was a dynamic investigation as readings were taken as the temperature rose. This experiment indicates that if the crystal is mounted carefully with adhesive then the results will not be significantly affected. An alternative explanation for the differences in the easy

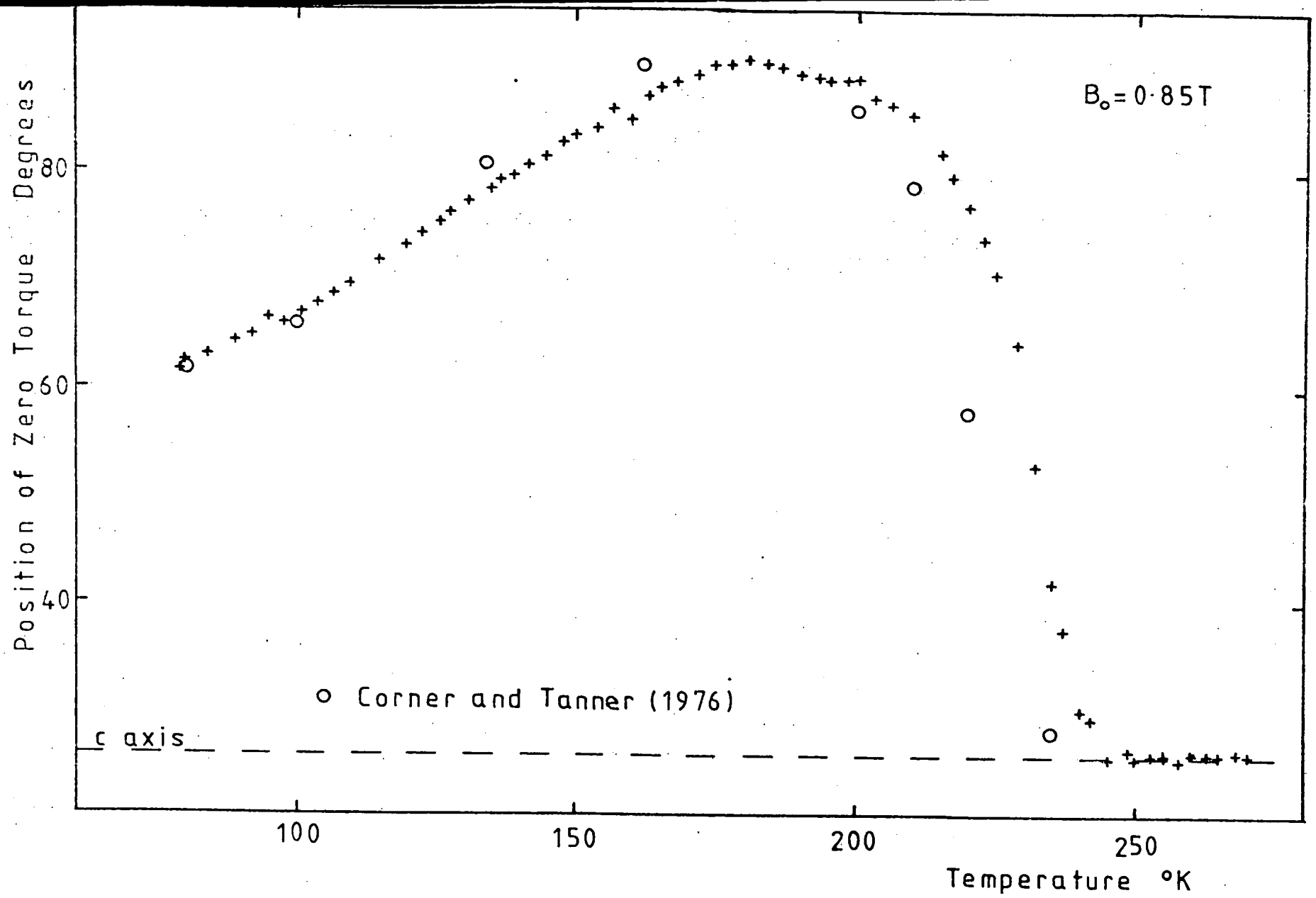

FIGURE 5.14 Direct Measurement of the Easy Direction

direction reported by various workers will be given in section 5.7.

5.5.3 Anisotropy Energy

The total anisotropy energy in a particular crystallographic direction is given by equation 4.5. A program was written to use the experimental data to determine the anisotropy energy surface at various temperatures. The program is given in Appendix IV and is written in Fortran IV. The program calculates the anisotropy energy for values of θ and φ at 5° intervals using the values of K_1, K_2, K_3 and K_4 for each temperature. The anisotropy energy surfaces are shown in Figures 5.15 and 5.16 for a $(11\bar{2}0)$ plane (which contains the c and b axis). These energy diagrams have been normalized to give zero anisotropy energy along the easy direction by the introduction of a temperature dependent parameter which has been identified with the quantity K_o of equation 4.5. The variation of this parameter with temperature is shown in Figure 5.17. The magnitude of the basal plane anisotropy is small on the scale of Figures 5.15 and 5.16 and contributes only a small 6 fold perturbation when rotating about the c axis. Darby and Taylor (1964) also calculated the anisotropy energy surfaces using the data of Corner et al. (1962) and a value of K_o from the magnetization data of Nigh et al. (1963). Their results are shown in Figure 5.18. The anisotropy energy surfaces show the same characteristic changes as the easy direction moves away from the c axis at about 240 K to form an easy cone. This, in effect, produces two easy directions in a $(11\bar{2}0)$ plane. If we plot $\sum K_n$ against temperature, Figure 5.19, we are in effect looking at the anisotropy energy in the basal plane ($\theta = 90^{\circ}$, $\varphi = 90^{\circ}$). Although the energy becomes very small in the temperature region 150 K to 240 K it is never zero and hence the basal plane does not become 'easy'. Darby and

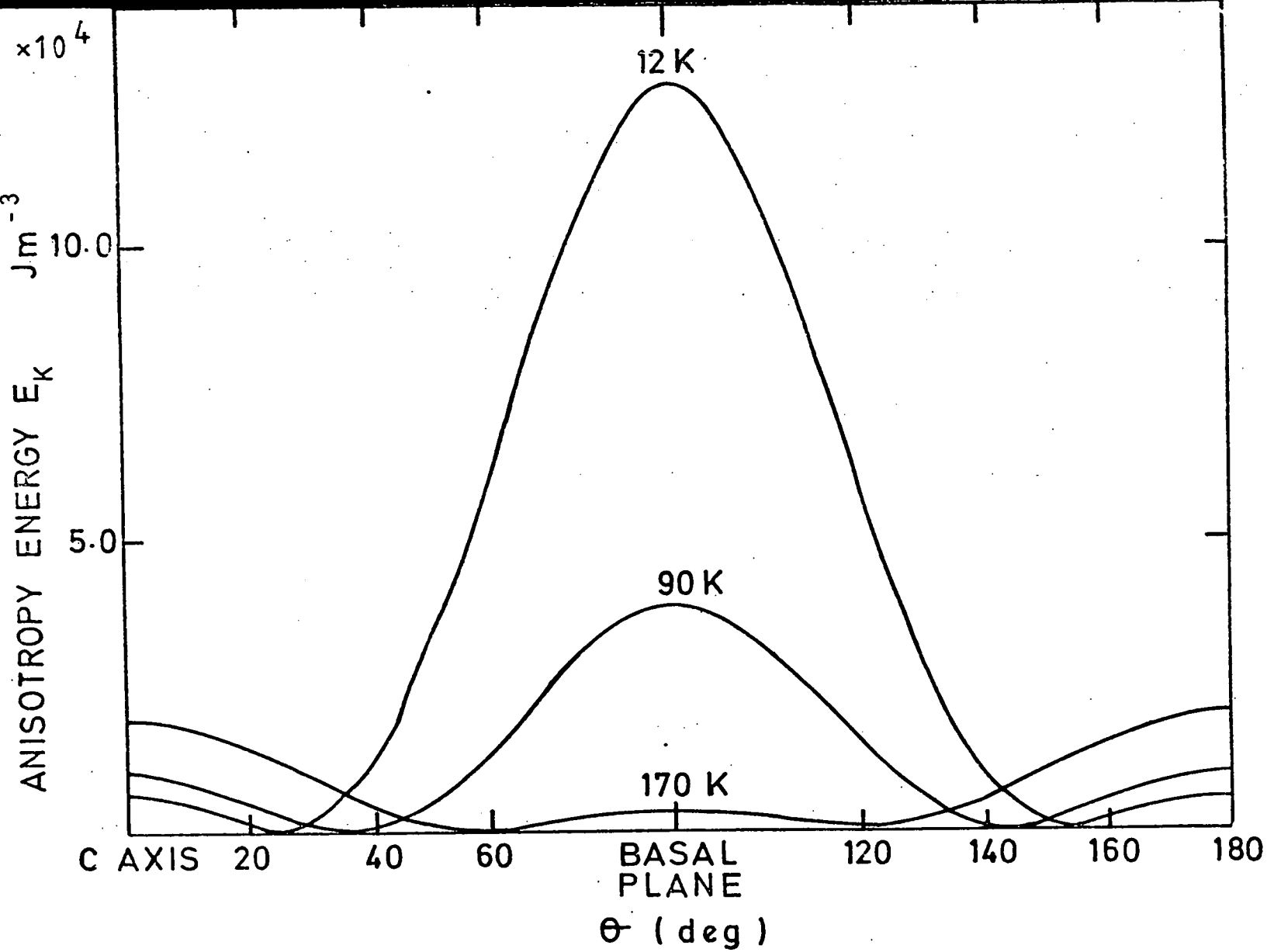

FIGURE 5.15 Anisotropy Energy Surfaces

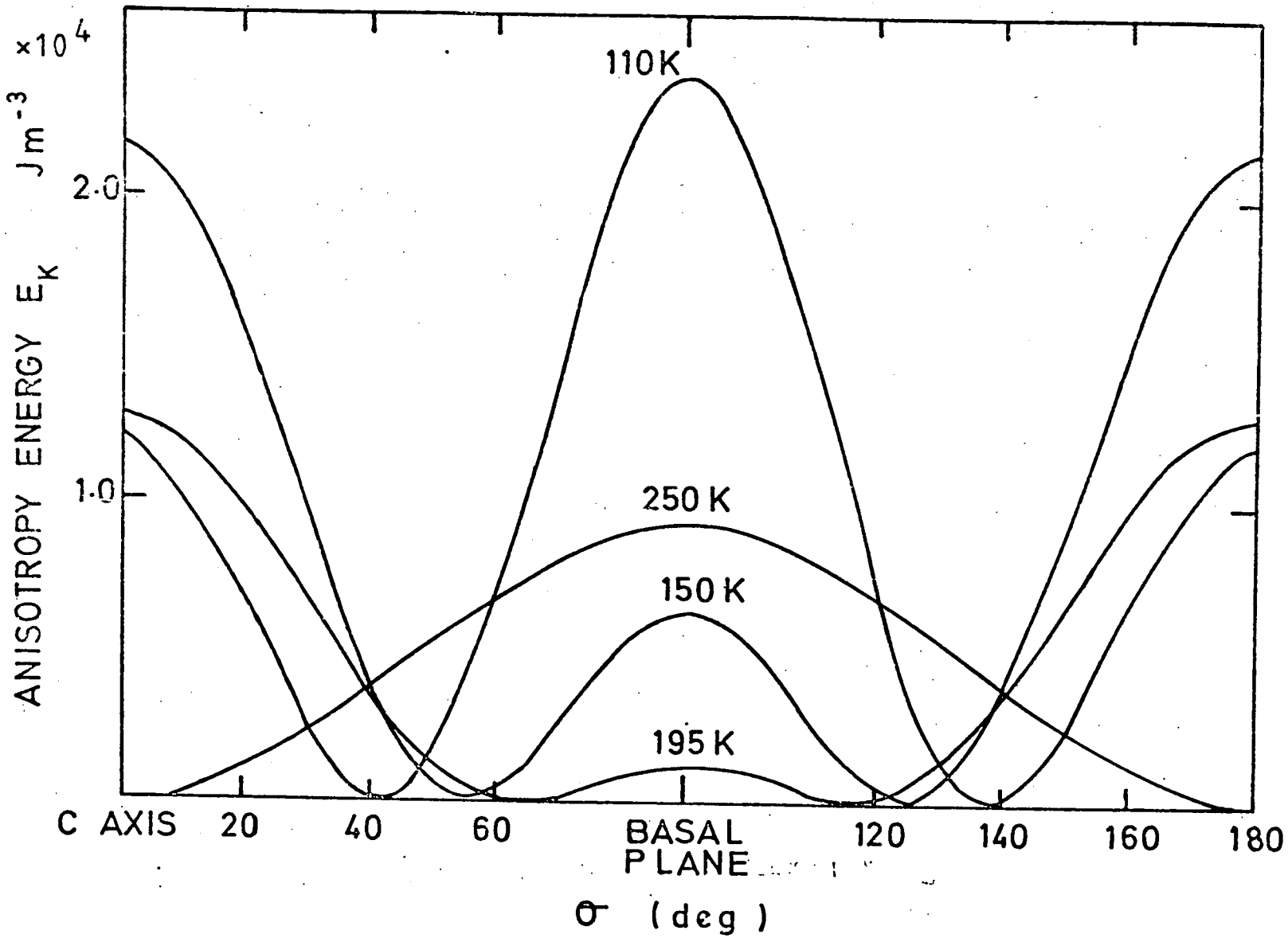

FIGURE 5.16 Anisotropy Energy Surfaces

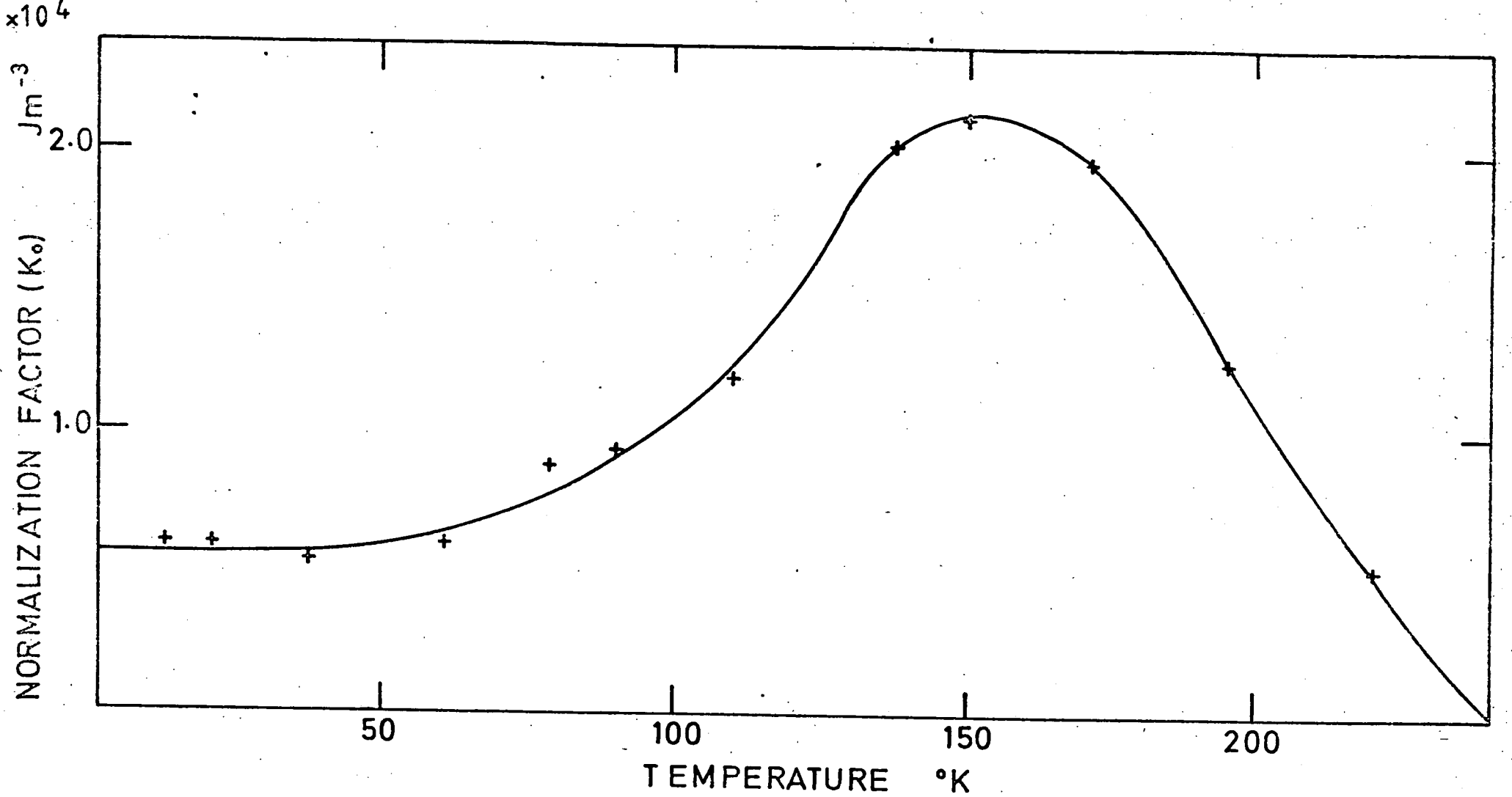

FIGURE 5.17 Temperature Dependence of K_o

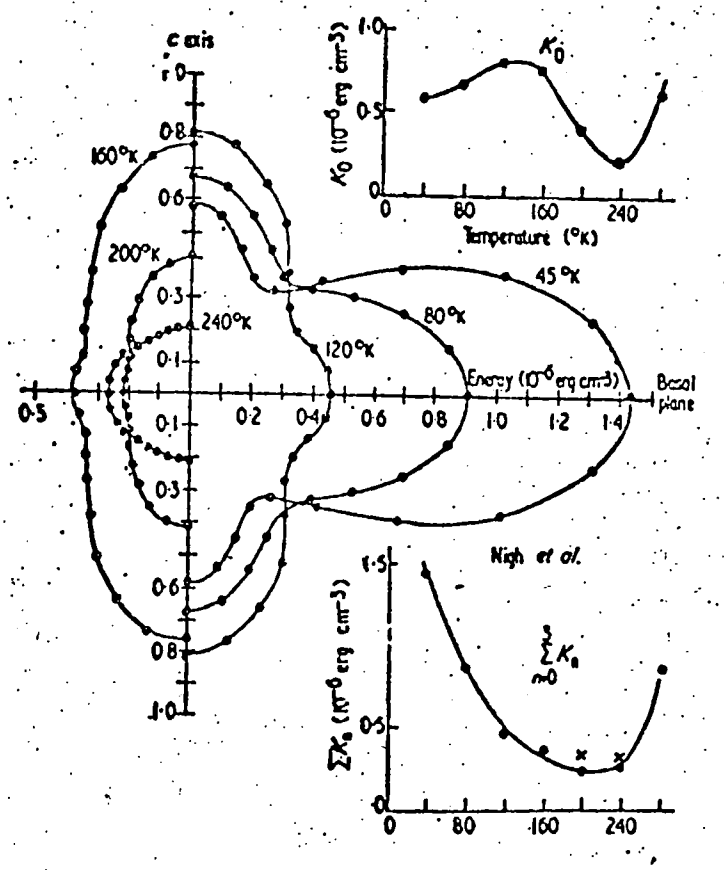

Polar energy diagrams in a plane containing the c axis at various temperatures, and variation of K_0 and $\sum_{n=0}^{3} K_n$ with temperature.

FIGURE 5.18 (AFTER DARBY and TAYLOR (1964))

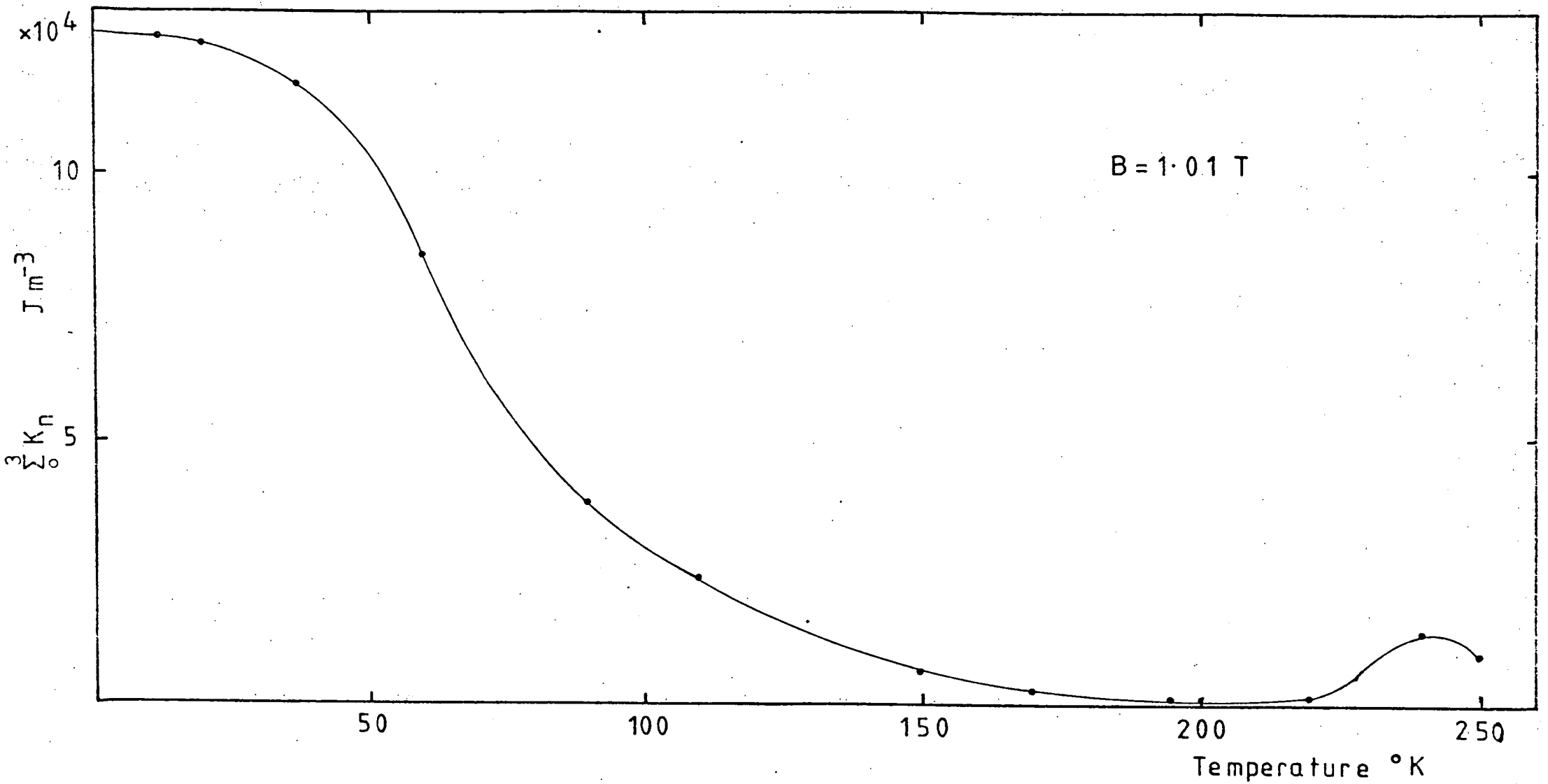

FIGURE 5.19 Temperature Dependence of ΣK_n

Taylor (1964) arrived at similar conclusions although their value of K_o was derived from the magnetization curves of Nigh et al. (1963). The validity of this procedure was discussed in section 4.2 and if we refer to the c axis magnetization curves of Roeland et al. (1975), Figure 5.20, the difficulties are apparent.

5.6 Theory of the Magnetocrystalline Anisotropy of Gadolinium

Following Callen and Callen (1966), who generalized the $l(l+1)/2$ power law for the single ion mechanism, there have been two detailed studies of the theory of magnetocrystalline anisotropy in gadolinium. Brooks and Goodings (1968) used a spin-wave model in which a crystal field of h.c.p. symmetry and magnetic dipole-dipole interactions were treated as first order perturbations to the isotropic exchange. They obtained the following relations for the temperature dependence of the anisotropy constants.

$$\begin{aligned} K_1(T) &= \left[K_1^{CF}(0) + \frac{8}{7} K_2(0) + \frac{8}{7} K_3(0) \right] M_T^{3} \\ &\quad - \left[\frac{8}{7} K_2(0) + \frac{144}{77} K_3(0) \right] M_T^{10} \\ &\quad + \frac{8}{11} K_3(0) M_T^{21} + E M_T^{2} \end{aligned} \tag{5.7}$$

$$K_2(T) = \left[K_2(0) + \frac{8}{11} K_3(0) \right] M_T^{10} - \frac{18}{11} K_3(0) M_T^{21}$$

$$K_3(T) = K_3(0) M_T^{21} \tag{5.8}$$

$$K_4(T) = K_4(0) M_T^{21}$$

Where M_T is the reduced magnetization and $K_n(0)$ the value of the anisotropy constant at OK. K_1^{CF} indicates the contribution to K_1 from the crystal field and E is the dipole-dipole contribution. The derivation of equations 5.7 and 5.8 used linearized spin wave theory and it is assumed that only the ground and first excited states are populated. Both these

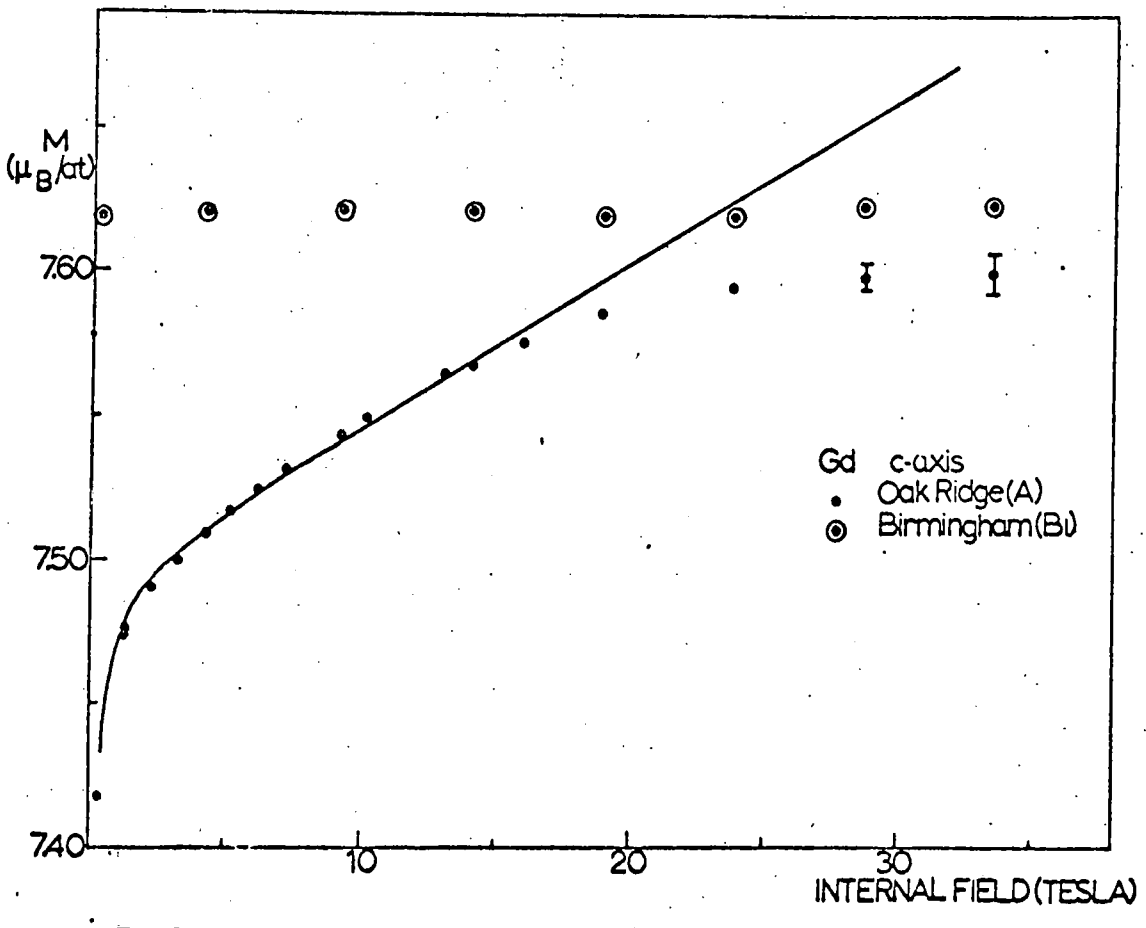

FIGURE 5.20 Magnetization at 4·2 K
(AFTER ROELAND et.al.(1975))

approximations apply only to low temperatures although Brooks and Goodings (1968) concluded that equations 5.7 and 5.8 should have a wider temperature range than spin wave theory would suggest. The expressions for K_2, K_3, and K_4 are in agreement with the low temperature approximation of Callen and Callen (1966) where

$$\hat{I}_{l+\frac{1}{2}} \rightarrow M_T^{l(l+1)/2}$$

The comparisons with the experimental results available at that time are shown in Figure 5.21(a). The value of E for gadolinium was determined to be 0.724×10^4 J_m^{-3} but even after correcting the experimental results of K_1 for magnetoelastic straining of the crystal, equation 4.14, no satisfactory agreement with equation 5.7 was found. It should be noted that the values of M_T were obtained from the data of Nigh et al. (1963) and would need slight modification in the light of the new value of the saturation magnetization as determined by Roeland et al. (1975).

Yang (1971) extended the ideas of Callen and Callen (1965) on the spin-orbit coupling mechanism of magnetostriction and derived a general expression for magnetic anisotropy in hexagonal crystals using quantum mechanical wave theories. These expressions, equations 4.31 and 4.32, include both single-ion and two-ion contributions with no correlation. The expressions were fitted to the data of Graham (1963) using the magnetization data of Nigh et al. (1963) and the results are shown in Figure 5.21(b). Analytically the results of Yang (1971) were expressed as

$$\frac{K_1(T, H)}{K_1(O, H)} = 13.31\,\hat{I}_{5/2}(T, H) - 3.63\,\hat{I}_{9/2}(T, H) - 8.5\,m^2(T, H) \qquad (5.9)$$

$$\frac{K_2(T, H)}{K_2(O, H)} = \hat{I}_{9/2}(T, H)$$

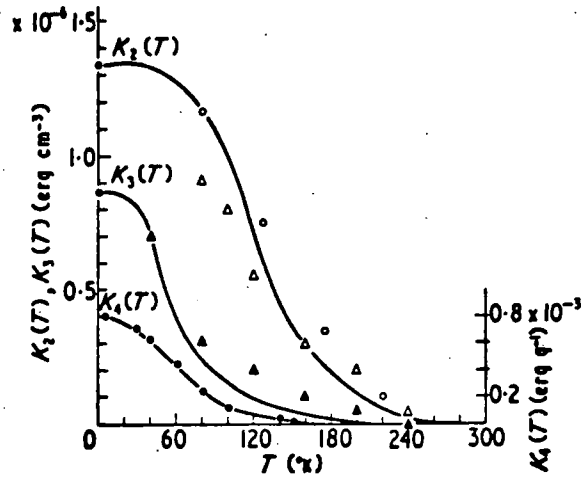

Temperature dependence of the second, third and fourth anisotropy constants. The full curves represent theoretical results using the magnetization data of Nigh *et al.* (1963). The theoretical curve for $K_4(T)$ is due to Graham (1966). The experimental data are represented by typical points: ▲ K_3 (Corner *et al.* 1962), △ K_2 (Corner *et al.* 1962), ○ K_2 (Graham 1963), ● K_4, $K_2(0)$, $K_3(0)$ (Graham 1966, Graham 1967, unpublished).

(a)

(AFTER BROOKS AND GOODINGS (1968))

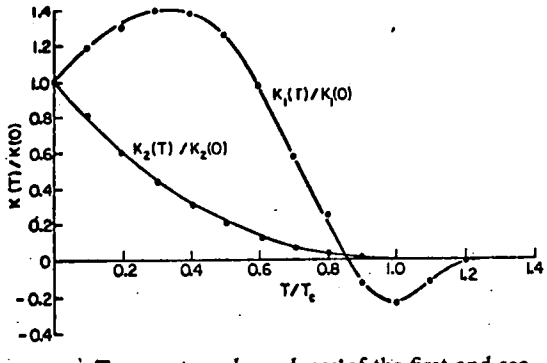

Temperature dependence of the first and second magnetic anisotropy constants of Gd. Solid curve represents the experimental data while dotted points are calculated from the theoretical equation.

(b)

(AFTER YANG (1971))

FIGURE 5.21

Yang (1976) notes that because of the large number of variable parameters used, four for K_1 and two for K_2, any set of experimental data could be matched by equations 4.31 and 4.32. The constants can, in principle, be calculated but greater detail of the crystal field than is available at present would be required.

The general conclusions of Brooks and Goodings (1968) and Yang (1971) are the same in that the anisotropy of gadolinium is due to both single and two ion contributions for K_1 while K_2 is of single ion origin only. Brooks and Goodings (1968) also conclude that K_3 and K_4 should be of single ion origin only. The present data for the magnetocrystalline anisotropy shows general agreement with the form of the experimental constants used by Brooks and Goodings (1968) and Yang (1971) (Corner et al., 1962; Graham, 1963, 1967) for K_1 and K_2. The reversal of the sign of K_1, which is not removed by any correction and must be correct for the easy direction to exhibit the behaviour that it does, is a strong argument that there are two competing interactions involved. K_2 shows a monotonic increase and is well behaved and gives reasonable agreement with the results of Yang (1971), the slight variations being due to a K_3 contribution not considered by Yang (1971). K_4 exhibits a similar behaviour to K_2. The results of Graham (1967) were fitted by a 21^{st} power law and they are in reasonable agreement with the present data. The behaviour of K_3 is not that predicted by Brooks and Goodings (1968). The values of K_3 down to 50 K are in reasonable agreement with the K_3 of Corner et al. (1962) but below that temperature, where Corner et al. (1962) indicate an increasing value of K_3, the present values decrease, Figure 5.11. The extrapolated values of K_3 show a more consistent behaviour with a gradual increase as the temperature decreases. The extrapolated value is in sharp contrast with that of Corner et al. (1962).

The only other measurements of K_3 have been made by the Japanese workers, Tajima (1971) and Tohyama and Chikazumi (1973) but comparisons are difficult for reasons already noted in section 5.5.1. Possible expanations for the behaviour of K_3 are as follows:

(a) K_3 could be very field dependent due to its small magnitude in comparison with K_1 and K_2.

(b) What we are observing as K_3 is, in fact, a K_3' in which a higher order anisotropy constant is a component.

(c) There could be a two-ion contribution to K_3. The fact that the values of K_3 are very erratic at low fields, Table 5.4, would suggest that (a) is the most likely cause of the odd behaviour of K_3, the extrapolated values giving the true indication of the behaviour of K_3.

5.7 The Effect of Nonmagnetic Inclusions on the Easy Direction

As mentioned in section 5.1 the previous investigations of the anisotropy and easy direction of gadolinium have been carried out using crystals of varying quality. In such material it was common to observe hexagonal platelets precipitated parallel to the basal plane. Figure 5.22 shows such a platelet in a crystal of gadolinium originally obtained from Metals Research Ltd., Cambridge. Its purity was given as 3N (99.9%) with respect to metallic impurities. The platelets were probably gadolinium oxide and from examination of micrographs such as Figure 5.22 the inclusion content can be estimated as typically 1 to 2% by volume. The crystals used in the present investigation showed no such inclusions. It will be shown in this section that the demagnetizing factor of these inclusions contributes a term to the uniaxial anisotropy which is sufficient to explain the variation in the measured values of the easy direction.

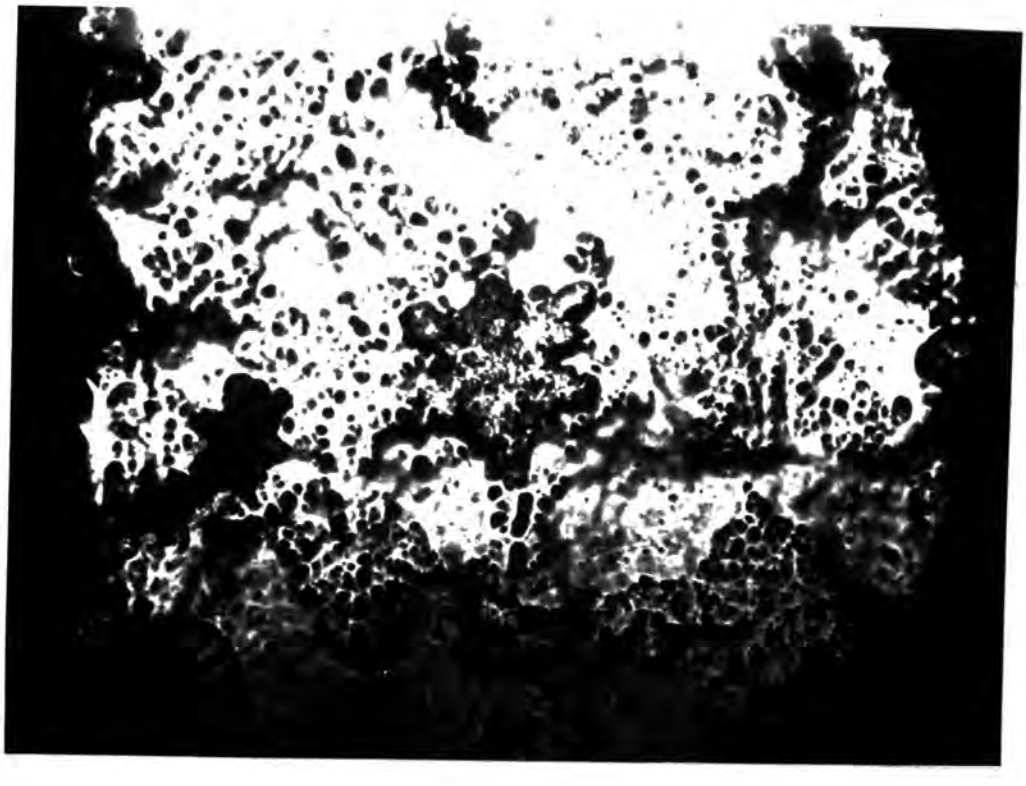

Gd F Basal Plane

200 μm

FIGURE 5.22 An Inclusion in a Gadolinium Crystal

At the surface of a non-magnetic inclusion embedded in a ferromagnetic body there appear 'free poles' the density of which is proportional to the intensity of the magnetization of the ferromagnet. The magnetic field induced by these 'free poles' is parallel to the magnetization and is given by

$$H_{in} = \frac{NM_s}{\mu_o} \qquad (5.10)$$

where N is the demagnetizing factor of a magnetic body of the same shape as the inclusion. The magnetostatic energy associated with the inclusion is thus

$$E_s = \frac{NM_s^2}{2\mu_o} \quad \text{per unit volume of inclusion}$$

For the purposes of this calculation we will consider the case of thin discs of diameter d and thickness t, ($d \gg t$), lying in the basal plane. Except with respect to the small basal plane anisotropy this is a good approximation to the hexagonal platelets observed. When the magnetization makes an angle θ to the c axis there is both a magnetocrystalline anisotropy term E_k and an inclusion shape anisotropy term E_s in the total anisotropy energy E_T. Thus for the total anisotropy energy per unit volume we have

$$E_T = E_k + E_s \qquad (5.11)$$

where
$$E_k = K_o + K_1 \sin^2\theta + K_2 \sin^4\theta + K_3 \sin^6\theta \qquad (5.12)$$

and
$$E_s = \frac{M_s^2 V}{2\mu_o} (N_\perp \cos^2\theta + N_{11} \sin^2\theta) \qquad (5.13)$$

Here $N_\perp$ and N_{11} are the geometric demagnetization factors perpendicular and parallel to the plane of the inclusion platelet and V is the volume fraction of inclusions. Therefore we have

$$E_T = (K_o + N_\perp V M_s^2/2\mu_o) + \left[K_1 - \frac{VM_s^2}{2\mu_o} (N_\perp - N_{11})\right] \sin^2\theta + K_2 \sin^4\theta + K_3 \sin^6\theta \qquad (5.14)$$

So to a first approximation the shape anisotropy predominantly affects the second term in the energy expansion, leading to an effective anisotropy constant K_1' given by

$$K_1' = K_1 - V M_s^2 (N_\perp - N_{11})/2\mu_o \qquad (5.15)$$

For a thin disc $N_\perp + 2 N_{11} = 1$ (5.16)

and equation 2.12 approximates to

$$N_{11} = \frac{\pi}{4k} \qquad (5.17)$$

where $k = \frac{d}{t}$

$$\text{Explicitly } K_1' = K_1 - \frac{V M_s^2}{8k\mu_o} (4k - 3\pi) \qquad (5.18)$$

Figure 5.23 shows the variation of K_1' at 170 K with the volume fraction of inclusions for various values of k. It can be seen that the presence of 1 to 2% volume fraction of inclusions can lead to a significant variation in the value of K_1.

The effective easy direction is given by

$$\theta_E = \sin^{-1}\left[\frac{-K_2 \pm (K_2^2 - 3 K_1' K_3)^{\frac{1}{2}}}{3 K_3}\right]^{\frac{1}{2}} \qquad (5.19)$$

Figure 5.24 shows the variation of the effective easy direction with inclusion content using the present values of the anisotropy constants at 1 Tesla. The presence of 0.8% of inclusions has a marked effect on the easy direction and yields a value in agreement with that of Corner et al. (1962). On increasing the oxide content to 1.5%, the easy direction enters the basal plane and this would seem to explain the results of Graham (1962) and Franse and Mihai (1977), although in the case of Franse and Mihai (1977) their crystal had also been used for

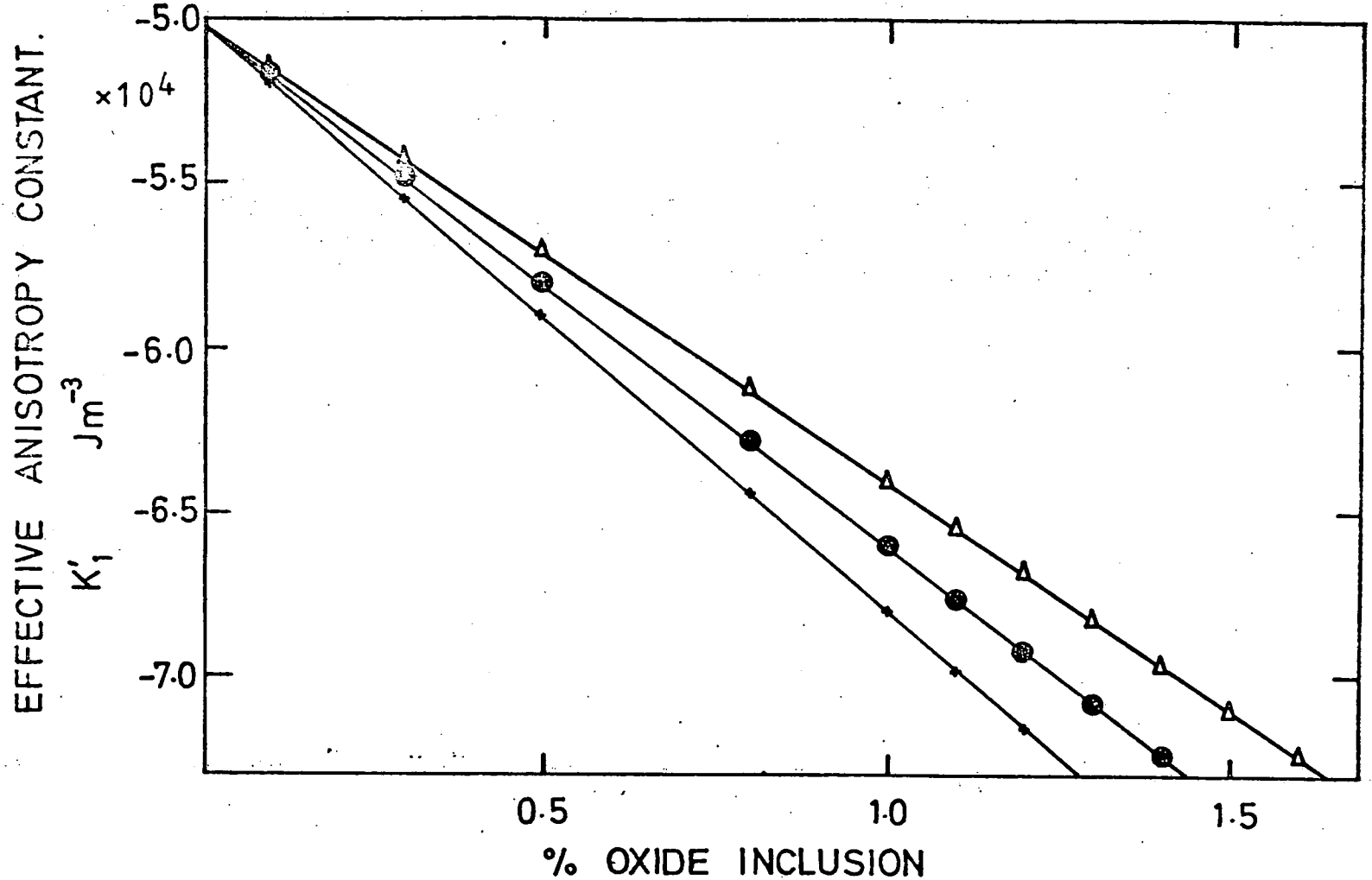

FIGURE 5.23 Variation of K_1 with Inclusion Content at 170 K

+ k = 100
• k = 20
Δ k = 10

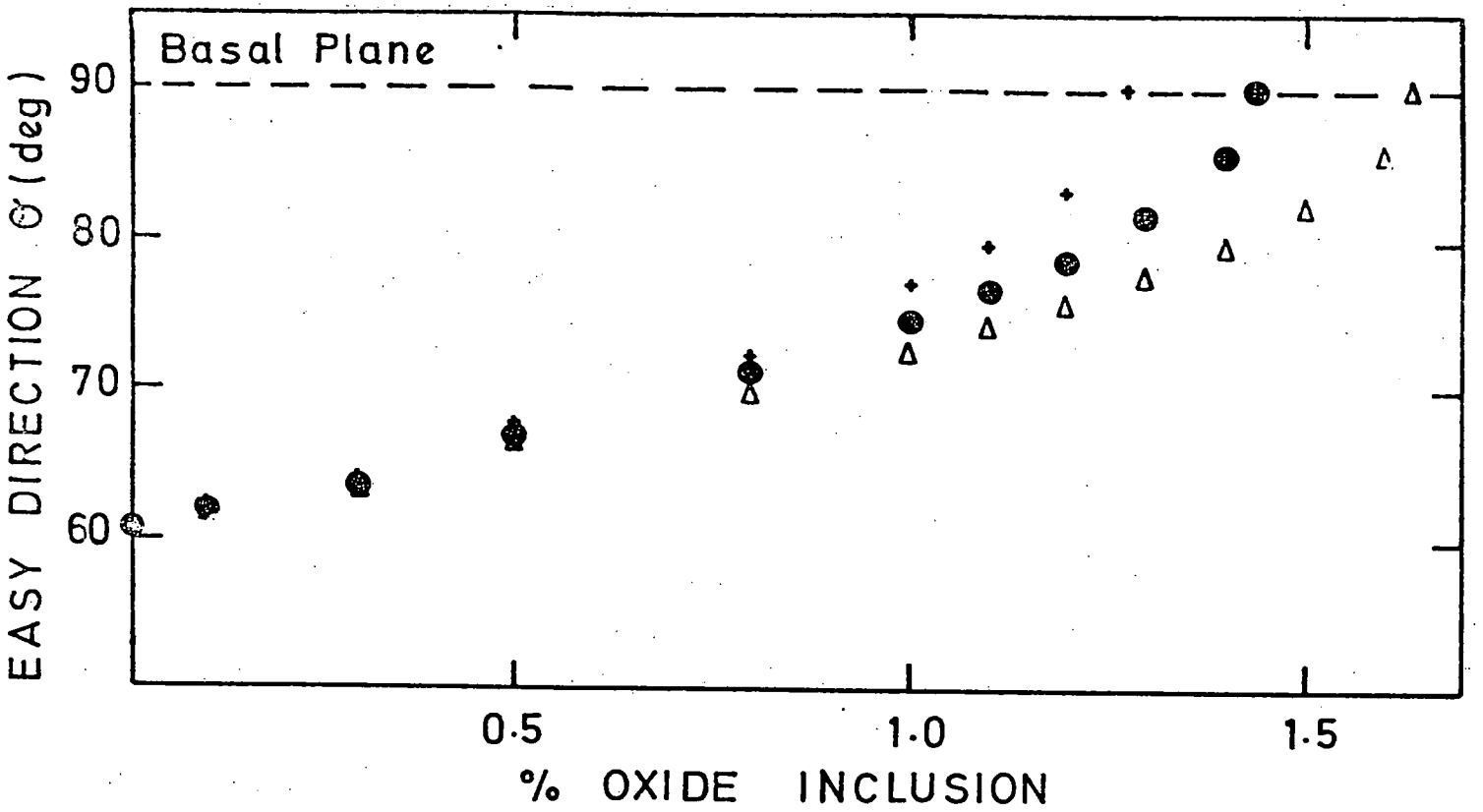

FIGURE 5.24 Variation of Easy Direction with Inclusion Content at 170 K

+ k = 100
• k = 20
Δ k = 10

high pressure experiments and strain could also have affected the measured easy direction. Figures 5.22 and 5.23 were plotted using the anisotropy constant values at 170 K. This temperature was chosen as the easy direction has its maximum value of cone angle, Figure 5.14, and Franse and Mihai report the basal plane to be easy, Figure 5.1(b).

This treatment gives a simple explanation of the various easy directions previously reported. It would also give rise to variations in the anisotropy constants. Only K_1 was considered here but a multipole expansion of equation 5.13 to take into account the exact shapes of the inclusions would introduce corrections to K_2 and K_3. The fact that all the measurements of K_4 are in reasonable agreement gives some support to this treatment as the platelets would have little effect on the basal plane anisotropy.

Lee (1977) has suggested that the variance in easy direction is due to a magnetostrictive contribution of the form of equation 4.14 arising from the differential thermal expansion of the inclusions and the bulk gadolinium. The effect of such a mechanism is difficult to calculate but if we assume isotropic magnetostriction then we can express the magnetoelastic energy E_σ as

$$E_\sigma = -\frac{3}{2} \lambda_s \sigma \cos^2\theta \qquad (5.20)$$

where λ_s is the magnetostriction constant, σ the applied stress and θ the angle between the magnetization and the stress. The stress due to an inclusion in the basal plane will be principally along the c axis. Therefore we have a contribution to K_1 of

$$K_1' = (K_1 + \frac{3}{2} \lambda_s \sigma) \qquad (5.21)$$

We can estimate the required value of σ to make the basal plane easy. At 170 K, taking λ_s from Corner and Hutchinson (1960), the required value of σ is approximately 10^9 N m^{-2}. Whether this order of stress could be

introduced by the inclusions is difficult to estimate. Any such stress effect would add to the magnetostatic effect (as λ_s is negative) and therefore reduce the amount of inclusion content required to make the basal plane easy.

The actual composition of the inclusions in the gadolinium crystals is unknown. The major impurity in the crystals used in the present work was oxygen (100 atomic p.p.m.). This would suggest that oxygen would also be the major impurity in poorer quality crystals and that the inclusions would be gadolinium oxide. It is important that when physical measurements are made on crystals the material used should be properly characterized with respect to impurities and lattice defects.

CHAPTER SIX

Magnetic Domains

6.1 Introduction

The concept of magnetic domains was introduced in Chapter 2 to explain how a ferromagnetic material can exist in a demagnetized state. It was also indicated in Chapter 2 that the formation of magnetic domains can dramatically reduce the large magnetostatic energy of a magnetized body. The first experimental evidence for the existance of magnetic domains was the discovery of the Barkhausen effect (Barkhausen (1919)) but it was not until thirteen years later that Bitter (1932) first observed magnetic domain structures on the surface of a ferromagnet and confirmed the domain hypothesis first put forward by Weiss (1907). Observations of magnetic domains have now been made on a wide variety of magnetic materials, including antiferromagnets, using a number of techniques. The theory of magnetic domains has also been extensively developed. The basics of domain theory are discussed in the classic review of Kittel and Galt (1956) and some experimental techniques for domain observation were treated by Carey and Isaac (1966).

6.2 Domain Walls

The introduction of ferromagnetic domains into a saturated magnetic material will reduce E_D and E_σ (equation 2.14) but will also introduce another energy term. The domain wall energy is just the total wall area times the wall energy per unit area, γ_w. The energy of a domain wall is principally determined by the magnetocrystalline anisotropy and the exchange energy. In an unstrained ferromagnetic material, with no external magnetic field acting upon it, the priciple domains are magnetized along the easy directions. Following Lilley (1950) we can derive an expression for the energy associated with rotating the magnetization from one easy direction to another i.e. the energy of a domain wall.

The turn angle between neighbouring spins is $\left(\frac{\delta\theta}{\delta x}\right) a$, where a is the lattice spacing and $\left(\frac{\delta\theta}{\delta x}\right)$ the spatial derivative of the angle of turn is not necessarily constant throughout the wall. The total exchange energy,

γ_E, in the wall due to the misalignment of the spins will be

$$\gamma_E = \frac{J S^2}{a} \int_{-\infty}^{\infty} \left(\frac{\delta\theta}{\delta x}\right)^2 dx \sin^2\psi \qquad (6.1)$$

per unit area of the wall surface. ψ is the angle between the magnetization vector, $\underline{M}_o$, and the normal to the domain boundary and θ is the angle between the projection of $\underline{M}_o$ on the boundary plane, $\underline{M}_p$, and some arbitrary (zero direction) in that plane, Figure 6.1. $\underline{M}_n$, the normal component of $\underline{M}_o$, should have the same value not only on each side of the boundary, but also within it. This corresponds to the absence of free poles in the transition region, i.e. $\nabla \cdot \underline{M} = 0$, so that there is no magnetostatic energy associated with the domain wall (Néel (1944)). The initial ($x = -\infty$) and final ($x = \infty$) directions of $\underline{M}_o$ are denoted by (ψ, θ_1) and (ψ, θ_2) respectively, i.e. these are the easy diections.

The total free energy per unit area of the domain boundary may be expressed in the form

$$\gamma_w = \gamma_A + \gamma_E \qquad (6.2)$$

where γ_A is the anisotropy energy associated with the boundary. Putting E_A equal to $\beta f_a(\psi, \theta)$, where βf_a is an expression for the reduced anisotropy energy so that βf_a is zero for the magnetization lying along an easy direction, the anisotropy energy in the boundary region is

$$\gamma_A = \int_{-\infty}^{\infty} \beta f_a \, dx \qquad (6.3)$$

per unit area.

Therefore

$$\gamma_{W_2} = \int_{-\infty}^{\infty} \left[\alpha a^2 \sin^2\psi \left(\frac{\delta\theta}{\delta x}\right)^2 + \beta f_a \right] dx \qquad (6.4)$$

where $\alpha = \frac{Js^2}{a^2}$

Using a simple variational procedure the stable spin arrangement can be obtained by minimizing the total energy for a small variation of the spin arrangement inside the wall.

When the angle θ of a spin at $x = x$ is changed by $\delta\theta$ the total wall energy is changed by

$$\delta\gamma = \int_{-\infty}^{\infty} \left[2\alpha a^2 \sin^2\psi \left(\frac{\delta\theta}{\delta x}\right)\left(\frac{\delta(\delta\theta)}{\delta x}\right) + \beta \frac{\delta}{\delta\theta} f_a(\psi,\theta) \, \delta\theta \right] dx$$

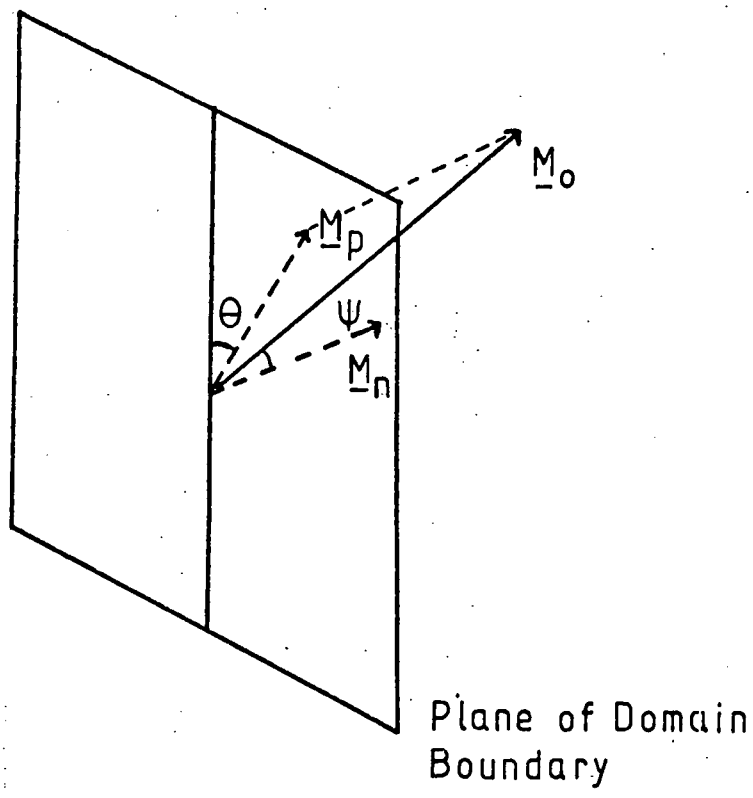

FIGURE 6.1 Domain Boundary Notation

which should vanish for a stable spin arrangement.

$$A s \int dx\, 2\alpha\, a^2 \sin^2\psi \left(\frac{\delta\theta}{\delta x}\right)\left(\frac{\delta(\delta\theta)}{\delta x}\right) \text{ is equal to}$$

$$\int -2\alpha\, a^2 \sin^2\psi \frac{\delta^2\theta}{\delta x^2}\, dx, \text{ we have}$$

$$\beta \frac{\delta f}{\delta \theta} a(\psi,\theta) \quad -2\alpha\, a^2 \sin^2\psi \left(\frac{\delta^2\theta}{\delta x^2}\right) = 0$$

This is an Euler equation which can be solved by multiplying by $\frac{\delta\theta}{\delta x}$ and then integrating, $\int_{-\infty}^{z=z} dz$.

$$\beta f_a(\psi,\theta) = \alpha\, a^2 \sin^2\psi \left(\frac{\delta\theta}{\delta x}\right)^2 \qquad (6.5)$$

This equation indicates that the exchange and anisotropy energy contributions are equal throughout the domain wall. Therefore we can write,

$$\frac{dx}{d\theta} = \left(\frac{\beta f_a}{\alpha a^2}\right)^{-\frac{1}{2}} \sin\psi \qquad (6.6)$$

If we substitute equation 6.6 into equation 6.4 we obtain

$$\gamma_w = 2 \left(\frac{Js^2}{a}\right)^{\frac{1}{2}} \sin\psi \int_{\theta_1}^{\theta_2} (\beta f_a)^{\frac{1}{2}}\, d\theta \qquad (6.7)$$

for the wall energy per unit area. The wall thickness will be given by

$$x = \frac{Js^2}{a} \sin\psi \int_{\theta}^{\theta} (\beta f_a)^{-\frac{1}{2}}\, d\theta \qquad (6.8)$$

To estimate the thickness of the domain wall we note that the maximum rate of change of angle occurs at x=0. By assuming this rate of change to be constant throughout the wall a minimum value of the wall thickness δ is given by

$$\delta = (\theta_2 - \theta_1)\left(\frac{dx}{d\theta}\right)_{x=o} \qquad (6.9)$$

$$= (\theta_2 - \theta_1) \left[\frac{a\, \beta f_a\left(\frac{\theta_2 - \theta_1}{2}\right)}{Js^2}\right]^{-\frac{1}{2}} \sin\psi$$

In a simple uniaxial material where,

$$E_a = \beta f_a = K_1 \sin^2\theta$$

then

$$\delta = \pi \left(\frac{A}{2K_1}\right)^{\frac{1}{2}}$$

with the exchange constant $A = \frac{2Js^2}{a}$

These calculations only consider the anisotropy and exchange energy contributions to the domain wall but in some cases, for example the heavy rare earths where the magnetostriction is large, a magnetoelastic contribution must be added. This can be taken into account by expressing βf_a as

$$\beta f_a = \beta f_c + \beta f_m \qquad (6.10).$$

where βf_c is the magnetocrystalline anisotropy contribution and βf_m is the magnetoelastic contribution.

6.3 Domain Structures

The combination of equations 2.14 and 6.7 should give the magnetic structure of an unstressed ferromagnet in the demagnetized state,

$$\text{i,e.} \qquad E_T = E_D + \gamma_W A \qquad (6.11)$$

where A is the total wall area.

The major factors governing the domain sturcture in any particular material are,

a) its shape
b) its saturation magnetization
c) the effective anisotropy
d) the exchange energy

In practice it is very difficult to make accurate predictions of the precise domain structure for a given material, but the general principle in such calculations is to minimize the amount of magnetostatic energy present by introducing various domain systems. A brief outline will be given here of the types of structure that have been predicted in uniaxial materials as these are of the type expected in gadolinium.

In a uniaxial material there is only one easy direction and the type of wall that would be expected involves a 180^o rotation of the spins. The idea of such a wall was first put forward by Bloch (1932) and it is often known as a Bloch wall. The first quantitative theory was derived by Landau and Lifshitz (1935) and they proposed a parallel-plate domain structure with triangular prism shaped closure domains to enclose the flux totally within the specimen, Figure 6.2a. This structure gives a total energy per unit volume of

$$E_T = \frac{\gamma L}{D} + \frac{KD}{2} \qquad (6.13)$$

where D is the width of the domains and L is the length of the crystal. Kittel (1949) proposed three models for a material where the anisotropy is very large and the formation of closure domains would be energetically unfavourable. They are illustrated in Figures 6.2 b, c and d and the energy associated with each model is as follows.

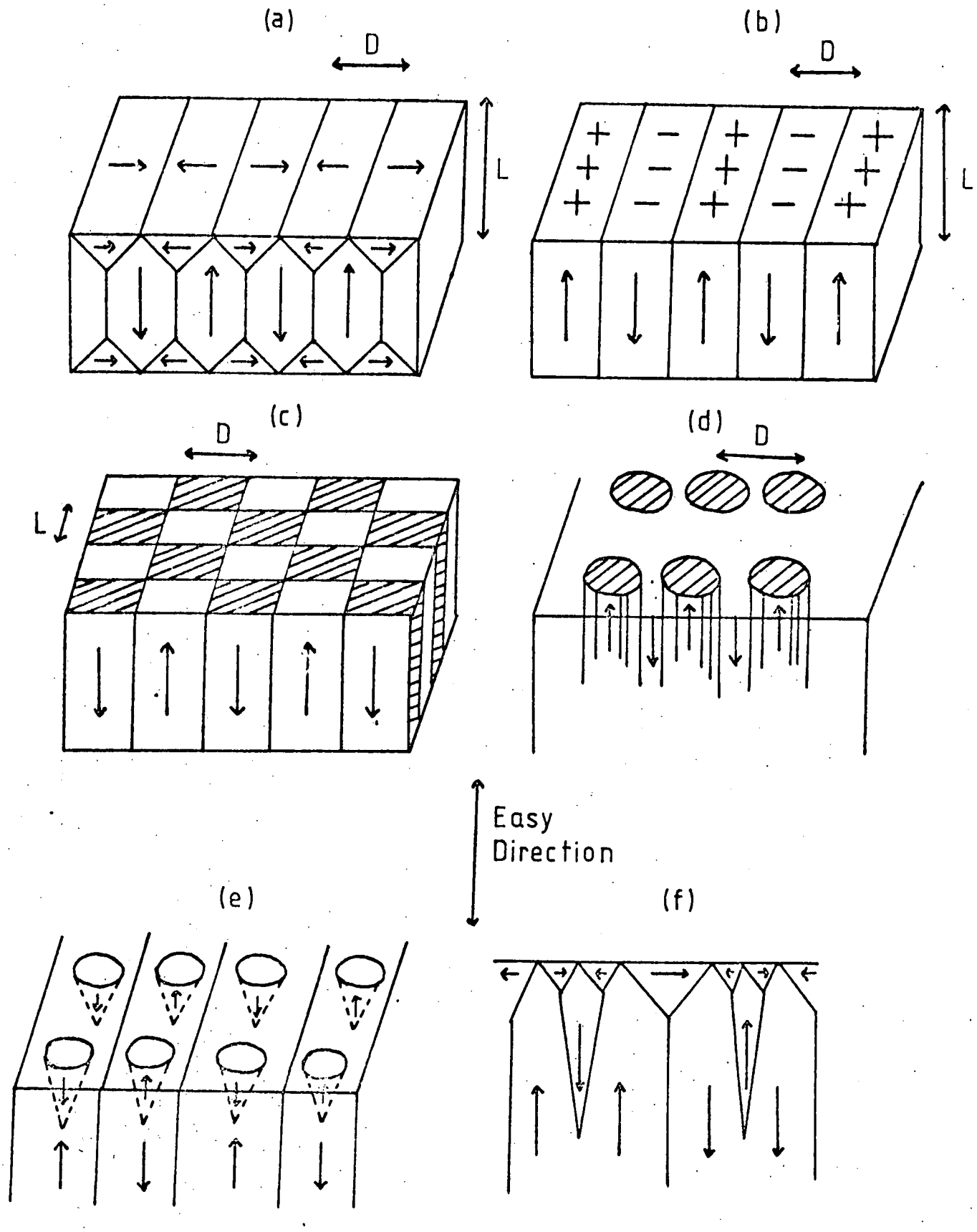

FIGURE 6.2 Uniaxial Domain Structure Models

Figure 6.2 b $$E_T = 1.705\ M_S^2 D + \gamma \frac{L}{D} \qquad (6.13)$$

Figure 6.2 c $$E_T = 0.53\ M_S^2 D + \gamma \frac{L}{D} \qquad (6.14)$$

Figure 6.2 d $$E_T = 0.374\ M_S^2 D + \gamma \frac{L}{D} \qquad (6.15)$$

Minimization of these expressions will yield the optimum value for the domain width, D_o.

$$D_o = \left(\frac{\gamma L}{C M_S^2} \right)^{\frac{1}{2}} \qquad (6.16)$$

where C is the appropriate geometric factor.

The expressions apply to an infinite parallel plate.

Goodenough (1956) put forward a reverse closure domain structure, Figure 6.2e, to minimize the surface magnetostatic energy with only a small increase in wall energy. This type of structure can become very complex in thick crystals where near the surface the walls show an undulatory deformation and the formation of multiple domains of reverse magnetization. This type of behaviour is shown in Figure 6.3a. The observation of such complex patterns on single crystals of BiMn alloys and cobalt have been intrepreted by Goodenough (1956), Tukata (1962), Kozlowski and Zietek (1966) and Kandaurova and Beketov (1975). Using a simple model of the observed surface structure they then minimized the surface magnetostatic energy with respect to the geometric factors of the model, Figure 6.3 b. Lifshitz (1944) proposed an alternative closure structure, Figure 6.2f, which extended the model of Landau and Lifshitz (1935) to take into account thick crystals as the Landau and Liftshitz (1935) model becomes unstable abo ve a certain crystal thickness. In certain materials where the anisotropy energy, K, is greater than the demagnetization energy, $2\pi M_s^2$ (for an infinite plate with M_s perpendicular to the plane of the plate), it is found that when the plate is thin enough isolated cylindrical domains can appear known as magnetic bubbles and are finding application in computer memory devices. An introduction to magnetic bubbles has been given by Jones (1976). Privorotskii (1976) has reviewed and extended the theories of Landau and Liftshitz (1935). He obtained relationships for the multiple branching of reverse domains illustrated in Figure 6.3 a, these were

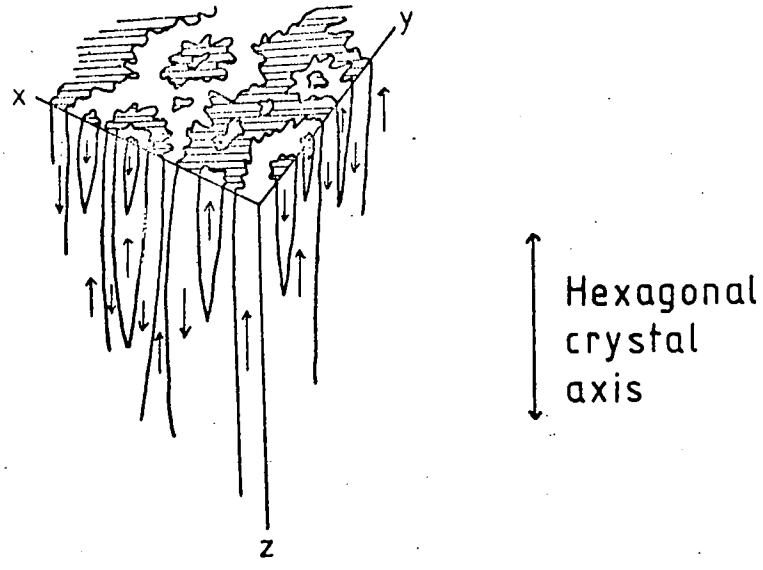

(a)

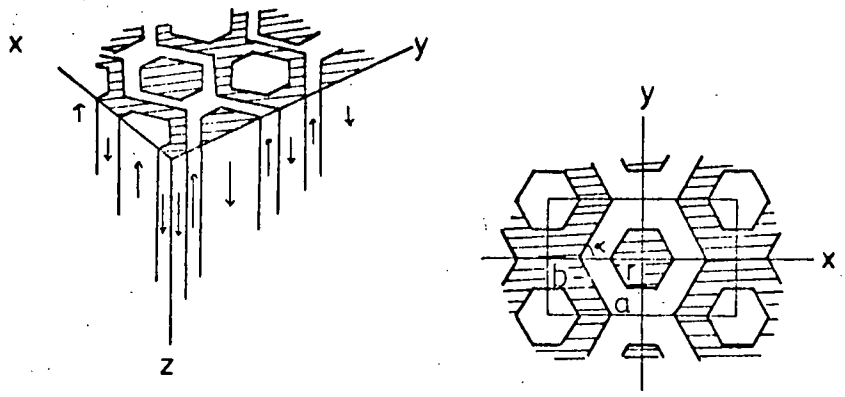

(b)

FIGURE 6.3 (a) Typical Domain Structure
(b) Simple Model of (a)
(AFTER KOZLOWSKI and ZIETEK(1965))

$$h = 0.117\, l$$
$$h_1 = h\left(1 - \frac{1}{3}\sqrt{3}\right) \qquad (6.17)$$
$$h_n = \frac{h_1}{(3\sqrt{3})^{n-1}}$$

where l is the thickness of the crystal, h the length of the largest reverse domain, and h_n the lengths of successively smaller reverse domains within each other.

A special case, when the anisotropy and magnetostriction disappear, has been discussed by Kittel and Gault (1956). Here all semblance of a discrete domain structure will disappear and the requirements of flux closure govern the orientation of the spins within the sample. This limiting case may be expected to occur when the Bloch wall width becomes comparable with the sample dimensions. The possible domain structures proposed by Kittel (1949) are shown in Figure 6.4 a and b.

In Figure 6.2. it is assumed that the magnetization in the main slab domains always lies parallel to the easy direction. However near to the surface the magnetization vector may be rotated slightly away from the easy direction due to the demagnetization field. This will produce a component of magnetization perpendicular to the easy direction. Thus, for small magnetization rotation, the material may be considered to have a constant, effective permeability, μ^*, perpendicular to the easy direction. Williams et.al. (1949) calculated a value for μ^* as

$$\mu^* = 1 + \frac{2\pi M_s^2}{K} \qquad (6.18)$$

6.4. Methods for Observing Magnetic Domains

6.4. 1 Colloid Techniques

The first direct method of observing magnetic domains was devised by Bitter (1931) who used a colloidal dispersion of magnetic iron oxide. If a small stray field exists on the surface of a magnetic sample, such as the intersection of a domain wall with the surface, the magnetic particles will be attracted by the stray field and thus produce a pattern determined by the

FIGURE 6.4 Possible Zero Anisotropy Domain Structures (AFTER KITTEL and GALT (1956))

stray fields, (Craik (1966)). This technique requires a well polished and strain free surface to produce domain patterns which represent the true domain structure. Surface strain can produce a thin layer of very fine domain structure which gives rise to 'maze' patterns.

As the methods of sample and colloid preparation have improved (Garrood (1962)) the Bitter technique has found widespread application in the study of magnetic domains. The technique has the advantages of being relatively simple to use and allowing some dynamic observations, e.g. the effect of magnetic field (Rosenberg et.al. (1964)) and applied stress (Corner and Mason (1967)), to be made. The disadvantages are that it only 'images' the surface stray fields, which are not necessarily representative of the internal domain structure. Also, because of the nature of the colloid suspension, it has a limited temperature range of about 220K to 370K. A modified colloid technique, now known as the dry colloid technique, was developed by Hutchinson et.al. (1966) and Essman and Trauble (1966) to study domains at very low or very high temperatures. It has also been used very successfully to study the magnetic flux distribution in superconductors, Sarma and Moon (1967) and Trauble and Essmann (1966). The colloid techniques will be discussed in further detail in section 6.5.

6.4.2 Magneto-optical Techniques

There are two magneto-optic effects which can be used to observe magnetic domains. These are the Kerr effect, where the plane of polarization of polarized light is rotated on reflection from a magnetic surface, and the Faraday effect, where the plane of polarization is rotated as it passes through a magnetic material. Obviously the Faraday effect can only be used for transparent magnetic materials such as garnets and orthoferrites. The degree and sense of the rotation of the polarized light is proportional to the direction and magnitude of the saturation magnetization of the magnetic material under observation. Therefore domains magnetized in different directions will produce different amounts of rotation and will be visible in light-dark contrast when viewed through an analyser. These techniques have the advantage that studies of rapid domain movement can be made, but they also require very good quality surfaces. The rotation effects are small and hence viewing is usually through nearly crossed polarizing elements and therefore high intensity illumination is required. Shilling and Houze (1974)

have reviewed the use of the Kerr effect on silicon-iron and Jones (1976) the use of the Faraday effect for observing domains in garnet materials.

6.4.3 Electron Microscopy

Under certain conditions the domain structure of thin foils and films can be seen in the transmission electron microscope (T.E.M.). This uses the Lorentz force on an electron in a magnetic field and is therefore known as Lorentz microscopy. It provides a means of observing fine scale domain phenomena and also their interaction with defects in the sample, which will also be imaged. The samples used in T.E.M. are very thin, of the order of 100 nm, and therefore the domain structures observed in them are not necessarily typical of the bulk material. It is possible using T.E.M. to measure the actual domain wall widths. Carey and Isaac (1966) gave a detailed treatment of T.E.M. as applied to the observation of magnetic domains.

Over the past decade the scanning electron microscope (S.E.M.) has been used to observe domain structures. This has several advantages over T.E.M. in that bulk samples can be investigated and the problems with the magnetic effect of the objective lens are removed. The magnetic contrast can be obtained in several ways and these have been discussed by Fathers and Jakubovics (1977).

The electron microscope can also be used in conjunction with the colloid technique. Here a carbon film replica of the colloid patterns is taken and then investigated using the T.E.M. to obtain high resolution, Craik and Tebble (1961).

6.4. 4 X-ray Diffraction

The application of X-ray techniques to the study of magnetic domains is unusual amo ng the methods described here in that it is the only method that does not interact directly with the magnetization. What is observed is the local variation in the X-ray diffaction conditions according to Bragg's Law due to the magnetostrictive deformation on either side of a domain wall. The method can show interior structures as well as surface domain configurations and also can image dislocations and low angle boundaries on the same X-ray topograph as the domains. One disadvantage of the method is that materials with a small magnetostriction do not give good contrast. A recent development which has dramatically reduced the exposure time required to take an X-ray topograph (usually of the order of 10-12 hours) is the use of synchrotron radiation. The application of X-ray techniques to domain studies has been

comprehensively reviewed by Tanner (1976).

6.4. 5 Neutron Diffraction

Neutrons are, because of their magnetic moment, a unique probe for the investigation of magnetic domains. They can be used to distinguish ferromagnetic domains through Larmor precession in simple transmission and both ferro and antiferromagnetic domains from Bragg diffraction experiments (in analogy with the X-ray techniques). The former method will give information about the relative numbers of various kinds of domains, domain distributions and average domain size. The second approach produces the same information as the X-ray techniques only the exposure times are much longer (of the order of days) and the resolution is not as good due to geometric factors such as the divergence of the diffracted beam. Schlenker and Baruchel (1978) have reviewed the progress of neutron diffraction as applied to magnetic domains.

6.4. 6 Other Techniques

All the techniques mentioned above will produce an image of the domain structure. A further technique which has been used to investigate domain structures is the use of a magnetic probe. This could be a search coil, magnetoresistance element or a Hall probe and a map of the magnetic field intensity above a magnetic surface can be plotted. Obviously, the resolution will depend upon the size of the probe and the accuracy of the scanning machinery. Such techniques were discussed by Carey and Isaac (1965) but are not in general use at the present time.

Another technique which has been used to observe domains is to electro-etch a magnetic material in the presence of a magnetic field, Evans and Garrett (1973). The exact mechanism which leads to the preferential etching of the domains is not known.

6.5. Techniques used in the Present Investigation

For observing domains in bulk gadolinium the Faraday effect (as the crystal is opaque), T.E.M. and neutron diffraction (due to the high absorbtion of neutrons by Gd.) cannot be considered. X-ray topography would be difficult due to the low magnetostriction of gadolinium.

Saad (1977) attempted unsuccessfully to use both the Kerr effect and S.E.M. The main problem with both these methods when applied to gadolinium, and the rare earths in general, is the preparation and maintenance of a perfectly flat and uncontaminated surface. For these reasons the wet and dry colloid techniques were used in the present work.

6.5. 1 Domain Pattern Formation by Fine Particles

Kittel (1949) and Bergmann (1956) derived limits for the formation of domain wall patterns by a colloid of fine, single domain magnetic particles. These may be summarized as

$$3\left(\frac{kT(1+\mu^*)}{2\pi M_s M_p \delta}\right)^{\frac{1}{2}} \leqslant d \leqslant 3\left(\frac{2kT}{\pi^2 M_s^2}\right)^{\frac{1}{3}} \qquad (6.19)$$

where, M_s is the saturation magnetization of the material under investigation.

M_p is the saturation magnetization of the fine particles.

δ is the domain wall width,

d is the diameter of the fine particles, assumed spherical.

Calculations based on this equation are approximate and usually at room temperature the colloid properties required are produced by trial and error. The room temperature colloid used in this work was a commercial water based magnetic fluid, 'Ferrofluid AO1', produced by Ferrofluidics Corporation, Massachusetts, U.S.A. This was found to be highly satisfactory when used in dilution.

Wyslocki and Zietek (1966) have discussed the interpretation of patterns obtained by the colloid technique in terms of the stray fields present in various situations.

6.5. 2 Production of Fine Particles for the Dry Colloid Technique.

The dry colloid technique, as used by Hutchinson et.al. (1965) and Essmann and Trauble (1966), uses fine magnetic particles produced by evaporation of the metal from a filament in a low pressure of an inert gas. In the present work the metal used was iron and the inert gas was helium. Investigations on fine particles produced by this technique have been carried out by a large number of workers over the past twenty years. This interest has been stimulated by the search for new magnetic

recording materials and also the investigation of quantum size phenomena in small particles. Most of these investigations have used particles produced at room temperature and the main results with regard to particle size will be summerized here. The five experimental parameters which govern the particle size are

a) the temperature of the filament,
b) the pressure of the inert gas (o.1 to 100 Torr)
c) the type of inert gas,
d) the type of metal to be evaporated,
e) the inert gas temperature.

The particles are assumed to grow from the vapour by two processes. First a condensation of the metal atoms take place to form small nuclei which then grow by coalescence. The exact theories of these growth processes have not been studied in detail and it is only recently that attempts have been made to quantify the processes (Kawamura (1973) and Kaito (1978)). In all the experimental investigations it was found that the pressure of the inert gas plays the major role in determining the size of the metal particles (Kimoto et.al. (1963), Wada (1967,1968)). Granquist and Buhrman (1976) investigated the size distribution of the particles and found that the logarithm of the particle volume has a Gaussian distribution which is what would be expected for a coalescence growth process. It should be noted that all the particles produced show distinct crystal habits (Uyeda (1974)).

Using equation 6.18 it should be possible to predict the size of the particles required to produce domain patterns at any temperature and hence the pressure of the inert gas required. Saad (1977) found extremely tight limits on the size of iron particles required to produce domain patterns on gadolinium at any particular temperature, but the estimation of the quantities μ^* and δ was extremely difficult.

It was found in the present work that domain patterms could be produced on silicon-iron at room temperature over a pressure range of 0.5 to 5 Torr of helium. The other two critical parameters to produce patterns are the amount of iron evaporated and the distance between the

specimen and the filament. These depend on the geometry of the evaporation system and must be determined by trial and error.

The dry colloid technique has been used successfully on a number of magnetic materials; Hutchinson et.al. (1965) and Caroni (1973) on silicon iron, Essmann and Trauble (1966) on cobalt, (both these investigations were at room temperature), Corner and Al-Bassam (1971) on terbium at 210K, Herring and Jakubovics (1973) on terbium and dysprosium at 4.2K and Corner and Saad (1977) on gadolinium at 77K.

CHAPTER SEVEN

Magnetic Domains in Gadolinium

7.1 Previous Work.

Magnetic domains in gadolinium were first observed by Birss and Wallis (1963) and Bates and Spivey (1964) using wet colloids modified for low temperature work. The former investigation was on a single crystal at 268K and the later was on a polycrystalline sample in the temperature region 180K to 210K. Both investigations suffered from poor contrast, but showed typical uniaxial type domain structures. Al Bassam and Corner (1969) used the wet colloid technique on good single crystals between 273K and 210K. They showed clearly the closure structure at a crystal edge on a $(11\bar{2}0)$ plane and complex patterns, with no perferred direction for the domain walls, on the basal plane. These observations were consistent with a uniaxial material with low basal plane anisotropy. This is what would be expected in gadolinium in that temperature range. Al Bassam and Corner (1969) also tried unsuccessfully to lower the temperature range by using the dry colloid technique. Corner and Saad (1977a, 1977b) have successfully used the dry colloid technique on good quality single crystals at 77K and interpreted the observed structure in terms of an easy cone of magnetization. Shilstein et.al.(1976) used the technique of small angle neutron scattering to investigate enriched Gd^{160} rolled sheet. They concluded that 180^{o} type boundaries are still preferred below 250K, i.e. the magnetization vector of neighbouring domains were located on different conical surfaces.

McKendrick et.al. (1977) and Chapman et.al.(1977) have investigated gadolinium foils using T.E.M. in the temperature range 160K to 300K. They observed parallel arrays of domain walls in basal plane foils, but these structures are thought to be a result of the foil

thickness (100μm) and the stress that had been introduced during their preparation.

In the present work the two magnetic phase transitions in gadolinium were investigated. These involve observations of domain structures around the Curie temperature (291K) and in the temperature region around and below 240K where the magnetization vector moves away from the c axis. For the former the Bitter wet colloid technique was used and for the low temperature work the dry colloid technique was employed.

7.2 Calculation of the Domain Wall Parameters.

Corner and Saad (1977b) have discussed the possible types of domain wall in an easy cone ferromagnet. Their results are summarised in Figure 7.1 where the 'possible modes' refer to the magnetization processes in a hexagonal crystal as discussed by Birss and Martin (1975). An estimation of the energy of each wall type was obtained by consideration of the anisotropy energy involved. Wall energy calculations have been made using equation 6.7, the full anisotropy expression (equation 4.5), the present values for the anisotropy energy at 90K and an estimation of the exchange energy obtained from the Curie temperature. The results are shown in Table 7.1. The integrations were carried out numerically using the values obtained for the anisotropy energy surfaces. The wall types 3b, 4a and 4b (Figure 7.1) have a very low energy which is to be expected as the basal plane anisostropy is very low. In the domain model of Corner and Saad (1977b) it is assumed that these wall types do not occur and that the magnetization is free to rotate about the easy cone. Wall type 3a has the next lowest energy, but it would produce a domain structure that would have a large magnetostatic energy associated with it. The present calculations confirm the estimates of Corner and Saad (1977b)

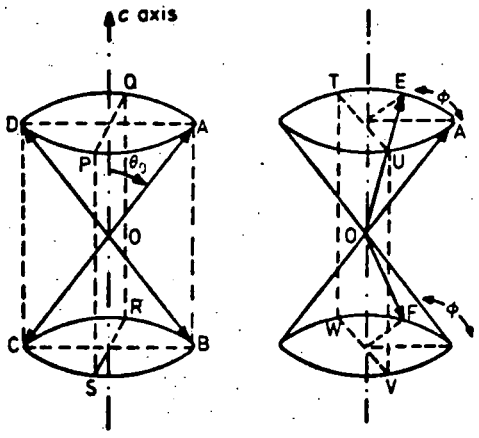

Magnetization directions and wall planes for various possible domain walls in an easy-cone ferromagnet

Characteristics of various possible walls in an easy-cone ferromagnet including relative wall energies for Gd at 77 K M_s is saturation magnetization.

Wall type	Possible modes	Separating magnetization directions	Angle through wall	Plane of wall	Normal component of magnetization	Maximum anisotropy energy term ($\times 10^6$ erg/cm^3)
1(a)	I, IIB	OA → OB	$\pi - 2\theta_0$	PQRS	$M_s \sin\theta_0$	$F_K(\pi/2) - F_K(\theta_0) + K_4 = 0{\cdot}525$
1(b)				ABCD	0	$F_K(\pi/2) - F_K(\theta_0) = 0{\cdot}523$
2	I	OA → OC	π	ABCD	0	$F_K(\pi/2) - F_K(\theta_0) + K_4 = 0{\cdot}525$
3(a)	I, IIC	OA → OD	$2\theta_0$	ABCD	0	$F_K(0) - F_K(\theta_0) = 0{\cdot}20$
3(b)				basal	$M_s \cos\theta_0$	$K_4 = 0{\cdot}002$
4(a)	I, IIC	OA → OE	$0 \rightarrow 2\theta_0$	TUVW	$M_s \sin\theta_0 \cos\frac{1}{2}\phi$	$K_4 = 0{\cdot}002$
4(b)				basal	$M_s \cos\theta_0$	$K_4 = 0{\cdot}002$
5(a)	I, IIB	OA → OF	$\pi - 2\theta_0 \rightarrow \pi$	TUVW	$M_s \sin\theta_0 \cos\frac{1}{2}\phi$	$F_K(\pi/2) - F_K(\theta_0) + K_4 = 0{\cdot}525$
5(b)				OAF	0	$F_K(\pi/2) - F_K(\theta_0) + K_4 = 0{\cdot}525$

FIGURE 7.1 (AFTER CORNER AND SAAD (1977b))

Wall Type	Wall Energy $J\ m^{-2}$
1b	$1{\cdot}03 \times 10^{3}$
2	$1{\cdot}43$
3a	$0{\cdot}40$
5b	$1{\cdot}82$

TABLE 7.1 Wall Energies at 90 K

that the most energetically favourable wall type is 1b. The estimation of the energy of wall type 5b is shown to be too small, the full integration procedure showing that the magnetization would sample a large section of the anisotropy surface in such a wall.

Using equations 6.7 and 6.9 and the anisotropy energy surface as above the temperature dependence of the wall energy and thickness was calculated. The calculation was for wall type 1b, which becomes a simple 180° Block wall above 240K. The results of the calculations are shown in Figures 7.2 and 7.3. The discontinuity of the curves is a result of the change of sign of K_1 at 240K and the very low total anisotropy energy in this region (Figure 5.19). If the total anisotropy energy did fall to zero then we would expect domain walls of zero energy and infinite thickness, i.e. a single wall throughout the whole crystal. Spin orientations of the type suggested by Kittel and Gault (1956) (Figure 5.4) would then be expected.

7.3 Experimental Techniques.

7.3.1 Bitter Wet Colloid Technique.

This technique was simple to use provided the surface of the crystal had been properly prepared. A drop of the Ferrofluid was placed on the crystal surface and then covered with a microscope cover slip to give a uniform film of colloid over the surface and reduce the evaporation rate of the colloid. Misting of the cover slip gave a lower temperature limit for this technique of 283K. Cooling was obtained by mounting the sample on a hollow copper block through which nitrogen gas was passed which had first been passed through a heat exchanger immersed in liquid nitrogen. The temperature could be controlled by varying the rate of flow of the nitrogen gas. The temperature was measured using a copper-constantan thermocouple, placed

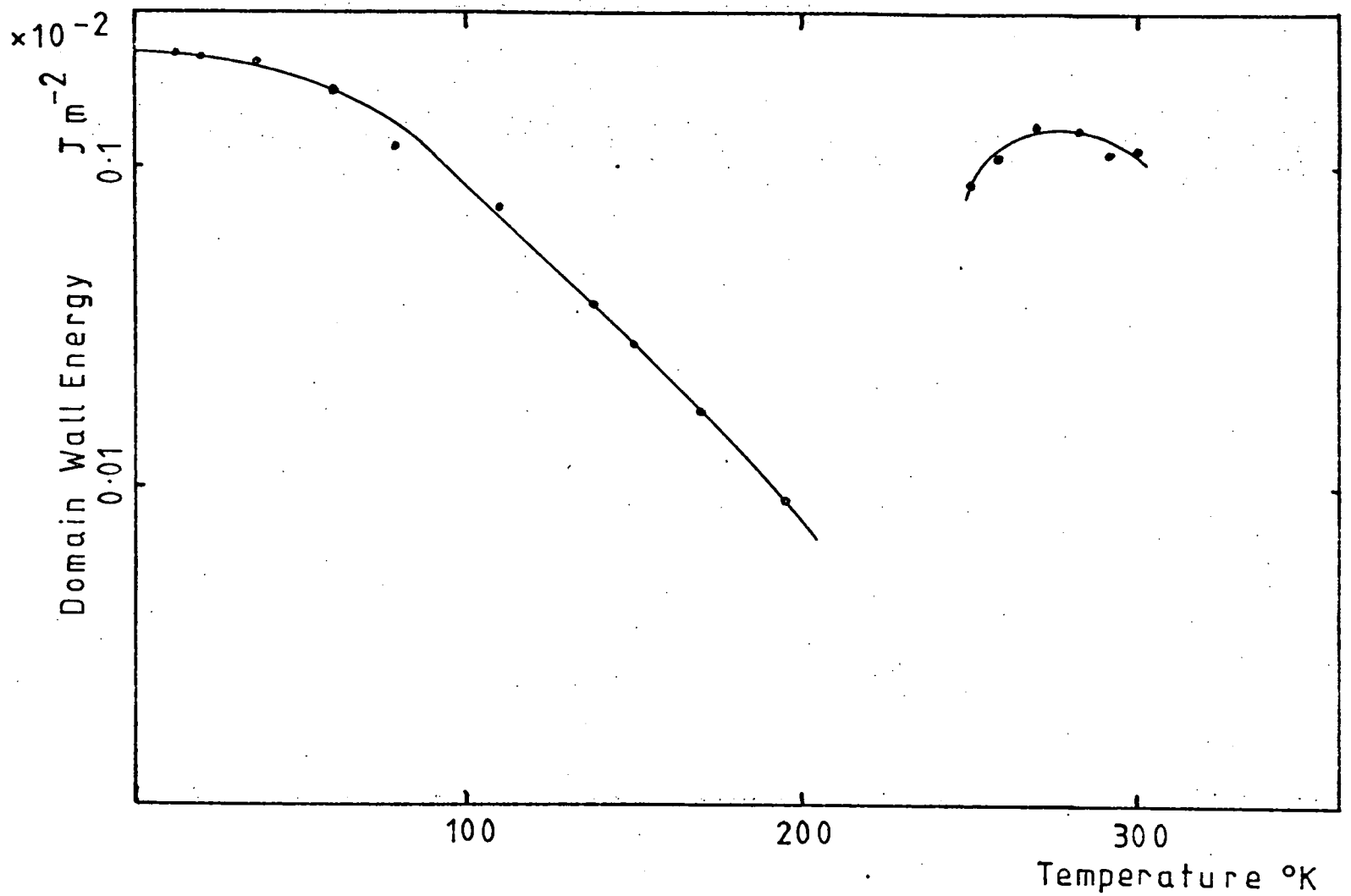

FIGURE 7.2 Calculated Domain Wall Energy
(Wall Type 1b)

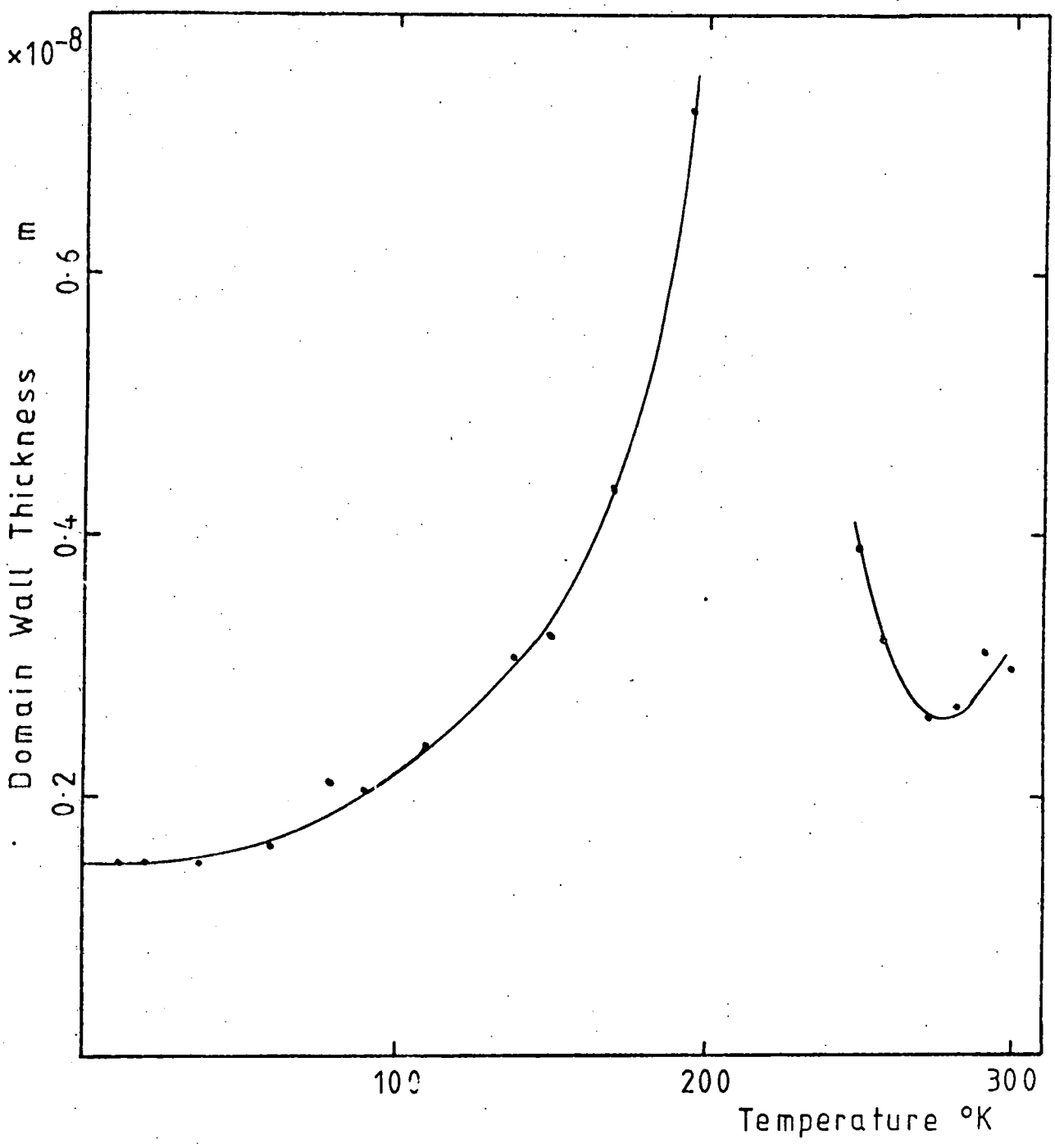

FIGURE 7.3 Calculated Domain Wall Thickness
(Wall Type 1b)

in a small hole on the top of the copper block near the sample, and a Noronix NTM 3 temperature meter. Magnetic fields could be applied by either small calibrated permanent magnets or a small electromagnet which fitted onto the microscope stage.

It is obvious that domain walls will be observed by this technique (section 6.4.1), but if a small magnetic field is applied perpendicular to the surface of the sample the Ferrofluid particles will be polarized and in turn will be attracted to domains magnetized in directions such that the surface has a suitable polarity. This mechanism is illustrated in Figure 7.4. for a single crystal of gadolinium. By reversing the applied magnetic field, the contrast in reversed (Figures 7.4b and 7.4c).

7.3.2 The Dry Colloid Technique.

The previous apparatus that had been used for observing domains on gadolinium at low temperatures (Saad 1977) had several disadvantages. It was very bulky and required a great deal of cooling and offered little control over the final temperature obtained. It also required a period of temperature stability, about 15 minutes, to allow the dry colloid particles to settle on the crystal surface under gravity. A new evaporation system was designed in order to give greater control over the temperature. In particular the system was inverted so that the crystal was mounted on a cold finger and the evaporation took place from below it. The particles were carried to the sample by the thermal currents produced by the hot filament. This method was successfully tested in a standard vacuum evaporation chamber at room temperatures. The use of a cold finger allowed the evaporation chamber to be made much smaller in diameter (4.5cm) and this could allow large external magnetic fields to be applied to the specimen.

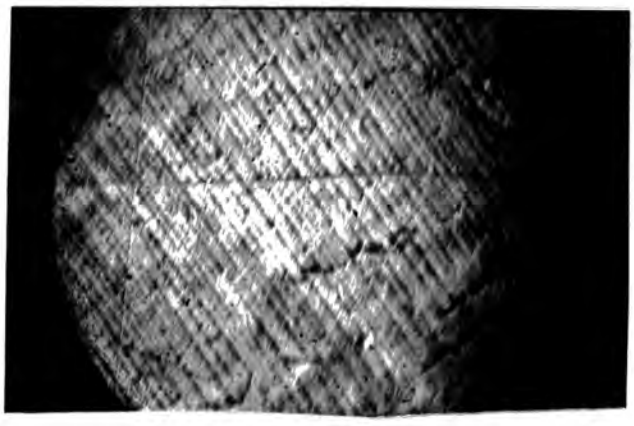

(a) Zero Field

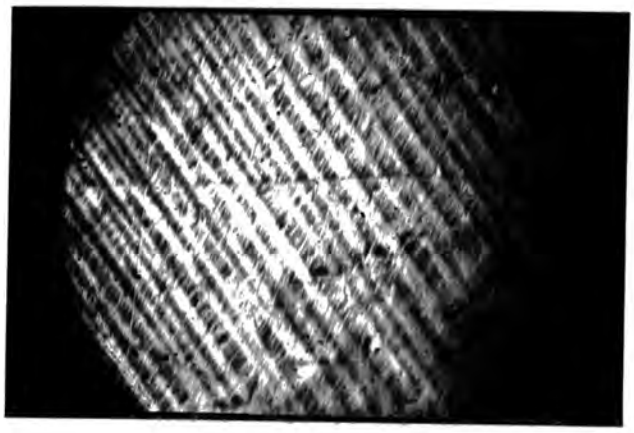

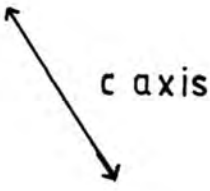

(b) ⊙ 1 mT

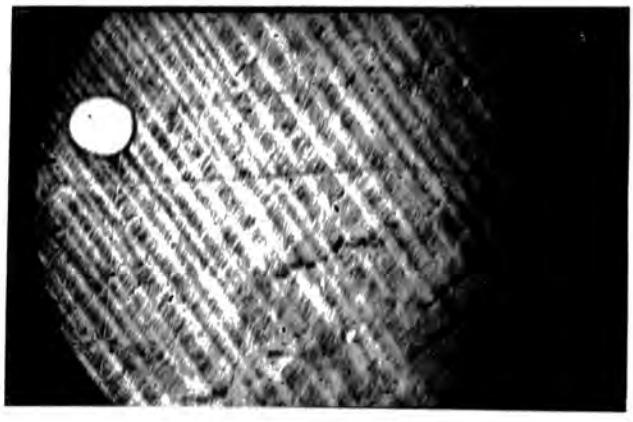

(c) ⊗ 1 mT

FIGURE 7.4 Gd C 285 K b Plane

This would be of particular use if the apparatus was used to study the ferromagnetic domain structure of other rare earth elements.

The apparatus is shown diagrammatically in Figure 7.5. The specimen was mounted using 'Durofix' onto a brass holder which was then screwed onto the cold finger of the glass cryostat. The evaporating heating source consisted of a 'V' shaped tungsten filament, 0.1cm diameter, of 99.97% purity. A new filament was used for each evaporation to reduce the risk of contamination of the specimen. The filament was a push fit into holes which had been drilled into the top of the brass electrodes. Iron wire was used throughout to produce the dry colloid particles. This was 0.027cm diameter wire of 99.99% purity. Before the wire was used the outer layers were stripped off using a pair of pliers to produce a shiny pure metal surface. The power to the filament was supplied by a mains rectified D.C. source capable of producing 120 amp at 5 V and controlled by a 'Variac'. The temperature was measured using a copper-constanan thermocouple, placed in a hole in the brass specimen mount, and a Noronix NTM 3 temperature meter. The double walled glass cryostat was useful in controlling the rate of cooling and the final temperature reached depending upon in which well the coolant was placed. Using liquid nitrogen the lowest temperature that could be obtained was 120K. This was due to the convective and conductive heat losses when the helium gas was introduced into the evaporation chamber. A later, temporary, modification which involved enclosing the main body of the evaporation chamber in a polystyrene nitrogen dewar reduced the lowest temperature obtainable to 90K. At low temperatures the convective transport of the iron particles was so efficient that a screen had to be introduced into the evaporation chamber to reduce the amount of iron deposited on the specimen. This consisted of a

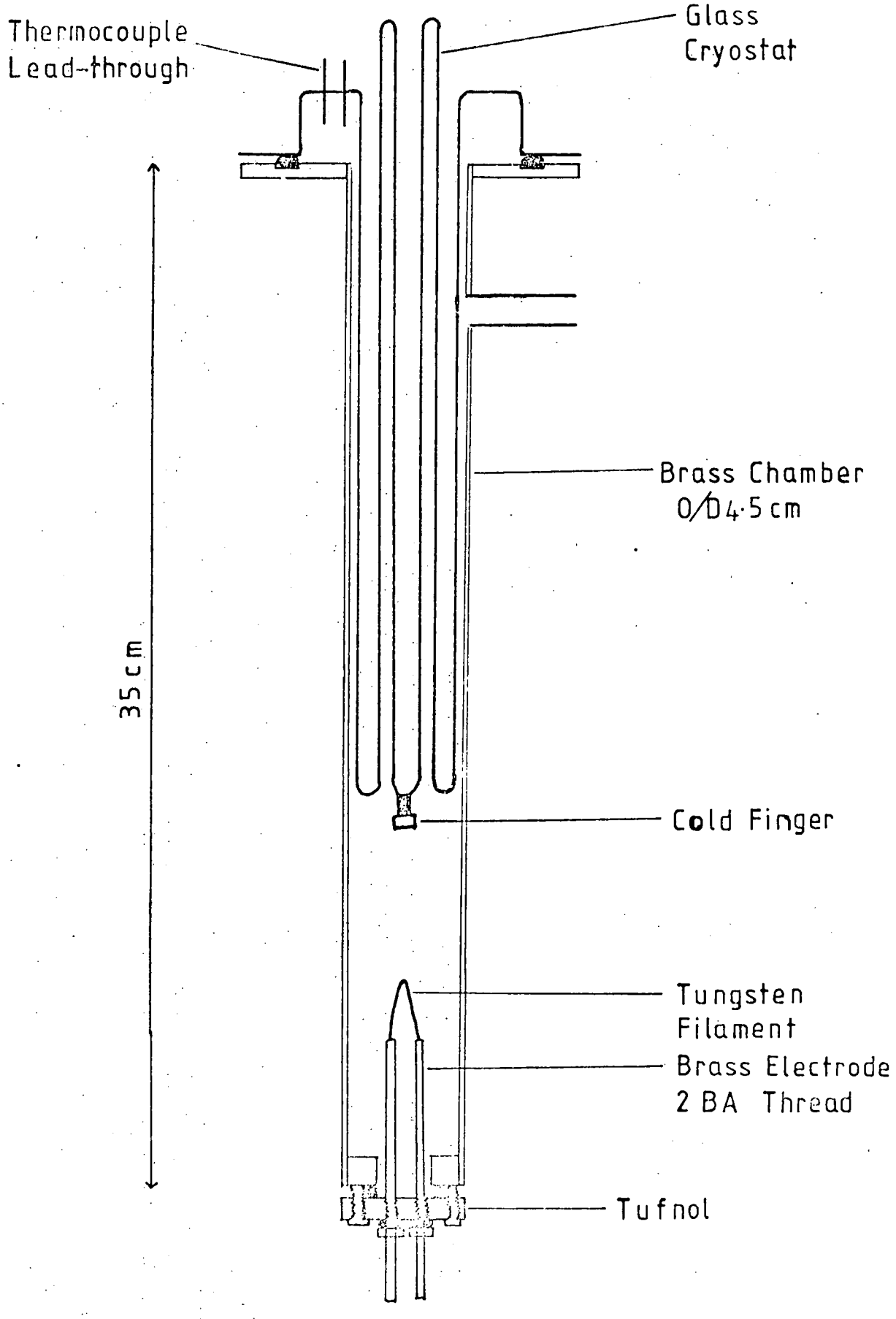

FIGURE 7.5 Dry Colloid Apparatus

1/2 x 1/2mm copper mesh mounted on the end of a plastic tube whose diameter gave a snug fit to the inside of the evaporation chamber. The length of the tube was such that the grid was supported mid-way between the filament and the specimen. To obtain good contrast on gadolinium a small vertical magnetic bias field was required. This was provided by a small ferrite magnet with a hole drilled in it so that it could sit above the specimen on the cold finger. It produced a vertical field of 14mT at the position of the specimen and a stray field of 4mT in the horizontal plane.

From preliminary experiments on silicon-iron polycrystalline samples the optimum evaporation conditions were determined. The main variables were the helium gas pressure, the filament to specimen distance, the amount of iron wire evaporated and the power supplied to the filament. At room temperature the optimum conditions were determined to be;

Helium gas pressure 1.5 Torr

Filament to specimen distance 4cm

Length of iron wire 7cm

Power to the filament 50amp at 2V for 15sec.

Before an evaporation was carried out the chamber was evacuated to a pressure less than 10^{-4} Torr by a standard diffusion and rotary vacuum pump system. The whole chamber was then flushed with high purity helium gas and then evacuated again. A low pressure of helium gas was then admitted and the system cooled to the temperature required. After the evaporation the whole system was warmed up to room temperature before the specimen was removed and then placed under the microscope. After each evaporation the chamber was thoroughly cleaned.

Figure 7.6 shows the patterns obtained on two polycrystalline silicon-iron samples at room temperature and 168K and also the pattern

300 μm

(a) Si-Fe Room Temperature

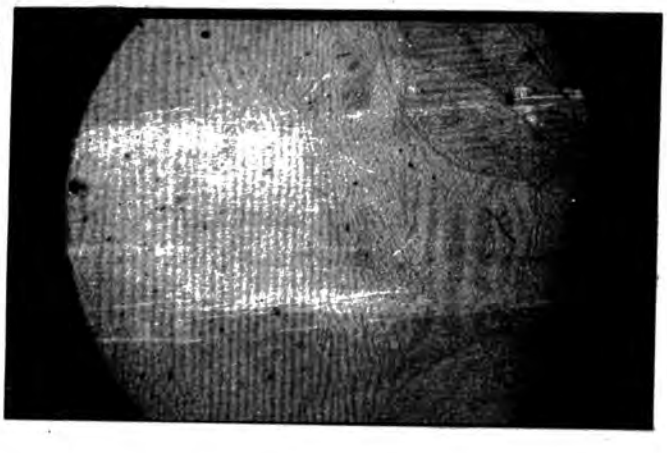

300 μm

(b) Si-Fe 136 ± 2 K

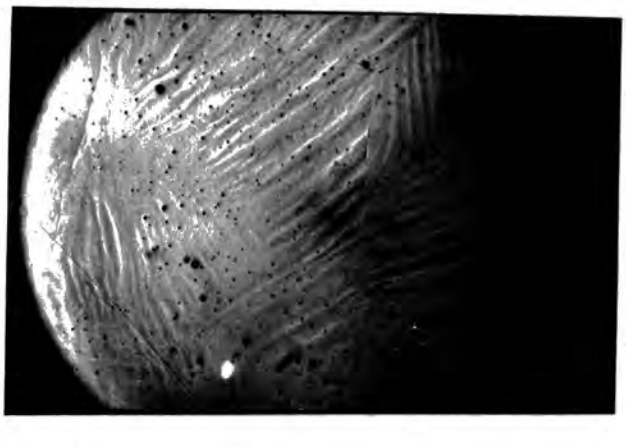

2000 μm

(c) Ni 168 ± 2 K ⊙ 14 mT

FIGURE 7.6 Dry Colloid Apparatus, Tests

obtained on a polycrystalline nickel disc. The effect of the grain boundaries on the domain structure can be clearly seen in each case.

7.3.3 The Specimens

The test samples of silicon-iron were obtained from commercially produced sheet material. After mechanically polishing, the surfaces were electrolytically polished using an electrolyte of chromic acid (25gm), acetic acid (133c.c.) and water (7.c.c.). The final surface of the polycrystalline nickel sample was obtained by chemically polishing with 50% acetic acid, 50% nitric acid. Etch pits are clearly visible in Figure 7.6c.

The gadolinium crystals were obtained from the Centre for Materials Science, Birmingham University and had been subjected to the solid state electrotransport technique. One crystal (F) had been obtained from Metals Research Ltd., Cambridge and was of 99.9% purity with respect to other metals. This sample contained a number of inclusions, Figure 5.22. The gadolinium samples had been cut using electrospark erosion by Saad (1977) and their orientation was checked using the back reflection Laue X-ray technique. The specimens are identified below:

Gd. A. This crystal has been described in section 5.3.

Gd. B. This crystal has been described in section 5.3.

Gd. C. This was a wedge-shaped crystal with a semi-circular cross-section. The maximum diameter was 4.5mm and the maximum thickness was 1.1mm. The large 'top' surface was a b-plane.

Gd. D. This was an elliptical disc of 7.5mm x 6.0mm x 0.75mm thick. The 'top' surface was a b-plane with the c-axis lying almost parallel to the semi-minor axis.

Gd. E. This was a circular disc of diameter 4mm and a maximum thickness of 0.7mm. The 'top' surface was a b-plane.

Gd. F. This was the Metals Research crystal and was a rectangular block 3.8mm x 1.4mm x 2.0mm. The 'top' (3.8 x 1.4) surface was a basal plane.

Gd. G. This was in the shape of an uneven rod, diameter 3mm and 10mm long. It was the anode end of the solid state electrotransport processed rod. It was polycrystalline in character.

The 'top' surfaces in each case were the ones used for the domain observations and these were mechanically polished using successively finer grades of emery paper (2/0, 3/0, 4/0) followed by a diamond compound paste (6/3 and 1/1/4μm) on the rotating wheel of a Metals Research Multipol polisher. To obtain a strain free surface a chemical polish was used comprising of 15ml nitric acid, 20ml lactic acid, 10ml acetic acid, 5ml orthophosphoric acid and 1ml sulphuric acid. This chemical polish is very effective provided that it remains uncontaminated. It was found when using the colloid techniques that the crystal would often require re-polishing chemically and occasionally mechanically after removing the colloid with ethanol. In one case, Gd, D, this resulted in a hole eventually appearing in the centre of the crystal. This is obviously a disadvantage of any technique that requires the re-polishing of the crystal sample after initial preparation.

7.3.4 Photography.

The domain structures were observed using a Cooke M40440 or a Vickers M.17 microscope at magnifications varying from 19x to 250x. Photographs were taken with a Pracktica LTL 35mm camera. Various

film types were tried for optimum performance and Ilford F.P.4 was found to give the best overall results. The photographs were printed on Kodak F4 Veribrom high contrast paper.

7.4 Observed Domain Structures.

7.4.1 The Curie Temperature.

Figure 7.7 shows the effect of reducing the temperature of a gadolinium crystal through the Curie temperature, 291K. The observations were made by placing the Ferrofluid on the surface of the sample and then cooling it very slowly by means of the nitrogen gas. The formation of domains can be clearly seen, Figure 7.7c, at the Curie temperature. The wall contrast was diffuse. This would be expected due to the low value of the saturation magnetization. On cooling a further degree Kelvin, Figure 7.7d, the definition was greatly improved. The domains were of the expected uniaxial type with 180° Block walls. On warming up the crystal it was often observed that the domain structure would remain visible to a temperature of about 293K. It was difficult to determine whether this was a genuine thermal hysteresis effect or whether it was due to the interia of the colloid particles. The effects were also studied using a 16mm cine camera mounted on the microscope to try to observe more precisely when the colloid patterns form. The film showed a gradual build up of colloid particles over the domain walls as the crystal was cooled through the Curie temperature.

7.4.2 The Effect of an Applied Magnetic Field.

Figure 7.8 shows the effect of a magnetic field applied to a gadolinium crystal at a temperature of 285K. At this temperature gadolinium exhibits simple uniaxial anisotropy. The main domains

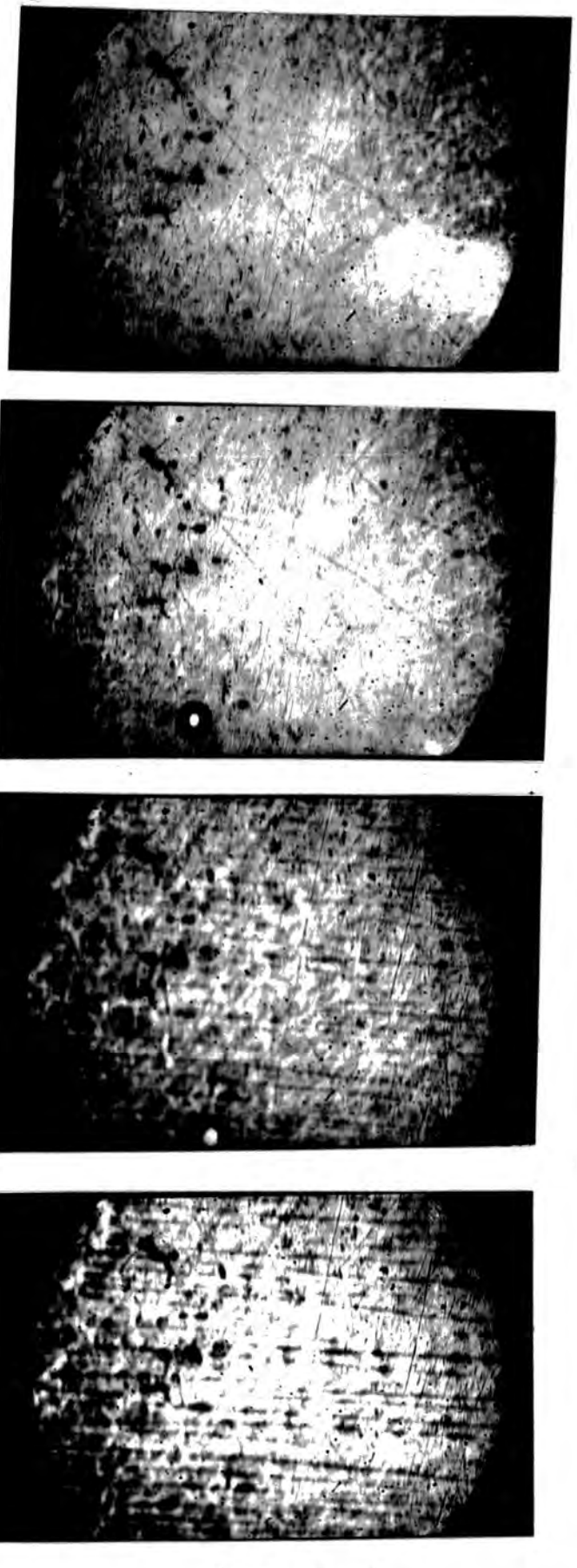

FIGURE 7.7 The Formation of Domains at the Curie Temperature

could be removed by the application of a relatively small field, 31mT, directed along the c-axis (Figure 7.8f). It should be noted that the type of contrast changes from wall contrast in Figure 7.8a to domain contrast in Figure 7.8b due to a small vertical component from the field of the electromagnet. Figure 7.9 shows the effect of reducing the applied field and a marked hysteresis effect was observed with a domain structure reappearing when the field was reduced to 8mT. On applying a magnetic field perpendicular to the c-axis (Figure 7.10) it was found impossible to destroy the domain structure even with the highest field obtainable from the electromagnet (62.5mT). As the crystal was circular in the magnetization plane (Gd. E) demagnetization effects can be ignored and therefore the observed behaviour can be accounted for in terms of the uniaxial anisotropy of gadolinium. In fact at this temperature K_1 is almost at its maximum positive value (Figure 5.11).

The basal plane domain structure observed, Figure 7.11, was that expected of a uniaxial material and was the same as that observed by Al.Bassam and Corner (1969). They also investigated the effect of applied magnetic fields on the basal plane domain structure. The contrast was found to be very poor without a magnetic field applied and the observations in Figure 7.11 were made using a small vertical bias field perpendicular to the basal plane so that areas of opposite polarity were observed. This was shown to be the case by reversing the areas of light and dark, Figures 7.11a and 7.11b.

7.4.3 Observations Using the Dry Colloid Technique.

Using the dry colloid technique described in section 7.3.2 an attempt was made to study the magnetic structure of gadolinium in the temperature region 120K to 290K. This region is particularly

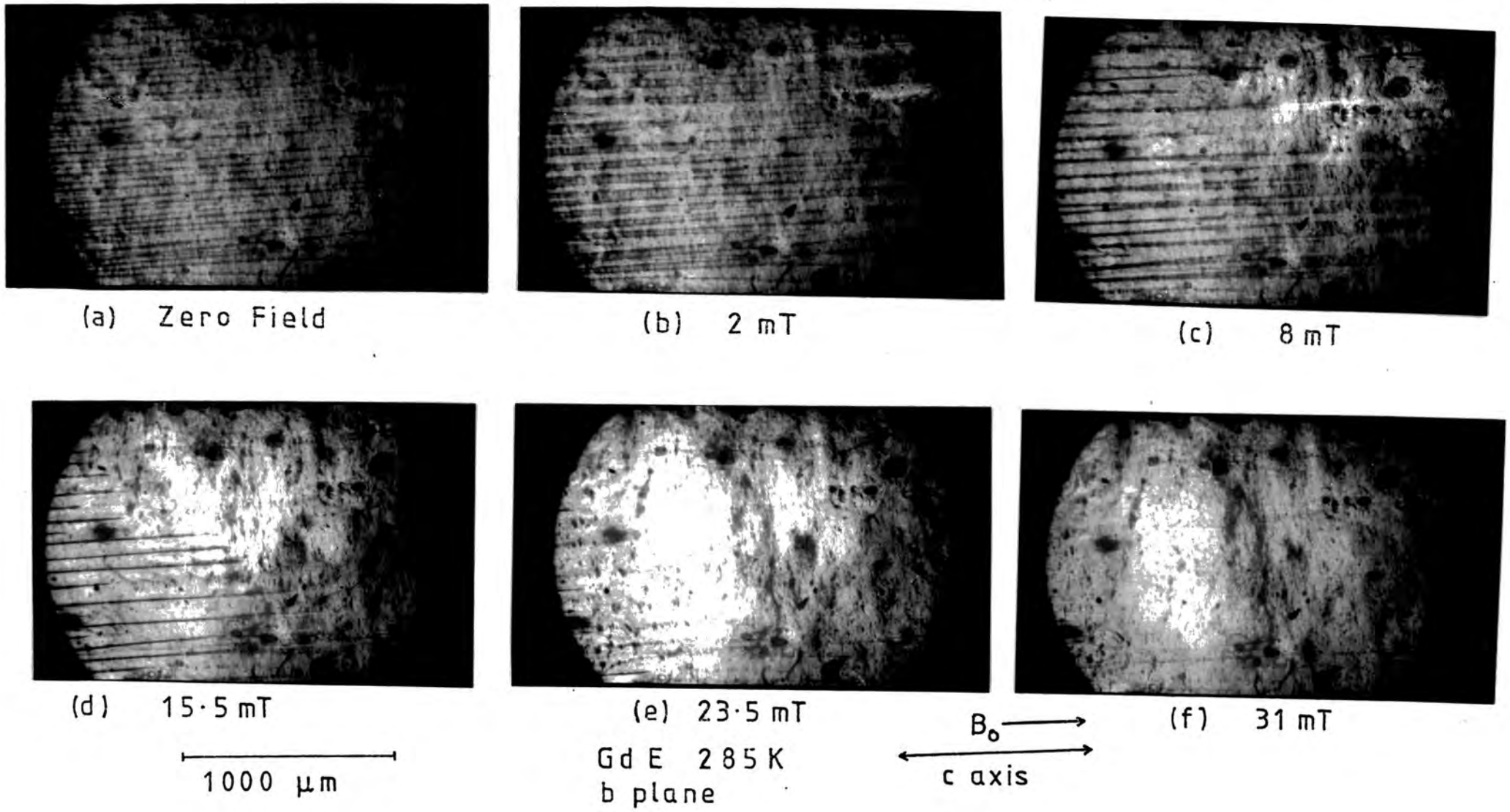

FIGURE 7.8 Magnetization Along the c Axis

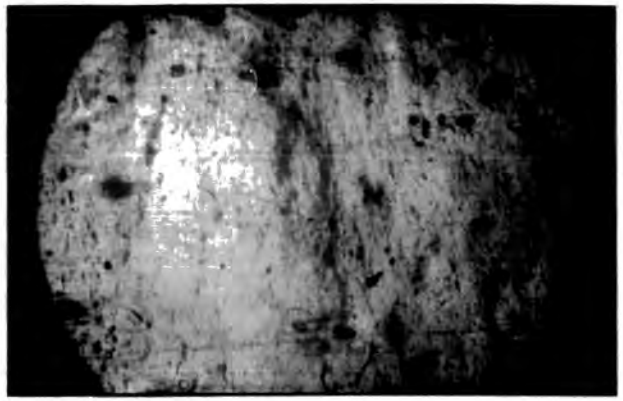

(a) 15·5 mT

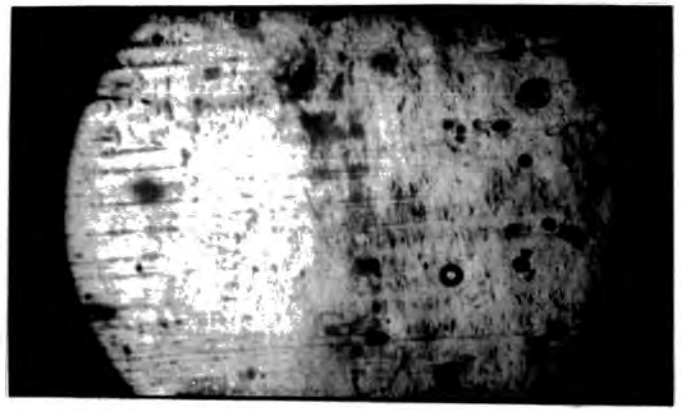

(b) 8 mT

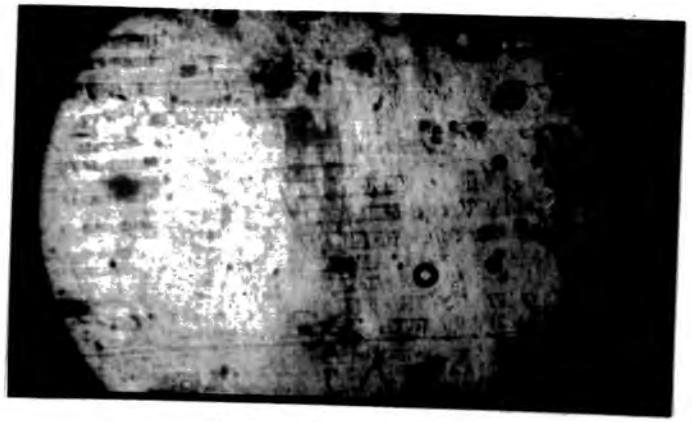

(c) 2 mT

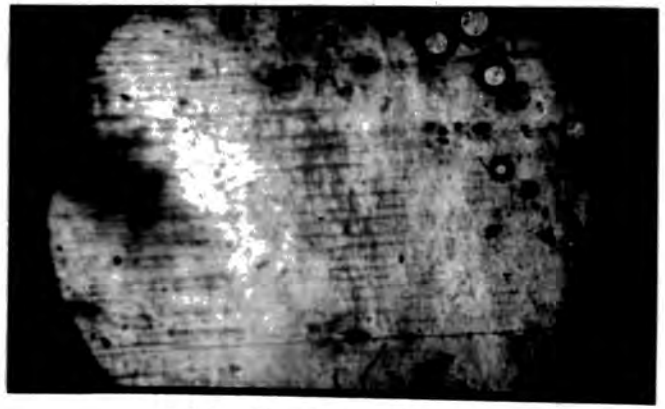

(d) Zero Field

B_o →

← c axis

Gd E 285 K
b plane

1000 μm

FIGURE 7.9 Demagnetization Along the c Axis

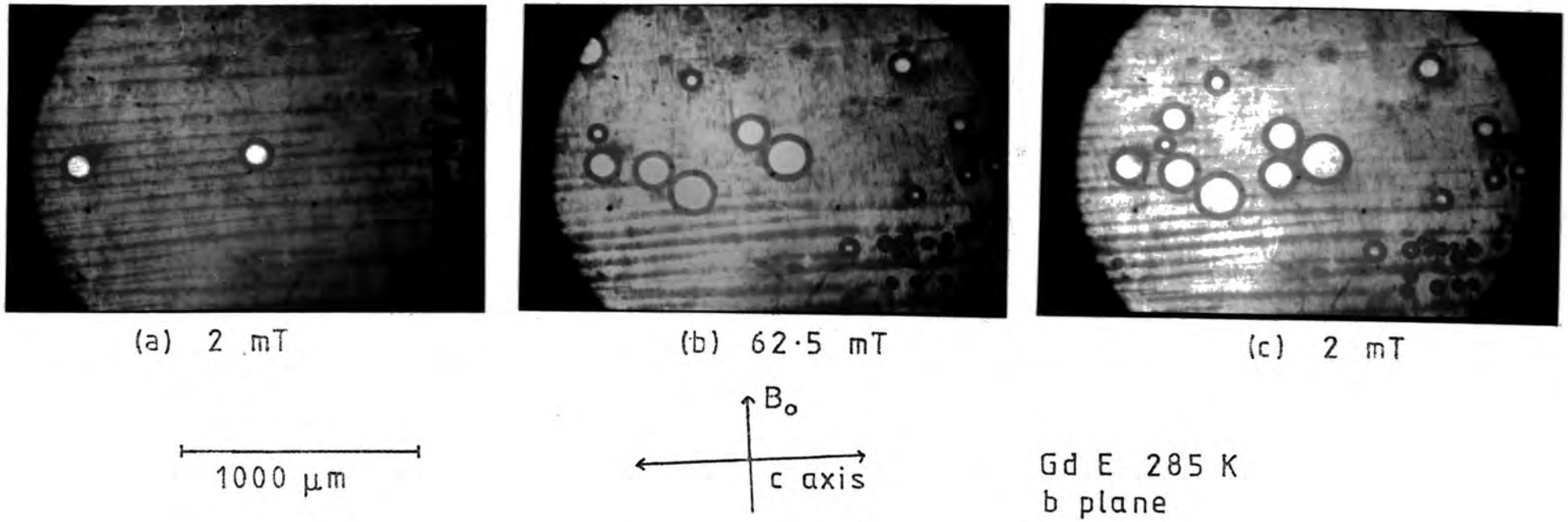

FIGURE 7.10 Magnetization and Demagnetization Perpendicular to the c Axis

(a) ⊙ 6 mT

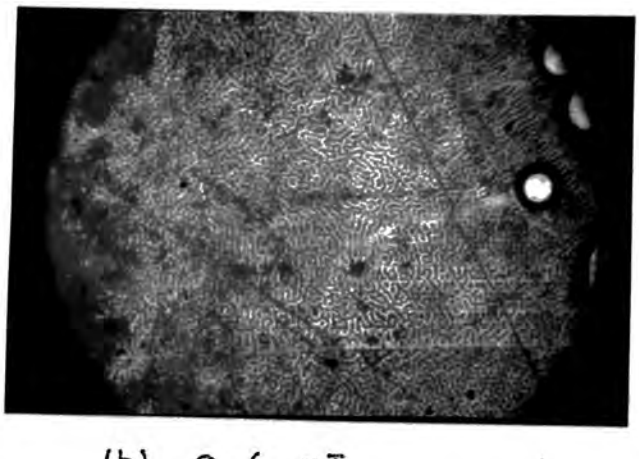

(b) ⊗ 6 mT

500 μm

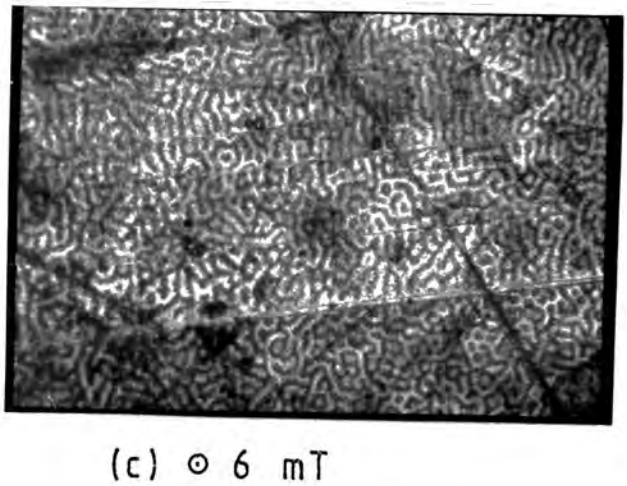

(c) ⊙ 6 mT

Gd B 287 K

300 μm

FIGURE 7.11 Basal Plane Domain Structure

interesting as it contains the transition point at 240K where the magnetization vector moves away from the c-axis to form an easy cone and also the region of maximum cone angle, Figure 5.13. No magnetic domains were observed in the present investigation below a temperature of about 230K. This is believed not to be due to the apparatus as it can produce clear and reproducible domain patterns on Si-Fe over its entire operating temperature range. The apparatus of Figure 7.5 was modified as noted in section 7.3.2 to enable it to reach a temperature of 90K, but this still failed to produce domain patterns on gadolinium. This is particularly surprising as Corner and Saad (1977a) produced clear domain patterns on gadolinium at 77K using the dry colloid technique. Recently Saad (1978) has produced domain patterns on a terbium crystal at 77K using the dry colloid technique. The behaviour of the domain structures that were observed will now be discussed.

Figure 7.12 illustrates the effect of reducing the temperature on the domain structure on a b-plane of gadolinium. At 251K, Figure 7.12a, a clear uniaxial type structure was observed with domains running parallel to the c-axis. Reverse dagger domains were observed coming from the edge of the crystal (left hand side of Figure 7.12a). On reducing the temperature to 241K and 234K the domain contrast deteriorated and a large number of striations appeared perpendicular to the principal domains (Figures 7.12b and 7.12c). Reducing the temperature further to 225K (Figure 7.12d) produced no obvious contrast. This behaviour is illustrated more clearly in Figure 7.13 which presents observations made on a basal plane. This shows a progressive change in the definition of the patterns obtained as the temperature was reduced. At 233K a faint pattern was still present (Figure 7.13c) but this disappeared completely on reducing the temperature a further 5 degrees Kelvin. Figure 7.14 again shows the same temperature effect

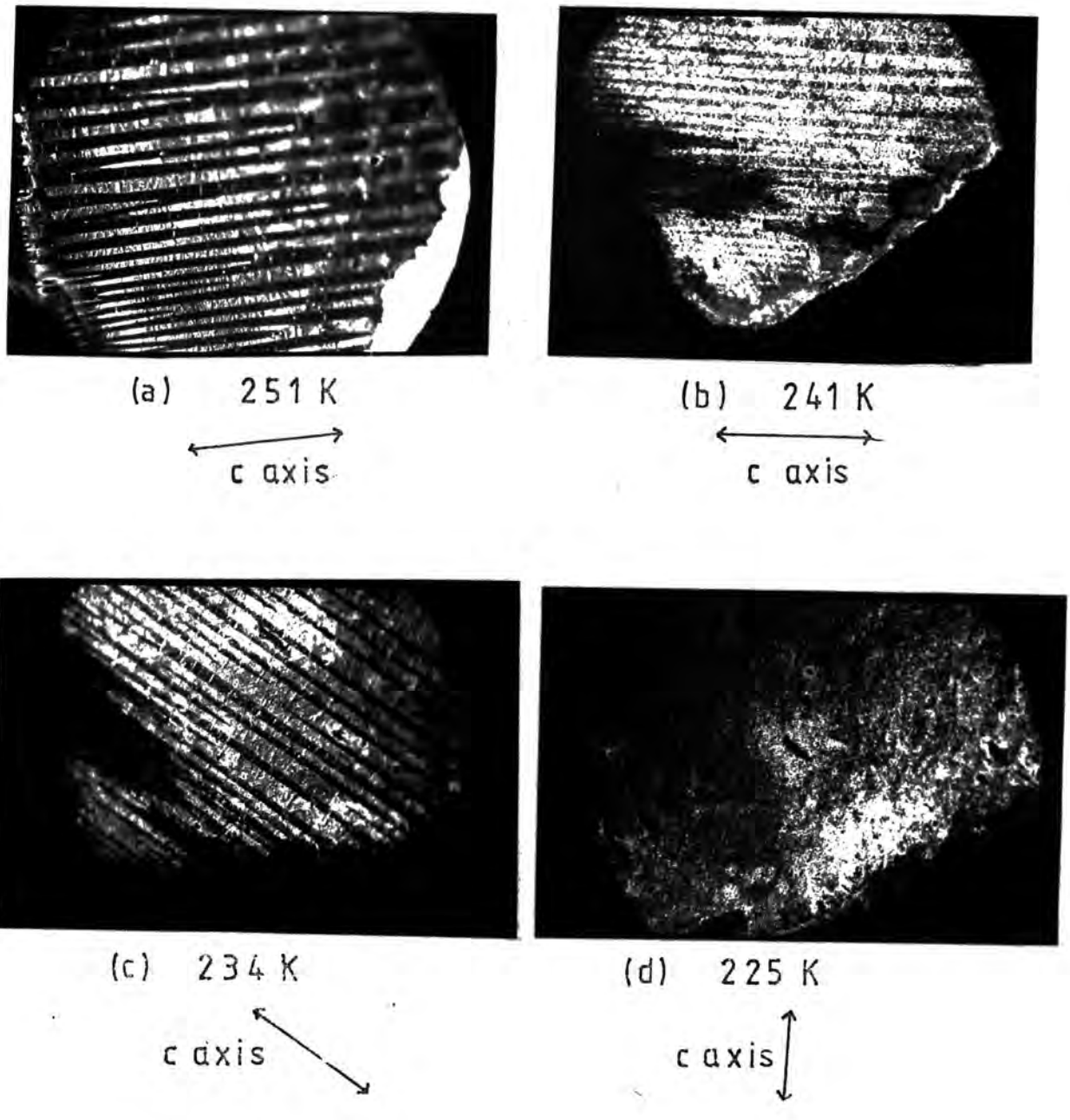

FIGURE 7.12 The Effect of Temperature on the b Plane Domain Structure

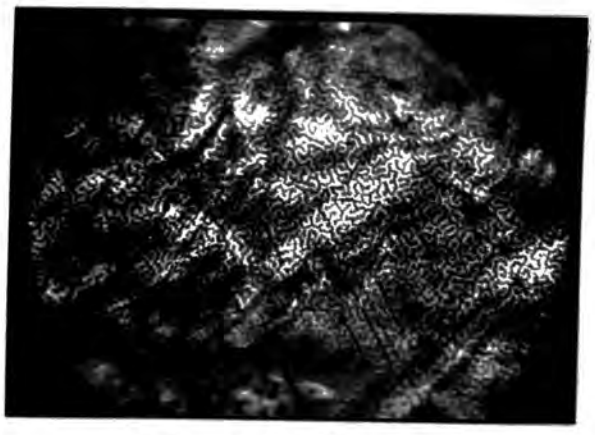

(a) 248 K

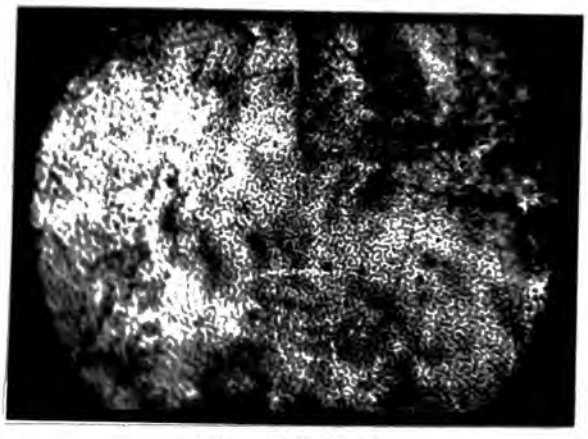

(b) 238 K

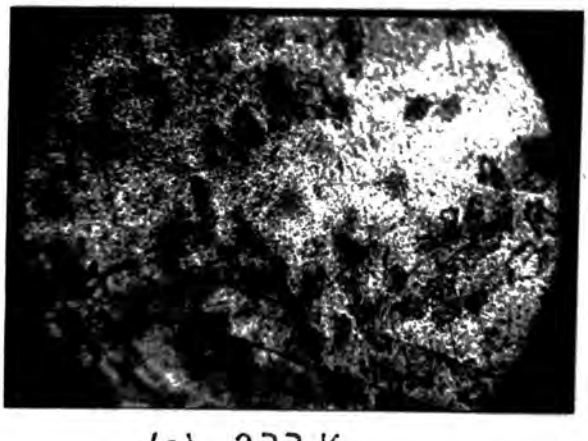

(c) 233 K

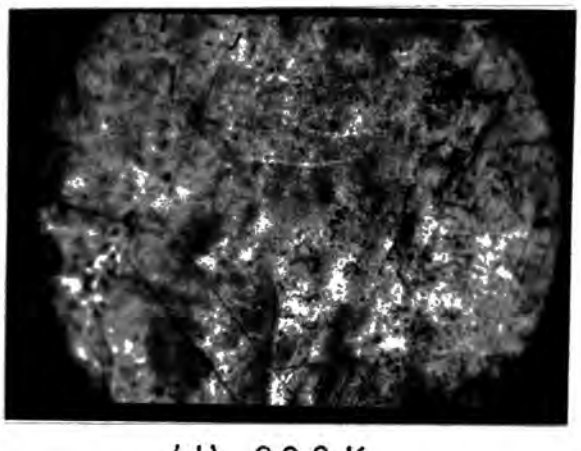

(d) 228 K

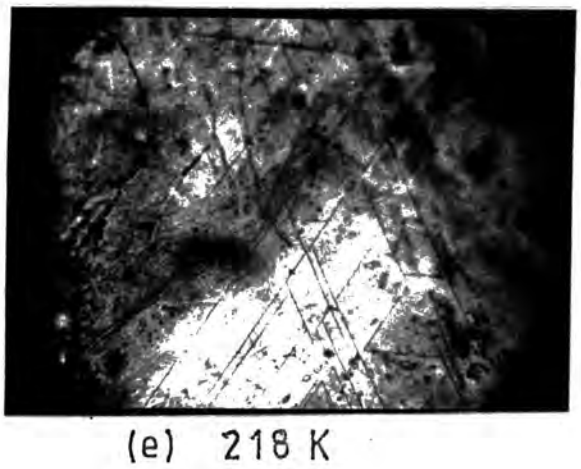

(e) 218 K

⊙ 14 mT
Gd B ±2 K

400 μm

FIGURE 7.13 The Effect of Temperature on the Basal Plane Domain Structure

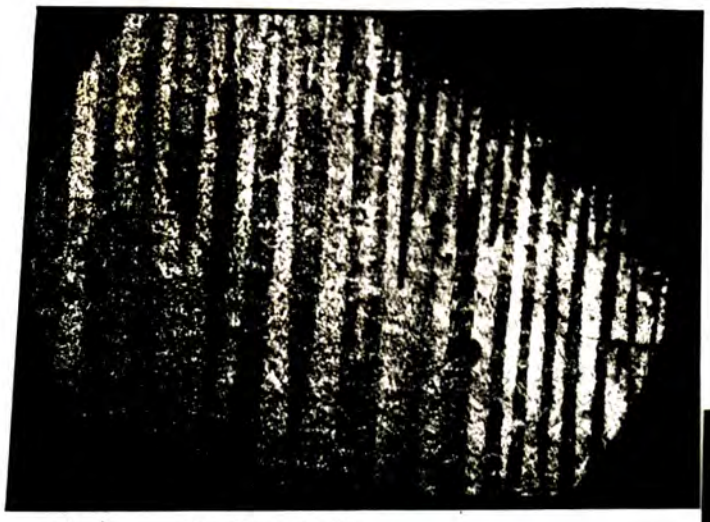

(a) 251 ± 2 K

c axis ↕

(b) 240 ± 2 K

↔

c axis

(c) 235 ± 2 K

⊙ 1 mT

Gd D

250 μm

(d) 227 ± 5 K

c axis

FIGURE 7.14 The Effect of Temperature on the b Plane Domain Structure

on another crystal (Gd. D). Figure 7.14d shows a domain structure observed at 227K which was the lowest temperature at which a domain pattern on gadolinium was observed. Unfortunately this particular experiment involved a large temperature error (± 5K) and the observation is therefore probably in agreement with the other observations.

The 'break-up' of the domain structure at about 240K to 230K would be expected considering the behaviour of the anisotropy in this temperature region. In a temperature region where the anisotropy is low, Figure 5.19, it would be energetically unfavourable to form domains and a similar type of spin system as proposed by Kittel and Galt (1956) (Figure 6.4) would predominate. The fact that domains were not observed below 150K is disturbing as at this temperature the anisotropy is certainly appreciable (Figure 5.19) and the easy cone well formed. The reasons why domains were not observed below 150K in the present work are not known. The effects of various rates of cooling, methods of mounting the crystal and applied magnetic fields were investigated but gave no more information about the non-appearance of a domain structure at low temperatures.

In Figure 7.15 the range of detail that was obtained with the dry colloid technique is illustrated. Figure 7.15a shows the domain structure over almost a complete crystal (Gd. C). This clearly illustrates the effect of the crystal thickness on the uniaxial domain structure as Gd. C was a wedge shaped crystal with the thinnest end running along the straight edge of the crystal. The thin crystal edge produces a very fine system of narrow domains and reverse daggers. At the thickest part of the crystal the domain structure is very simple, composed of slab domains running parallel to the c-axis separated by 180^{o} Bloch walls. Figure 7.15b shows the intricate pattern of alternating polarities on the basal plane at high magnification and indicates

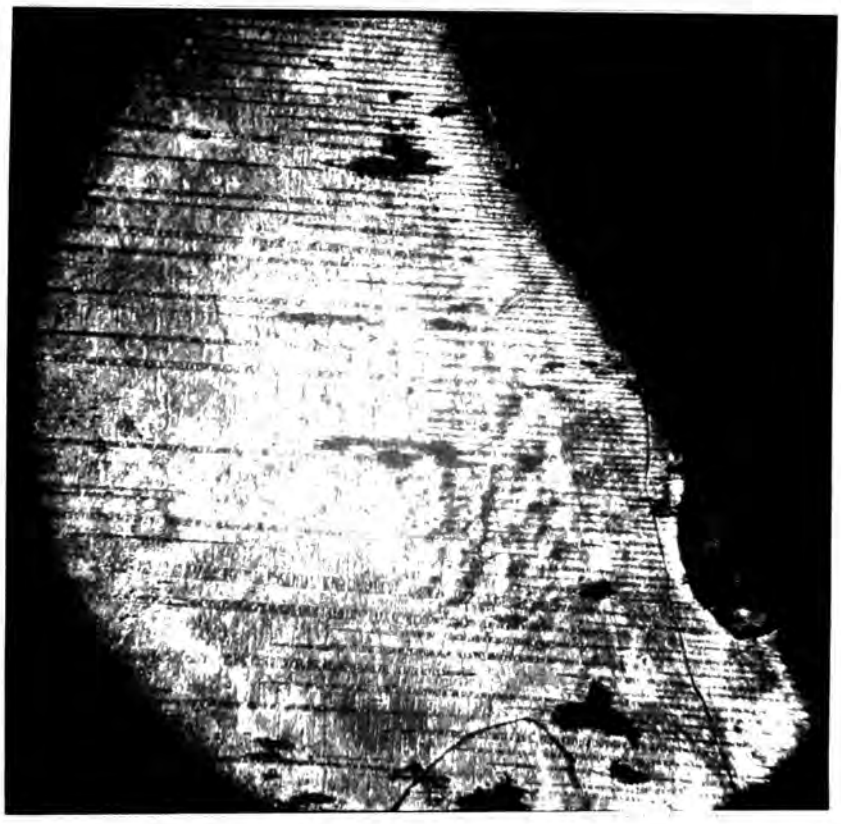

(a) Gd C 234 K b Plane
⊙ 14 mT

1000 μm

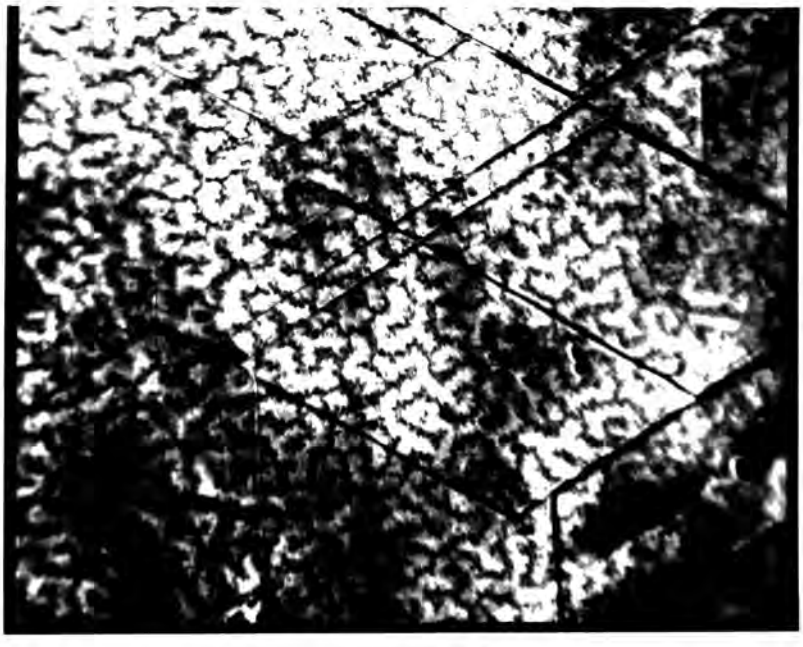

(b) Gd B 249 K Basal Plane
⊙ 14 mT

150 μm

FIGURE 7.15 Dry Colloid Technique

the limit of resolution on the dry colloid technique due to the particle size.

7.4.4 The Effect of Defects on the Domain Structure.

If the crystal used for domain observations contains defects of various types these can dramatically affect the domain structure. In the case of Figure 7.16a there is a grain boundary running across the centre of the photograph. Even though the misorientation of the grains is small a large number of reverse daggers are nucleated to reduce the magnetostatic energy of the free pole distribution along the grain boundary.

In Figure 7.16b we see a basal plane domain structure which varies dramatically in size from one area to another. This is in sharp contrast with the uniform structure observed in Figure 7.11. Gd. F is the Metals Research crystal containing inclusions and Al Bassam (1969) has shown that the variation in the spacing of the domain structures is due to the inclusions forming different effective thicknesses of pure gadolinium within the crystal.

Figures 7.16c and 7.16d show the effect of scratches and surface defects on the domain structure in a b-plane. Again, as in the case of Figure 7.16a, reverse dagger domains form to minimize the magnetostatic energy of the free poles. The main domain structure is then unaffected by the presence of such defects provided they are not too numerous.

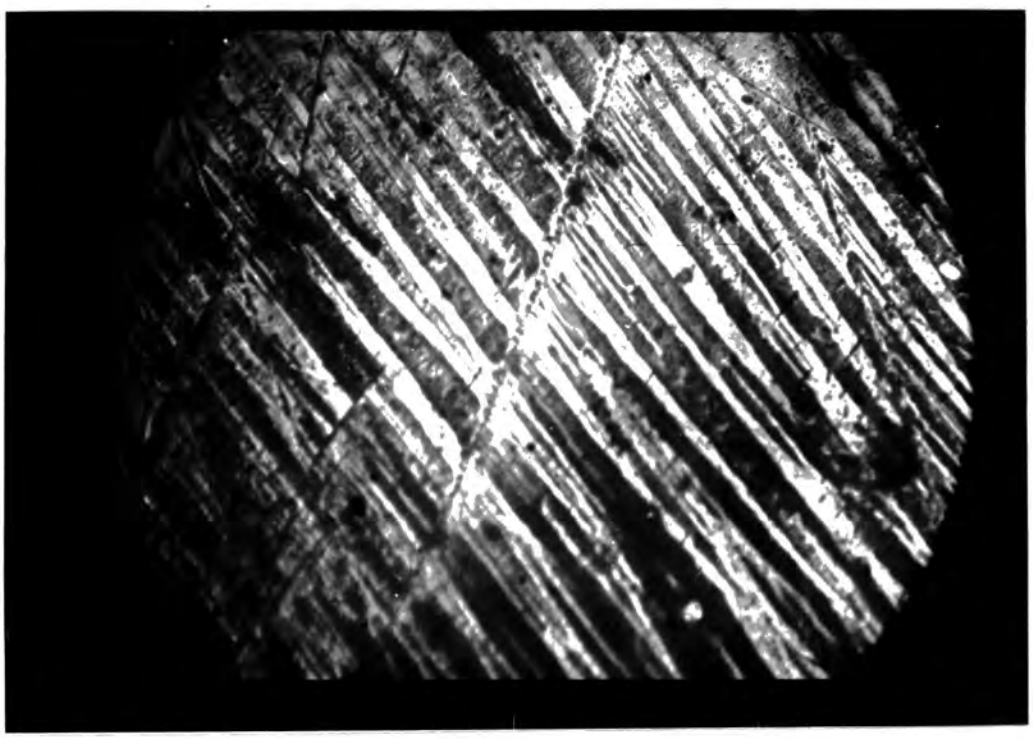

(a) Gd G 288 K ⊙ 1 mT 250 μm

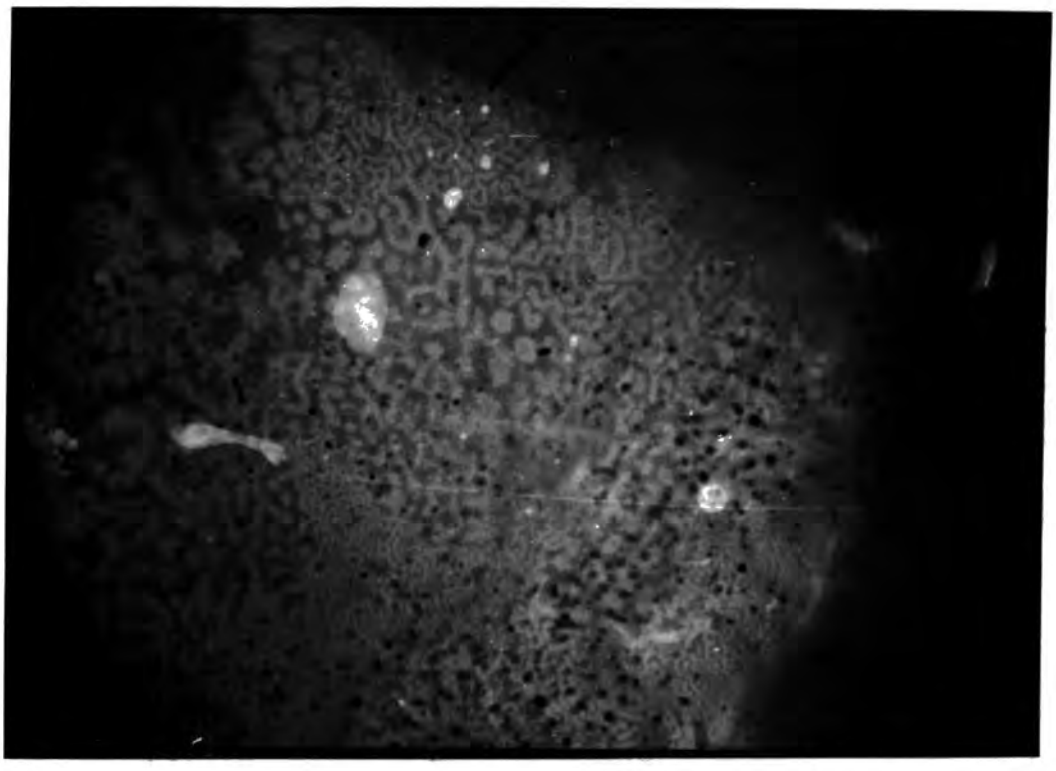

(b) Gd F Basal Plane 288 K ⊙ 1 mT 100 μm

FIGURE 7.16 The Effect of Crystal Defects on the Domain Structure (Ferrofluid)

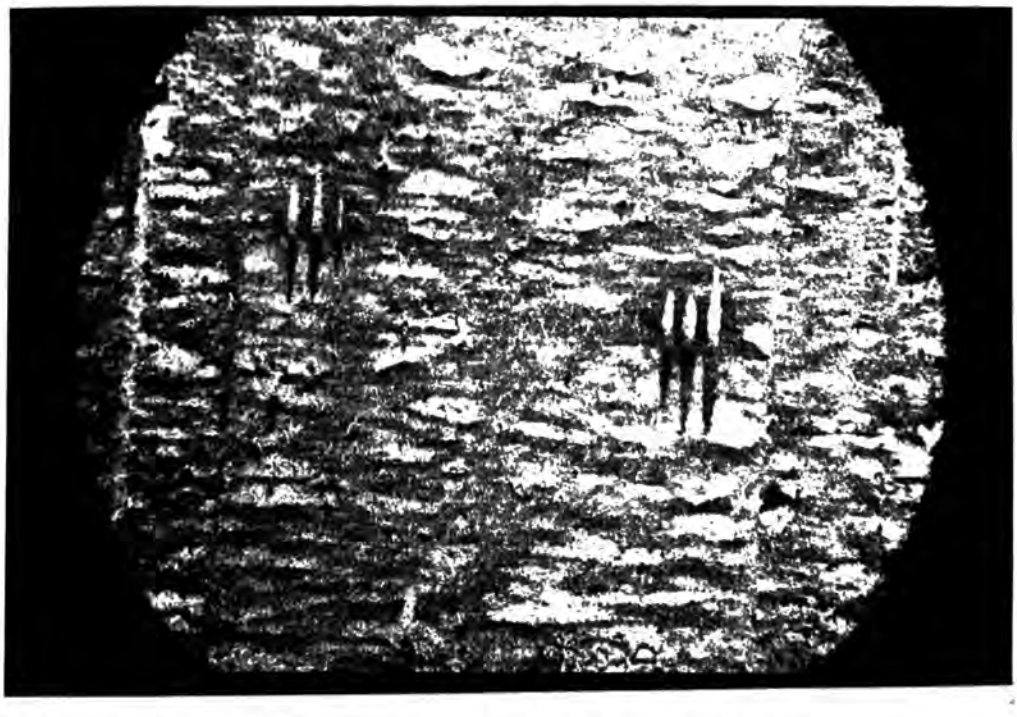

(c) Gd D b plane 252 K ⊙ 7 mT

200 μm

(d) Gd A b plane 234 K ⊙ 14 mT

250 μm

FIGURE 7,16 (cont.)

(Dry Colloid)

CHAPTER EIGHT

Conclusions

8.1 The Magnetocrystalline Anisotropy of Gadolinium.

The redetermination of the anisotropy constants was thought to be necessary due to the lack of agreement in the previous measurements and the recent controversy about the easy direction of magnetization (Corner and Tanner (1976), Franse and Mihai (1977)). The use of high quality single crystals of gadolinium, which have recently become available, would also yield more reliable results than the previous determinations which had used uncharacterized crystals from various sources.

The results of the present measurements of the anisotropy, as described in Chapter 5, are shown in Figures 5.11 and 5.12. These results are in agreement with the general temperature dependence of the constants as previously determined, but are significantly different in the actual values of the anisotropy constants. It would perhaps appear that the present determination has produced just one more set of constant values, albeit on much better quality crystals. The determination of the easy direction is a critical test in this case. Corner and Tanner (1976) determined the easy direction directly using the same crystals as the one used above. Their easy direction was in excellent agreement with the neutron diffraction result of Cable and Wollan (1968). The easy direction of magnetization determined in the present work by calculation using the anisotropy constants, inspection of the experimental torque curves and also a further direct measurement using a different crystal mounting technique gave consistent results which were in good agreement with the result of Corner and Tanner (1976) and hence that of Cable and Wollan (1968). These results are also in serious disagreement with

those of Franse and Mihai (1977).

In section 5.7 a theory was developed which can explain the lack of agreement in previously determined anisotropy constants and easy direction. This involved the calculation of the magnetostatic energy of a platelet inclusion lying in the basal plane of a crystal of gadolinium and its contribution to the total directionally dependent magnetic energy of the crystal. Such inclusions were commonly observed in the crystals used for the previous determinations of the anisotropy constants and the easy direction and a few percent by volume of such inclusions would account for the various results. In particular if enough inclusions were present the easy direction could be driven into the basal plane. No such inclusions were observed in the crystals used in the present work. The crystal used in the neutron diffraction work of Cable and Wollan (1968) would probably have contained such inclusions in reasonable quantities, enough to affect the easy direction measurements if they had been made by a magnetic technique. The neutron measurements were made without the application of an external magnetic field and hence the crystal would be in its demagnetized state, i.e. it would have a domain structure. Carey and Isaac (1964) and Carey and Thomas (1972) have shown that if inclusions are present in a uniaxial crystal then reverse dagger domains will nucleate around the inclusion to reduce the amount of free pole present and hence the magnetostatic energy. Such domains are commonly observed. Figure 7.16c and 7.16d show reverse dagger domains nucleated on scratches and surface defects. These will have the same magnetostatic properties as an inclusion. Figure 8.1 shows schematically the domain structure expected in an uniaxial crystal containing platelet inclusions lying perpendicular to the easy direction. These inclusions have little effect on the

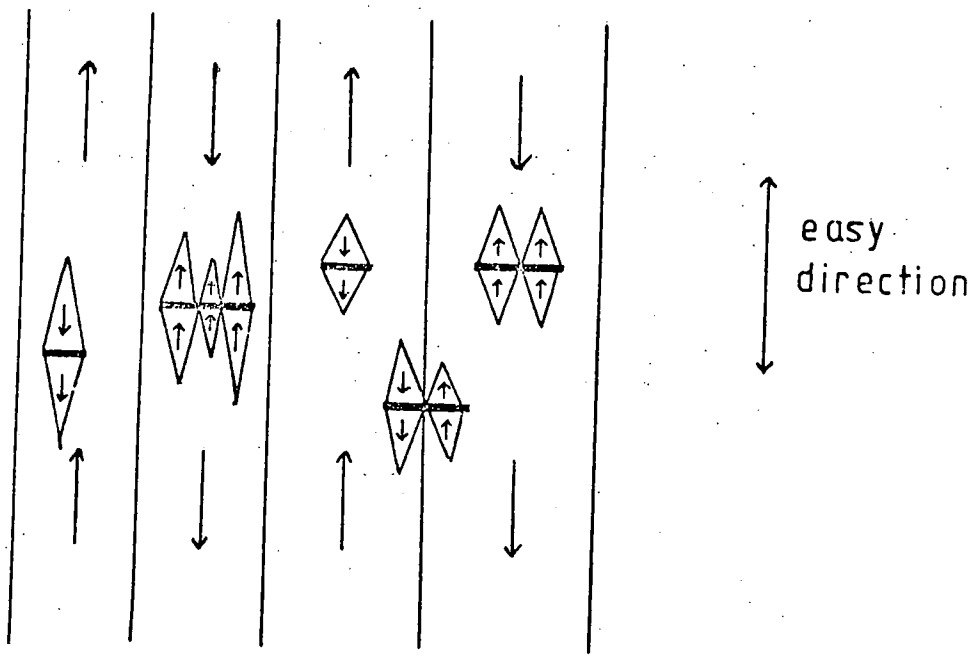

FIGURE 8.1 Reverse Dagger Domains
Around Nonmagnetic Inclusions

bulk domain structure. This is the situation that would be expected in the neutron diffraction work and hence the inclusions would have little effect on the results since the easy directions would remain those determined by the magnetocrystalline anisotropy. The crystal quality seems to have little effect on the basal plane anisotropy, Figure 5.12, and this would be expected if the magnetostatic inclusion model is correct. Strain effects, although principally along the c-axis, would be expected to show quite a large contribution to the basal plane anisotropy.

From the above arguments it can be concluded that the easy direction of gadolinium is now firmly established as having the form of Figure 5.13 and that the present values of the anisotropy constants are the most reliable available.

As the temperature dependences of the anisotropy constants, with the exception of K_3, are of the same form as those determined previously no new information on the origins of the magnetocrystalline anisotropy in gadolinium can be obtained. The change of sign of K_1 clearly indicates that the anisotropy must have a two-ion as well as a single-ion origin which have different temperature dependences. This conclusion was arrived at by both Brooks and Goodings (1968) and Yang (1971). K_2 and K_4 both seem to be of single-ion origin, as does K_3 if the extrapolated value is taken to indicate its true behaviour (section 5.6). The anisotropy energy surfaces (Figures 5.16 and 5.17) show the basic mechanism of the temperature dependence of the anisotropy as proposed by Akulov (1936) (Figure 4.2).

8.2 The Domain Structure of Gadolinium.

For the investigation of the effects of the magnetocrystalline anisotropy on the magnetic domain structure gadolinium is an extremely

interesting ferromagnet. The change in the easy direction and the formation of the easy cone due to the large changes in the anisotropy energy with temperature allow observations of the domain structure at various temperatures to be linked directly to the anisotropy. Marti and Paul (1977) have carried out an investigation of the effects of anisotropy on domain wall widths in crystalline and amorphous metal films using Lorentz microscopy but only small changes in K_1 were studied. Gadolinium also provides a unique opportunity to study the formation of magnetic domains at the Curie temperature.

In the present work an investigation of the two magnetic phase transitions, the Curie temperature and uniaxial to easy cone transition, was carried out. The results, discussed in Chapter 7, showed the formation of domains as the crystal was cooled through the Curie temperature and the disappearance of an observable domain structure at approximately 230K. The behaviour of the domain structure in the temperature range 230K to 291K was shown to be consistent with the uniaxial anisotropy of gadolinium in this temperature region.

Corner and Saad (1977a) have shown that a domain structure exists at 77K where there is an easy cone of magnetization. The transition from the uniaxial structure to the easy cone structure would be expected to occur at about 230K and, due to the small anisotropy energy (Figure 5.19), some intermediate spin system would be expected around this temperature. This would not necessarily be a definite domain structure but would be a closure spin system of the types illustrated in Figure 6.4. This analysis would seem to fit the observations with the exception that, using the present apparatus, no reformation of a domain structure was obtained at low temperatures (down to 90K). The reasons for not observing a domain structure below about 150K, where the easy cone is firmly established and the anisotropy is large

Durham University SCIENCE - 7 FEB 1979 SECTION Library

are not clear. The apparatus has produced domain patterns on other materials at low temperatures, Figure 7.6. The possibility that the crystal was severely strained by the cooling procedure, which would affect the domain structure, was investigated. The rate of cooling, the lowest temperature reached and the amount of thermal cycling that had taken place made no difference to the observations. If the evaporation was carried out below 230K no patterns were observed and if it was carried out above 230K then clear uniaxial type structures were observed. The unlikely possibility that the bias field used in the apparatus was saturating the crystal as it passed through the low anisotropy region was shown not to be the case by using an external bias field and applying it only after the specimen had been cooled down. This still failed to produce an observable domain structure.

8.3 Suggestions for Further Work.

With respect to the magnetocrystalline anisotropy it is suggested that more work should be carried out on the theoretical aspects of the anisotropy. This would probably follow the work of Yang (1971) rather than that of Brooks and Goodings (1968) as the former provides a more general treatment. In particular the work should concentrate on obtaining detailed expressions for the parameters of equations 4.31 and 4.32 which depend upon the crystal structure and the electronic structure. If these parameters were known then a critical comparison with the experimental data could be made. The present anisotropy data could supply a set of values for the parameters of equations 4.31 and 4.32, but these would not necessarily be unique values and would add little to our present understanding of the magnetocrystalline anisotropy.

The magnetic domain structure of gadolinium has not been completely elucidated by the present and previous investigations and therefore further work would be useful. In particular work on the region of the easy cone of magnetization at high cone angles, i.e. around 170K, would help to complete the understanding of the changes in domain structure with the anisotropy. It is possible that a different technique than the one used in the present work will be required. In Chapter 6 the possible methods of domain observation and their application to gadolinium were discussed. The most promising alternative method would be S.E.M. provided that suitable surfaces could be prepared. The dry colloid technique is fairly insensitive to small order topographical changes of a sample whereas the S.E.M. technique is very sensitive to such changes. If a suitable apparatus could be developed to reach 4.2K it would be interesting to see if the magnitude of K_4 is sufficient to affect the basal plane domain structure.

The present dry colloid apparatus would provide a suitable system for investigating the domain structure of terbium and also dysprosium. The apparatus would need to be modified to reduce heat losses and be able to maintain a temperature of 77K. This could possibly be achieved by replacing the present brass evaporation chamber with a stainless steel double walled chamber which could be evacuated. This would retain the possibility of using the apparatus in conjunction with large external magnetic fields.

REFERENCES

AL BASSAM T.S. (1969) Ph.D.Thesis. Univ. Durham.

AL BASSAM T.S. and CORNER W.D. (1969) Coll. Int. du C,N.R.S. 180, 47.

ALSTAD J. and LEGVOLD S. (1965). J.App.Phys. 35, 1752.

AMIGHIAN J. (1975) Ph.D. Thesis, Univ. Durham.

AMIGHIAN J. and CORNER W.D. (1976). J.Phys. F. 6, L309.

ARKULOV N. (1936) Z.Phys. 100, 197.

ASADA T. (1973) J.Phys.Soc. Japan 35, 85.

BAGGULEY D.M.S. and LIESEGANG J. Proc. Roy. Soc. A300, 497.

BANISTER J.R., LEGVOLD S and SPEDDING F.H. (1954) Phys.Rev. 94, 1140.

BARKHAUSEN H. (1919) Physik Z. 20, 401.

BATTALLAN F and SOMMERS C. (1977) Physica B 86-88, 28.

BATES L.F. and SPIVEY S. (1964). Brit. J.App. Phys. 15. 705.

BELOV K.P. and PED'KO A.V. (1962) Soviet Phys. JEPT 15, 62.

BERGMANN W.H. (1956) Z.Angew Phys. 11, 559.

BIRSS R.R. (1959) Advances in Physics, 8, 252.

BIRSS R.R. and WALLIS P.M. (1963) Physics Letters 4, 313.

BIRSS R.R. (1964) Symmetry and Magnetism, North Holland.

BIRSS R.R. and WALLIS P.M. (1964). Proc. Int. Conf. on Magnetism Nottingham (Bristol IOP). 744.

BIRSS R.R. and HEGARTY B.C. (1967) J.Sci.Inst. 44, 621.

BIRSS R.R. and KEELER G.J. (1974) Phys. Stat. Sol.(b) 64, 357

BIRSS R.R. and MARTIN DJ. (1975) J.Phys.C. 8, 189.

BIRSS R.R.,KEELER G.J. and POMFRET D. (1976) J.Phys. E 9, 635.

BIRSS R.R., KEELER G.J. and SHEPHERD C.H. (1976) J.Phys. E 9, 963.

BITTER F (1931) Phys. Rev. 38, 1903.

BITTER F (1932) Phys. Rev. 41, 507.

BLOCH F (1930) Z.Phys. 61, 206.

BLOCH F (1932) Z.Phys. 74, 295.

BLY P.H. (1967) Ph.D. Thesis Univ.Durham.

BOZORTH R.M. and WAKIYAMA T. (1963) J.Appl.Phys. 34, 1351.

BROOKS M.S.S. and GOODINGS D.A. (1968) J.Phys. C1, 1279.

BROOKS M.S.S. and EGAMI T. (1973) J.Phys. C6, 513.

BROWN G.V. (1976) J.App.Phys. 47, 3673.

BROWN W.F. (1963) Micromagnetics, Wiley

CABLE J.W. and WOLLAN E.O. (1968) Phys. Rev. 165, 733.

CALLEN E.R. and CALLEN H.B. (1960) J.Phys.Chem. Solids 16. 310.

CALLEN E.R. and CALLEN H.B. (1965) Phys.Rev. 139, A455.

CALLEN E.R. and CALLEN H.B. (1966) J.Phys.Chem.Solids 27, 1271.

CAREY R and ISAAC E.D. (1964) Brit. J.App.Phys. 15, 551.

CAREY R and ISAAC E.D. (1966) Magnetic Domains and Techniques for their Observation, E.U.P.

CAREY R and THOMAS B.W.J. (1972) J.Phys. D 5, 200.

COLEMAN W.E. and PAVLOVIC A.S. (1964) Phys. Rev. 135, A426.

CAMPBELL I.A. (1972) J.Phys. F. 2, L47.

CARONI C.A., MANGHI E and de RECA N.E.W. (1973) IEEE Trans Mag. 9, 647.

CHAPMAN J.N., McKENDRICK W.H., FERRIER R.P. and HUKIN D.A. (1977) Proc. Conf. Rare Earths and Actinides, Durham, Inst. Phys. Conf. Ser. 37.

COOPER B.R. (1968) Solid State Physics 21, 393.

COQBLIN B (1977) The Electronic Structure of Rare Earth Metals and Alloys - The Magnetic Heavy Rare Earths, Academic Press.

CORNER W.D. and HUTCHINSON (1960) Proc. Phys.Soc. 75, 781.

CORNER W.D. , ROE W.C. and TAYLOR K.N.R. (1962) Proc.Phys.Soc. 80, 927.

CORNER W.D. and MASON J.J. (1964) Brit.J.App.Phys. 15, 709.

CORNER W.D. and AL BASSAM (1971) J.Phys.C. 4, 47.

CORNER W.D. and TANNER B.K. (1976) J.Phys.C. 9, 627.

CORNER W.D. and SAAD F.M. (1977a) Physica B 86-88 1331

CORNER W.D. and SAAD F.M. (1977b) Proc.Conf. Rare Earths and Actinides, Durham, Inst.Phys.Conf. Ser. 37.

CRACKNELL A.P. (1971) Advances in Physics 20, 1.

CRAIK D.J. and TEBBLE R.S. (1961) Rep.Prog.Phys. 14, 116.

CRAIK D.J. (1966) Brit.J.App.Phys. 17, 873.

DARBY M.I. and TAYLOR K.N.R. (1964) Proc.Int.Conf. on Magnetism, Nottingham (Bristol I.OP) 742.

DARBY M.I. and ISAAC E.D. (1974) IEEE Trans.Mag. 10, 259.

DARNELL F.J. (1963) Phys. Rev. 130, 1825.

EAGLES D.M. (1975) Z.Physik B 21, 69.

EAGLES D.M. (1975) Z.Physik B 21, 79.

EAGLES D.M. (1975) Z.Physik B 21, 171.

EAGLES D.M. (1975) Z.Physik B 21, 177.

EDWARDS J. (1977) Private Communication.

ELLIOTT R.J. (ed) (1972) Magnetic Properties of Rare Earth Metals, Plenum.

ESSMANN U., TRAUBLE H. (1966). J.Sci.Inst. 43, 344.

EVANS D.J. and GARRETT H.J. (1973) IEEE Trans. Mag. 9, 197.

FATHERS D.J. and JAKUBOVICS J.P. (1977) Physica B 86-88, 1343.

FERON J.L. (1969a) C.R.Acad. Sci. Paris, 269B, 549.

FERON J.L. (1969b) C.R.Acad. Sci. Paris, 269B, 611.

FRANSE J.J.M. and MIHAI V. (1977) Physica B 86-88, 49.

FUJII H., HUSHIMOTO Y., MISHIMA A., SHOHATA N. and OKAMOTO T. (1976). J.Phys.Soc. Japan, 41, 1179.

FUJIWARA H., TOKUNAGA T., TANGE H., and GOTO M. (1977) J.Phys. Soc. Japan, 43, 1554.

FUREY W.N. (1967). Ph.D. Thesis, Harvard Univ. U.S.A.

GADSDEN C.J. and HEATH M.J. (1978) J.Phys.F. 8, 521.

GARROOD J.R. (1962). Proc. Phys. Soc. 79, 1252.

de GENNES P.G. (1962). J.Phys. et. Rad. 23, 510.

GOODENOUGH J.B. (1956) Phys. Rev. 102, 356.

GRAF H., HOFMANN W., KUNDIG W., MEIER P.F., PATTERSON B.D. and REICHART W, (1977) Solid State Comm. 23, 653.

GRAHAM C.D. (1962). J.Phys. Soc. Japan, 17, 1310.

GRAHAM C.D. (1967). J.App. Phys. 28, 1375.

GRANQUIST C.G. and BUHRMAN R.A. (1976). Solid State Comm. 18, 123.

GRIFFEL M., SKOCHDOPOLE R.E. and SPEDDING F.H. (1954). Phys. Rev. 93, 657.

GUPTA R.P. and LOUCKS T.L. (1968). Phys. Rev. 176, 848.

HEISENBERG W. (1928) Z.Phys. 49, 619.

HERRING C.P. and JAKUBOVICS J.P. (1973). J.Phys.F. 3, 157.

HUTCHINSON R.I., LAVIN P.A. and MOON J.R. (1965). J.Sci.Inst. 42, 885.

ITO T. (1973). J.Sci. Hiroshima Univ. Ser.A 37, 107.

JACKSON S. (1978). Private Communication.

JENSEN J. (1976). Phys. Rev. Lett. 37, 951.

JENSEN J. (1977). Physica B 86-88, 32.

JONES D.W., FARRANT S.P., FORT D. and JORDAN R.G. (1977) Proc. Conf. Rare Earths and Actinides, Durham, Inst. Phys. Conf. Ser. 37.

JONES G.A.(1976) Science Progress 63, 219.

JORDAN R.G. (1974). Contemp. Phys. 15, 375.

JORDAN R.G., JONES D.W. and HALL M.G. (1974) J.Cryst. Growth 24-25, 568.

KAITO C. (1978). Jap. J.App.Phys. 17, 601.

KANDAUROVA G.S. and BEKETOV V.N. (1975). Sov. Phys. Solid State 16, 1213.

KAMAMURA K. (1973). Jap. J.App.Phys. 12, 1685.

KASUYA T. (1956). Prog. Theor. Phys. Japan 16, 45.

KIMOTO K., KAMIYA Y., NONOYUMA M and UYEDA R. (1963). Jap. J. App. Phys. 2, 702.

KITTEL C. (1948). Phys. Rev. 73, 155.

KITTEL C. (1949). Rev. Mod. Phys. 21, 541.

KITTEL C. and GALT J.K. (1956). Solid State Physics 3, 439.

KITTEL C. (1968). Solid State Physics 22, 1.

KITTEL C. (1971). Introduction to Solid State Physics 4th ed., Wiley.

KOEHLER W.C. (1972) Chapter 3 of Elliott (1972).

KOUVEL J.S. and GRAHAM C.D. (1956). AIEE Cong. Mag. Mag. Mat. Boston.

KOZOLOWSKI G. and ZIETEK W. (1966). Acata Physica Polonica 29, 261.

KUBO R. and NAGAMIYA T. (1969). Solid State Physics, McGraw Hill.

KUCHIN V.M., SOMENKOV V.A., SHIL'SHSTEIN S.Sh. and PATRIKEEV Yu B. (1969). Soviet Physics JEPT 28, 649.

LANDAU L.D. and LIFSHITZ E.M. (1935). Phys. Z. Sowj. 8, 153.

LEE E.W. (1955) Reports Prog.Phys. 18, 184.

LEE E.W. (1959). Advances in Physics 8, 292.

LEE E.W. (1977). Private Communication.

LILLEY B.A. (1950). Phil Mag. 41, 792.

LINDGÅRD P.A. (1976a). Phys. Rev. Lett. 36, 385.

LINDGÅRD P.A. (1976b). Phys. Rev. Lett. 37, 954.

LINDGÅRD P.A. (1978). Phys. Rev. B 17, 2348.

MARTI J., and PAUL D.I. (1977). J.Appl. Phys. 48, 4678.

MASON W.P. (1951). Phys. Rev. 82, 715.

MASON W.P. (1954). Phys. Rev. 96, 302.

MATTOCKS P.G. and YOUNG R.C. (1977). J.Phys. F. 7, 1219.

McEWEN K.A. and TOUBORG P. (1973). J.Phys. F. 3, 1903.

MILSTEIN F. and ROBINSON L.B. (1969). Phys. Rev. 177, 904.

MISHIMA A., FUJII H. and OKAMOTO T. (1976). J.Phys. Soc. Japan, 40, 962.

McKENDRICK W., CHAPMAN J.N., FERRIER R.P. and HUKIN D.A. (1977) Physica B 86-88, 1335.

MOON R.M., KOEHLER W.C., CABLE J.W. and CHILD H.R. (1972) Phys.Rev. B5, 997.

MORRISH A.H. (1965). The Physical Principles of Magnetism, Wiley.

NÉEL L. (1944). Cahiers de Phys. 25, 1.

NIGH H.E., LEGVOLD S. and SPEDDING F.H. (1963). Phys. Rev. 132, 1092.

OSBORNE J A. (1945). Phys. Rev. 67, 351.

PALMER S.B., LEE E.W. and ISLAM M.N. (1974). Proc. Roy. Soc. London A 338, 341.

PENOYER R.F. (1959). Rev. Sci. Inst. 30, 711.

PRIVOROTSKII I. (1976). Thermodynamic Theory of Domain Structures, Wiley.

RHYNE J.J (1972). Chapter 4 of Elliott (1972).

RHYNE J.J. and McGUIRE T.R. (1972) IEEE Trans.Mag. 8, 105.

ROBINSON K. and LANCHESTER P.C. (1978). Phys. Lett. 64A, 467.

ROE W.C. (1961). Ph.D. Thesis Univ. Durham.

ROELAND L.W., COCK G.J., MULLER F.A., MOLEMAN A.C. McEWAN K.A., JORDAN R.G. and JONES D.W. (1975). J.Phys. F. 5, L233.

ROSENBERG M., TANASOIU C. and RUSU C. (1964). Phys. Stat. Sol. 6, 141.

RUNDERMANN M.A. and KITTEL C. (1954). Phys. Rev. 96, 99.

SAAD F.M. (1977). Ph. D. Thesis Univ. Durham.

SAAD F.M. (1978). Private Communication.

SALMONS L.R., STRNAKT K. and HOFFER G.I. (1968). Tech. Report AFML-68-159, Wright-Patterson Air Force Base, Ohio, U.S.A..

SARMA N.V. and MOON J.R. (1967). Phil Mag. 16, 433.

SCHLENKER M. and BARUCHEL J. (1978). J.Appl.Phys. 49, 1996.

SHILLING J.W. and HOUZE G.L. (1974) IEEE Trans.Mag. 10, 195.

SHIRBER J.E., SCHMIDT F.A., HARMON B.N. and KOELLING D.D. (1976). Phys. Rev.Lett. 36, 448.

SHILSTEIN Sh.S., SOMENKOV V.A., KALJNOV M. and ELYUTIN N.O. (1976). Sov. Phys. Solid State 18, 1886.

SLATER J.C. (1936). Phys. Rev. 49, 537.

SMITH D.A. (1976). J.Mag. Mat. 1, 214.

STEVENS K.W.H. (1952). Proc. Phys. Soc. A65, 209.

STONER E.C. (1938). Phil Mag. 25, 899.

STONER E.C. (1945). Phil Mag. 36, 803.

SWIFT W.M. (1973). IEEE Trans.Mag. 9, 348.

SYDNEY K.R., CHAPLIN D.H., and WILSON G.V.H. (1976). J.Mag.Mat. 2, 345.

TAJIMA K. (1971). J.Phys. Soc. Japan 31, 441.

TAKASHI M., KADOWAKI S., WAKIYAMA T., ANAYAMA T. and TAKAHASHI M. (1978). J.Phys.Soc. Japan. 44, 825.

TAKATA Y. (1962). J.Phys. Soc. Japan 18, 87.

TANNER B.K. (1976). X-Ray Diffraction Topography, Pergoman A76.

TAYLOR K.N.R. (1970). Contemp. Phys. 11, 423.

TAYLOR K.N.R. (1971). Advances in Physics 20, 551.

TAYLOR K.N.R. and DARBY M.I. (1972). Physics of Rare Earth Solids, Chapman and Hall.

TEMPLE J.A.G., FAIRBAIN W.M. and PICKETT G.R. (1977). J.Phys. F 7, 1039.

TOHYAMA K., TAJIMA K., CHIKAZUMI S. and SAWAOKA A. (1969). J.Phys. Soc. Japan 27, 1070.

TOHYAMA K. and CHIKAZUMI S. (1973). J.Phys. Soc. Japan 35, 47.

TONEGAWA T. (1964). J.Phys. Soc. Japan 19, 1168.

TRAUBLE H.and ESSMANN U. (1966). Phys. Stat. Solidi 18, 813.

URBAIN G, WEISS P. and TROMBE F. (1935). C.R.Acad.Sci.Paris 200, 2132.

UYEDA R. (1974). J.Cryst. Growth 24-25, 69.

VAN VLECK J.H. and FRANK A. (1929). Phys. Rev. 34, 1494.

VAN VLECK J.H. and FRANK A (1929). Phys. Rev. 34, 1625.

VAN VLECK J.H. (1932). Theory of Electric and Magnetic Susceptibilities, OUP.

VAN VLECK J.H. (1956). AIEE Conf. Mag. Mag. Mat., Boston.

WADA N. (1967). Jap.J.Appl. Phys. 6, 553.

WADA N. (1968). Jap.J.Appl. Phs. 7, 1287.

WARNOCK F. (1975). M.Sc. Thesis Univ. Durham.

WEISS P (1907). J.Phys. et Rad. 6, 661.

WELFORD J. (1974). Ph. D. Thesis Univ. Durham.

WELLS P., LANCHESTER P.C., JONES D.W. and JORDAN R.G. (1974). J. Phys. F 4, 1729.

WILL G., NATHANS R. and ALPERIN H.A. (1964). J.App. Phys. Supp. 35, 1045.

WILLIAMS H.J., BOZORTH R.M. and SHOCKLEY W. (1949). Phys. Rev. 75, 155.

WOHLFARTH E.P. (1959). Advances in Physics 8, 87.

WYSLOCKI B., and ZIETEK W. (1966). Acta Physica Polonica 29, 223.

YANG J.J.H. (1971). Ph.D. Thesis Univ. California L.A.

YANG T.T. (1976). Jap. J.App. Phys. 15, 279.

YOSIDA K. (1957). Phys. Rev. 106, 893.

ZENER C. (1954). Phys. Rev. 96, 1335.

APPENDIX I

Program for the Analysis of Basal Plane Torque Curves

P.L.1

```
KAYC:PROCEDURE OPTIONS(MAIN);
DECLARE (A(2,6),AMP(2,6),AC(2),CALIB,DIFF,DY,HYST,K4,LL,PHASE(2,6),PRODS
(2,2,6),PROS(2,36),RMS(2),RS(2,36),SCALE,TRIG(2,6,36),WT)DEC FLOAT(6),
(I,J,K,L,NC,SW)BINARY FIXED(15,0),(DATE)CHARACTER(15);
DECLARE(K)A,K2A,K3A,K1,K2,K3,K1V,K2V,K3V)DEC FLOAT(6);
DECLARE(FIELD,TEMP)CHARACTER(5),(K4V,DENSITY)DEC FLOAT(6);
SETUP:DO L=1 BY 1 TO 6;
DO J=1 BY 1 TO 36;
TRIG(1,L,J)=SIND(10*L*(J-1));
TRIG(2,L,J)=COSD(10*L*(J-1));
END;
END;
ON CONVERSION PUT LIST(ONSOURCE,ONCHAR);
GET LIST(CALIB,WT,DENSITY);
START:SW=0;
ON ENDFILE(SYSIN) GOTO LAST;
GET LIST(DATE,NO,SCALE,DY,LL,((RS(I,J) DO J=1 TO 36)DO I=1,2));
GET LIST(FIELD,TEMP);
PUT EDIT('DATE','NUMBER',NO,'SCALE',SCALE,'V/CM','DY=',DY,'LL=',LL)
(PAGE,A(14),X(2),A(8),F(4,0),X(2),A(7),F(8,5),X(1),A(8),X(2),A(4),F(6,2
),X(2),A(5),F(4,2));
PUT EDIT('MAG.FIELD=',FIELD,'TEMP=',TEMP)(SKIP,A(10),A(5),X(5),
A(5),A(5));
PUT EDIT('MEASURED VALUES')(SKIP,A(18));
PUT EDIT('CW.RDGS.',RS(1,*),'ACW.RDGS.',RS(2,*))(2(SKIP,A(8),12(X(2),
F(6,2)),2(SKIP,X(8),12(X(2),F(6,2)))));
IF DY¬=0 THEN DO;
DO I=1,2;
DO J=1 BY 1 TO 36;
RS(I,J)=(COS(ATAN(DY,LL)))*(RS(I,J)+((J+1)*DY/35));
END;
END;
PUT EDIT('VALUES CORRECTED FOR SHEAR')(SKIP,A(27));
PUT EDIT('CW.RDGS.',RS(1,*),'ACW.RDGS.',RS(2,*))(2(SKIP,A(8),12(X(2),
F(6,2)),2(SKIP,X(8),12(X(2),F(6,2)))));
END;
CALC:DO I=1,2;
DO K=1,2;
DO L=1 BY 1 TO 6;
PRODS(K,I,L)=(SUM(RS(I,*)*TRIG(K,L,*)))/18;
END;
END;
END;
DO I=1,2;
AC(I) = (SUM(RS(I,*)))/36;
DO L=1 BY 1 TO 6;
A(I,L)=SQRT((PRODS(1,I,L))**2+(PRODS(2,I,L))**2);
AMP(I,L)=(A(I,L)*CALIB*SCALE)/(WT);
PHASE(I,L)=ATAND(PRODS(2,I,L)/PRODS(1,I,L))/(2*L);
END;
END;
END;
HYST=(AC(2)-AC(1))*SCALE*CALIB*6.2832/(WT);
K1A=(AMP(1,1)+AMP(2,1))/2;
K2A=(AMP(1,2)+AMP(2,2))/2;
K3A=(AMP(1,3)+AMP(2,3))/2;
K3=(16*K3A)/3;
K2=(2*K2A+8*K3A);
K1=(K1A-(2*K2A)-(3*K3A));
K3V=K3*DENSITY;
K2V=K2*DENSITY;
K1V=K1*DENSITY;
RCRS=0;
DO I=1,2;
RCRS(I,*) = AC(I);
DO J=1 BY 1 TO 36;
DO L=1,2,3,6;
RCRS(I,J)=RCRS(I,J)+A(I,L)*SIND(2*L*(5*(J-1)+PHASE(I,L)));
END;
END;
END;
PUT EDIT('VALUES CALC FROM 2,4,6,12FOLD COMPONENTS')(SKIP,A(45));
PUT EDIT('CW.RDGS.',RCRS(1,*),'ACW.RDGS.',RCRS(2,*))(2(SKIP,A(8),12(X(
2),F(6,2)),2(SKIP,X(8),12(X(2),F(6,2)))));
DO I=1,2 ;
RMS(I)=0 ;
DO J = 1 BY 1 TO 36;
RMS(I)=RMS(I)+(RS(I,J)-RCRS(I,J))**2;
END;
RMS(I)=(RMS(I)/36);
END;
PUT EDIT('MEAN','2FOLD','4FOLD','6FOLD','8FOLD','12FOLD','12FOLD',
'AMPS(CW)',AC(1),AMP(1,*),'PHASE(CW)',PHASE(1,*),'AMPS(ACW)',AC(2),AMP(
2,*),'PHASE(ACW)',PHASE(2,*))(SKIP,X(18),7(X(4),A(7)),2(SKIP,A(18),7(X
(1),F(10,3)),SKIP,A(18),X(11),6(X(1),F(10,3))));
PUT SKIP EDIT('HYSTERESIS ESTIMATE=',HYST,'JKG-1 PERREV',
'MEAN K3=',K3,'JKG-1','K3V=',K3V,'J M-3',
'MEAN K2=',K2,'JKG-1','K2V=',K2V,'J M-3',
'MEAN K1=',K1,'JKG-1','K1V=',K1V,'J M-3',
'RMS ERROR=',RMS)
(X(5),A(22),F(10,3),X(2),A(14),3(SKIP,X(17),A(10),F(10,3),X(2),A(7),
X(11),A(5),F(10,3),X(2),A(5)),
SKIP,X(15),A(22),F(10,3),X(3),F(10,3));
IF SW=0 THEN GOTO START;
LAST:END KAYC;
```

ND OF FILE

APPENDIX II

Program for the Analysis of b Plane Torque Curves

P.L.1

```
1        [illegible]
2        DECLARE(A(2,6),AMP(2,4),AC(2),CALIB,DIFF,DY,HYST,LL,PHASE(2),PRODS
3        (2,2,6),RCFS(2,9,36),RMS(2,9),RS(2,36),SCALE,TRIG(2,6,36),WT)
4        DEC FLOAT(6),
5        (I,J,K,L,NO,SW)BINARY FIXED(15,0),(DATE)CHARACTER(15);
6        DECLARE(K1A,K2A,K3A,K4A,K1,K2,K3,K1V,K2V,K3V)DEC FLOAT(6);
7        DECLARE(FIELD,TEMP)CHARACTER(5),(DENSITY)DEC FLOAT(6);
8        SETUP:DO L=1 BY 1 TO 6;
9        DO J=1 BY 1 TO 36;
10       TRIG(1,L,J)=SIND(10*L*(J-1));
11       TRIG(2,L,J)=COSD(10*L*(J-1));
12       END;
13       END;
14       ON CONVERSION PUT LIST(ONSOURCE,ONCHAR);
15       GET LIST(CALIB,WT,DENSITY);
16       START:SW=0;
17       ON ENDFILE(SCARDS) GOTO LAST;
18       GET LIST(DATE,NO,SCALE,DY,LL,((RS(I,J) DO J=1 TO 36)DO I=1,2));
19       GET LIST(FIELD,TEMP,(PHASE(I) DO I=1,2));
20       PUT EDIT(DATE,'NUMBER',NO,'SCALE',SCALE,'V/CM','DY=',DY,'LL=',LL)
21       (PAGE,A(16),X(2),A(8),F(4,0),X(2),A(7),F(8,5),X(1),A(5),X(2),A(4),F(6,2
22       ),X(2),A(5),F(6,2));
23       PUT EDIT('MAG.FIELD=',FIELD,'TEMP=',TEMP)(SKIP,A(10),A(5),X(5),
24       A(5),A(5));
25       PUT EDIT('MEASURED VALUES')(SKIP,A(18));
26       PUT EDIT('CW.RDGS.',RS(1,*),'ACW.RDGS.',RS(2,*))(2(SKIP,A(8),12(X(2),
27       F(6,2)),2(SKIP,X(8),12(X(2),F(6,2)))));
28       IF DY^=0 THEN DO;
29       DO I=1,2;
30       DO J=1 BY 1 TO 36;
31       RS(I,J)=(COS(ATAN(DY/LL)))*(RS(I,J)+((J-1)*DY/35));
32       END;
33       END;
34       PUT EDIT('VALUES CORRECTED FOR SHEAR')(SKIP,A(27));
35       PUT EDIT('CW.RDGS.',RS(1,*),'ACW.RDGS.',RS(2,*))(2(SKIP,A(8),12(X(2),
36       F(6,2)),2(SKIP,X(8),12(X(2),F(6,2)))));
37       END;
38       CALC:DO I=1,2;
39       DO K=1,2;
40       DO L=1 BY 1 TO 6;
41       PRODS(K,I,L)=(SUM(RS(I,*)*TRIG(K,L,*)))/18;
42       END;
43       END;
44       END;
45       DO I=1,2;
46       AO(I) = (SUM(RS(I,*)))/36;
47       DO L=1 BY 1 TO 6;
48       A(I,L)=SQRT((PRODS(1,I,L))**2+(PRODS(2,I,L))**2);
49       END;
50       END;
51       DECLARE(ANG(3,2,36),RMSMIN(2),X(2))DEC FLOAT(6);
52       DO I=1,2;
53       DO L=1 BY 1 TO 3;
54       DO J=1 BY 1 TO 36;
55       ANG(L,I,J)=SIND(L*2*(5*(J-1)+PHASE(I)));
56       END;
57       END;
58       END;
59       DO I=1,2;
60       DO J=1 BY 1 TO 36;
```

```
      RCRS(I,1,J)=AO(I)+A(I,1)*ANG(1,I,J)+A(I,2)*ANG(2,I,J)+A(I,3)*
      ANG(3,I,J);
      RCRS(I,2,J)=AO(I)+A(I,1)*ANG(1,I,J)+A(I,2)*ANG(2,I,J)-A(I,3)*
      ANG(3,I,J);
      RCRS(I,3,J)=AO(I)+A(I,1)*ANG(1,I,J)-A(I,2)*ANG(2,I,J)-A(I,3)*
      ANG(3,I,J);
      RCRS(I,4,J)=AO(I)+A(I,1)*ANG(1,I,J)-A(I,2)*ANG(2,I,J)+A(I,3)*
      ANG(3,I,J);
      RCRS(I,5,J)=AO(I)-A(I,1)*ANG(1,I,J)+A(I,2)*ANG(2,I,J)+A(I,3)*
      ANG(3,I,J);
      RCRS(I,6,J)=AO(I)-A(I,1)*ANG(1,I,J)+A(I,2)*ANG(2,I,J)-A(I,3)*
      ANG(3,I,J);
      RCRS(I,7,J)=AO(I)-A(I,1)*ANG(1,I,J)-A(I,2)*ANG(2,I,J)-A(I,3)*
      ANG(3,I,J);
      RCRS(I,8,J)=AO(I)-A(I,1)*ANG(1,I,J)-A(I,2)*ANG(2,I,J)+A(I,3)*
      ANG(3,I,J);
      END;
      END;
      DO I=1,2;
      DO L=1 BY 1 TO 8;
      DO J=1 BY 1 TO 36;
    RMS(I,L)=RMS(I,L)+(RS(I,J)-RCRS(1,L,J))**2;
      END;
      END;
      END;
      DO I=1,2;
      DO L=1 BY 1 TO 8;
      RMS(I,L)=SQRT(RMS(I,L)/36);
      END;
      END;
      RMSMIN(1)=RMS(1,1);
      X(1)=1;
      RMSMIN(2)=RMS(2,1);
      X(2)=1;
      DO I=1,2;
      DO L=1 BY 1 TO 7;
      IF RMS(I,L+1)<RMSMIN(I) THEN DO;
      RMSMIN(I)=RMS(I,L+1);
      X(I)=L+1;
      END;
      END;
      END;
      DO I=1,2;
      IF X(I)=2 THEN A(I,3)=-A(I,3);
      IF X(I)=3 THEN DO;
      A(I,2)=-A(I,2);
      A(I,3)=-A(I,3);
      END;
      IF X(I)=4 THEN A(I,2)=-A(I,2);
      IF X(I)=5 THEN A(I,1)=-A(I,1);
      IF X(I)=6 THEN DO;
      A(I,1)=-A(I,1);
      A(I,3)=-A(I,3);
      END;
      IF X(I)=7 THEN DO;
      A(I,1)=-A(I,1);
      A(I,2)=-A(I,2);
      A(I,3)=-A(I,3);
      END;
      IF X(I)=8 THEN DO;
```

```
      A(I,1)=-A(I,1);
      A(I,2)=-A(I,2);
      END;
      END;
      DO I=1,2;
      AO(I)=(AO(I)*SCALE*CALIB)/WT;
      DO L=1 BY 1 TO 6;
      AMP(I,L)=(A(I,L)*CALIB*SCALE)/(WT);
      END;
      END;
      HYST=(AC(2)-AO(1))*6.2832;
      K1A=(AMP(1,1)+AMP(2,1))/2;
      K2A=(AMP(1,2)+AMP(2,2))/2;
      K3A=(AMP(1,3)+AMP(2,3))/2;
      K4A=(AMP(1,5)+AMP(2,5))/2;
      K3=(-16*K3A)/3;
      K2=(2*K2A+8*K2A);
      K1=(-K1A-2*K2A-3*K3A);
      K3V=K3*DENSITY;
      K2V=K2*DENSITY;
      K1V=K1*DENSITY;
      PUT EDIT('VALUES CALC FROM 2,4,6 FOLD COMPONENTS')(SKIP,A(45));
      PUT EDIT('CW.RDGS.',RCRS(1,X(1),4),'ACW.RDGS.',RCRS(2,X(2),4))
     (2(SKIP,A(8),12(X(2),F(6,2)),2(SKIP,X(8),12(X(2),F(6,2)))));
      PUT EDIT('MEAN','2FOLD','4FOLD','6FOLD','8FOLD','10FOLD','12FOLD',
      'AMPS(CW)',AO(1),AMP(1,*),'AMPS(ACW)',AC(2),AMP(2,*))
     (SKIP,X(18),7(X(4),A(7)),2(SKIP,A(18),7(X(1),E(10,3))));
      PUT SKIP EDIT('HYSTERESIS ESTIMATE=',HYST,'JKG-1 PERREV',
      'MEAN K3=',K3,'JKG-1','K3V=',K3V,'J M-3',
      'MEAN K2=',K2,'JKG-1','K2V=',K2V,'J M-3',
      'MEAN K1=',K1,'JKG-1','K1V=',K1V,'J M-3',
      'RMS ERROR=',RMS(1,X(1)),RMS(2,X(2)))
      (X(5),A(22),E(10,3),X(2),A(14),3(SKIP,X(17),A(10),E(10,3),X(2),A(7),
      X(11),A(5),E(10,3),X(2),A(5)),
      SKIP,X(15),A(22),E(10,3),X(3),E(10,3));
      IF SW=0 THEN GOTO START;
      LAST:END KAYC;
END OF FILE
```

APPENDIX III

Program for a Least Squares Fit of a Straight Line

FORTRAN IV

```
LIST FCRISE
    1       *COMPILE
    2       C PROGRAM LSE
    3               REAL SDC,SDB,B,C,SX,SY,SXY,SX2,A(25,4),CE(25),BE(25),SCE,SB
    4               INTEGER N,I,J
  4.1       1       READ(5,13)ID
  4.2       13       FORMAT(A4)
  4.3               WRITE(6,14)ID
  4.4       14       FORMAT(//,2X,A4)
    5               READ(5,10) N
    6       10      FORMAT(I2)
  6.5               IF (N.LT.1) GO TO 8
    7       C DATA READ IN AS PAIRS OF X,Y VALUES
    8               I=0
    9               J=0
   10               DO 2 I=1,N
   11         2     READ(5,11)(A(I,J),J=1,2)
 11.5          11  FORMAT(2F10.4)
 11.6               WRITE(6,12)((A(I,J),J=1,2),I=1,N)
 11.7       12      FORMAT(/,10X,'X',14X,'Y',/,2(5X,F10.4))
   12               I=0
   13               J=0
   14               DO 3 I=1,N
   15               A(I,3)=A(I,1)*A(I,2)
   16         3     A(I,4)=A(I,1)**2
   17               SX=0.0
   18               SY=0.0
   19               SXY=0.0
   20               SX2=0.0
   21               DO 4 J=1,N
   22               SX=SX+A(J,1)
   23               SY=SY+A(J,2)
   24               SXY=SXY+A(J,3)
   25               SX2=SX2+A(J,4)
   26         4     CONTINUE
   27               B=(N*SXY-SY*SX)/(N*SX2-SX*SX)
   28               C=(SY*SX2-SX*SXY)/(N*SX2-SX*SX)
   29               WRITE(6,5)B,C
   30         5     FORMAT(/,3X,'Y=BX+C',7X,'B=',F10.4,5X,'C=',F10.4)
   31               SCE=0.0
   32               SBE=0.0
   33               I=0
   34               J=0
   35               DO 6 I=1,N
   36               CE(I)=C-(A(I,2)-B*A(I,1))
   37               BE(I)=B-((A(I,2)-C)/A(I,1))
   38               SCE=SCE+CE(I)**2
   39               SBE=SBE+BE(I)**2
   40         6     CONTINUE
   41               SDC=SQRT(SCE/(N*(N-1)))
   42               SDB=SQRT(SBE/(N*(N-1)))
   43               WRITE(6,7)SDB,SDC
   44         7     FORMAT(/,'STAND.DEVS',4X,'SDB=',F10.4,3X,'SDC=',F10.4)
   45               GOTO 1
   46         8     STOP
   47               END
```

APPENDIX IV

Program for the Calculation of Anisotropy Energy Surfaces FORTRAN IV

```
$COMPILE
C PROGRAM FOR ANISOTROPY ENERGIES
      REAL A,B,K1V,K2V,K3V,K4V
      INTEGER C
      DIMENSION E(37,37)
100   READ(5,1) TEMP,K1V,K2V,K3V,K4V
  1   FORMAT(A4,4E10.4)
      IF (K1V.EQ.0.0) GO TO 12
      DO 2 I=1,37,1
      A=0.0
      A=SIN(5.0*(I-1.0)*3.1416/180.01
      DO 3 J=1,37,1
      B=0.0
      B=COS(30.0*(J-1.0)*3.1416/180.01
      E(I,J)=(K1V*A**2)+(K2V*A**4)+(K3V*A**6)+(K4V*B*A**6)
  3   CONTINUE
  2   CONTINUE
      WRITE(6,4) TEMP
  4   FORMAT('1',//,'    ANISOTROPY ENERGY SURFACE AT ',A4)
      DO 5 I=1,37,1
      C=5*(I-1)
      WRITE(6,10) C
 10   FORMAT(1X,'THETA=',I3,10X,'PHI VALUES')
      WRITE(6,11)(E(I,J),J=1,37,1)
11    FORMAT(1X,10(F10.2,1X))
  5   CONTINUE
      GO TO 100
 12   STOP
      END
$DATA
$STOP
```

Durham University
SCIENCE
7 FEB 1979
SECTION
Library